The Theory of Two-Electron Atoms: From the Ground State to Complete Fragmentation

Gregor Tanner, Klaus Richter*, Jan-Michael Rost†
Basic Research Institute in the Mathematical Sciences
HP Laboratories Bristol
HPL-BRIMS-98-17
July, 1998

two-electron atoms, quantum chaos, electron-correlation, review

The evolution of understanding and predicting spectra of two-electron atoms including doubly excited resonance states which are strongly influenced by *correlated* electron-electron dynamics is reviewed. In a first part we summarize the historical development and introduce common techniques to measure and calculate two-electron atom states. Part two gives an introduction into approximate quantum methods developed for two-electron atoms, in particular adiabatic and group theoretical approaches. These methods explain and predict the striking regularities of two-electron resonance spectra by identifying approximate quantum numbers corresponding to collective, correlated electron-pair dynamics. The quantum numbers are very different from the independent particle classification, suitable for low lying states in atomic systems, only. Part three describes modern semiclassical concepts and their application to two-electron atoms. Simple interpretations of the approximate quantum numbers can be given in terms of a few key periodic orbits of the classical three body problem. Qualitative and quantitative semiclassical estimates for doubly excited states are obtained for both, regular and chaotic classical two-electron dynamics using modern semiclassical techniques.

Internal Accession Date Only

*Max-Planck Institut für Physik Komplexer Systeme, Dresden,Germany
†Fakultät für Physik der Universität Freiburg,Freiburg, Germany

CONTENTS

I. Introduction 4
A. Scope of this review and related work 4
B. Content of the review 5
II. Helium-like systems: from old to modern quantum theory 7
A. Early calculations of two-electron ground states 8
1. The failure of the "old quantum theory" 8
2. Semiclassical perturbative and variational approaches 12
a. Planetary atoms 12
b. Percival's treatment 13
c. Solov'ev's adiabatic perturbative treatment 13
d. Discussion and summary of further approaches 14
3. Wavemechanical perturbative and variational results 14
B. Doubly-excited states: basic spectral structure and experimental developments 15
1. Basic spectral properties 16
2. Early experimental observation of electronic correlations 17
3. Overview over modern spectroscopical techniques 19
a. Double excitation of helium using synchrotron radiation 19
b. Laser double excitation of alkaline earth atoms 21
4. Further methods for double excitation 22
a. Laser excitation of H^- 22
b. Dielectronic recombination 22
c. Electron impact experiments 23
C. Doubly-excited states: numerical approaches and spectra 23
1. Brief review of modern numerical methods 23
a. Feshbach projection formalism 23
b. Hyperspherical approaches 23
c. R-matrix method 24
d. Stabilization method 24
e. Multi-configurational Hartree–Fock method 24
2. Calculation by complex rotation 25
3. The helium $^1S^e$ energy level diagram 26
III. Approximate quantum mechanical concepts for two-electron dynamics 28
A. Overview 28
B. The molecular adiabatic approximation 30
1. Symmetries and wavefunctions 30
2. Quasiseparability and quantum numbers 32
3. Propensity rules for radiative and non-radiative transitions 33
a. Autoionization 33
b. Dipole transitions 36
4. The molecular description of planetary states 36
a. Characteristics of planetary states 36
b. Structure of planetary states from the adiabatic approximation 37
c. Decay widths 38
5. Conclusions from the adiabatic molecular treatment 39
C. The algebraic approach 39
1. Dynamical SO(4) representations for one and two electron atoms 39
2. The energy level multiplets for intrashell doubly-excited states 40
3. Supermultiplets for two-electron states 41
D. The hyperspherical adiabatic approximation 42
1. Potential curves and channel functions 43
2. Nodal pattern of wavefunctions and propensity rules 44
E. Other quantum mechanical concepts for two-electron resonances 45
1. Dimensional scaling 45
2. The grandparent model and the double Rydberg formula 46
3. Work in the limit of large nuclear charge Z 46
IV. Semiclassical theory for two-electron atoms 47
A. Introduction to modern semiclassical theory 47
1. The semiclassical Green function 48
2. From classical paths to periodic orbits: trace formulae and semiclassical zeta functions 49

a. Semiclassical trace formula for chaotic systems 49
b. The spectral determinant and semiclassical zeta functions 51
c. The S–matrix and periodic orbits 52
3. Semiclassical quantization for integrable and chaotic dynamics: EBK–quantization and periodic orbit expansions 53
a. Einstein Brioullin Keller (EBK) quantization 53
b. Periodic orbit quantization for chaotic systems 53
B. Two-electron atoms: a classical analysis 56
1. General overview: Integrals of motion, scaling properties and regularisation techniques 56
a. The Hamiltonian and scaling properties 56
b. Regularisation of the two–body collisions 57
c. Symmetries and invariant subspaces 58
2. Invariant subspaces: collinear configurations and the Wannier ridge 58
a. Collinear Helium: the Hamiltonian and general properties 58
b. The symmetry plane of the Wannier ridge 62
C. Qualitative semiclassical analysis of the two-electron spectrum from fundamental periodic modes 64
1. Classical interpretation of the spectral structure of two–electron atoms 64
2. Single periodic orbit quantization 65
a. The frozen planet orbit 65
b. The Langmuir orbit 67
c. The asymmetric stretch orbit 67
3. Spectral Fourier analysis 69
D. Quantitative determination of resonances from semiclassical summation techniques 70
1. EBK–quantization of asymmetric electronic excitations 70
2. Semiclassical zeta function and symmetrically excited states 71
3. Rydberg series and semiclassical quantum defect theory for collinear eZe – states 73
V. Conclusion and Outlook 76
A. Summary 76
1. Helium after 1920: The quest for quantum mechanics 76
2. Helium after 1960: The need to go beyond the Hartree-Fock approximation 76
3. Helium after 1990: The quest for new concepts to understand the extreme excitation regime 76
B. Outlook 77
C. Acknowledgements 77
References 78

I. INTRODUCTION

Moon-earth-sun, the oldest, best known but least understood three body problem (Gutzwiller (1994)) – this is, how Martin Gutzwiller summarized research on the gravitational dynamics of three masses in a recent Review of Modern Physics (Gutzwiller (1998)). Probably a similar statement applies to the corresponding microscopic three-body system, the dynamics of three massive point charges, most abundantly exemplified in nature by two–electron–atoms. The reason is, in both cases, the chaotic nature of the classical dynamics of the three-body system.

Two–electron atoms have played an important role for the development of theoretical physics in this century: They were a catalyst for the quantum theory in the mid twenties since the old quantum mechanics of Niels Bohr and others could not cope with the seemingly simple problem to calculate the ground state of helium. The discovery of strong electron-electron correlation effects in doubly excited resonant states of helium in a seminal experiment by Madden and Codling in 1963 has triggered the development of group-theoretical and adiabatic quantum approximations to understand these unexpected correlations. Almost 70 years after the failure of the Bohr-Sommerfeld quantization for helium, two–electron dynamics, again, was at the forefront of a revival of the old quantum theory. New semiclassical concepts were introduced by Gutzwiller and others in the early 70ies for which Heller and Tomsovic (1993) have coined the term *post modern quantum mechanics*. In contrast to the old quantum theory, which was based on (mostly) ad hoc quantization rules for certain classical orbits, modern semiclassical theory exploits the full classical dynamics in a systematic way. Based on these ideas the first successful semiclassical quantization of helium was performed by Ezra et al. in 1991.

Bound states of two-electron atoms have been understood quickly with the help of the overwhelmingly successful Hartree-Fock self consistent field method. In fact, they can be handled to such an accuracy today that they are used for high precision measurements and calculations to improve on fundamental physical constants. Hence, over the last 35 years, the struggle to understand doubly-excited states has been the focus of theoretical research on two-electron atoms: what are the energetic positions of the resonances, their lifetimes, and their excitation mechanisms? Understanding meant and means in this context more than the ability to numerically calculate these resonance properties, an ability which we have gained only over the last decade.

From the point of view of many-particle physics, two-electron atoms may appear to be rather simple systems; their Hamiltonian involves nothing more but the three mutual Coulomb interactions. However, this impression is misleading. Due to the increasing role which electron correlation plays for higher and higher excitation, correlated three-body Coulomb dynamics generates an extremely rich and complicated resonance spectrum. Hence, two electron atoms represent a prototype of a (few body) system strongly affected by electronic correlation.

From a general perspective the complexity of the atomic three-body problem can be related to the underlying chaotic classical dynamics, in particular if the system is highly excited in an energy regime where infinitely many resonances exist. In this respect, two electron atoms are of basic interest not only in atomic physics but also for the development of concepts of quantum chaos (see Berry (1983), Gutzwiller (1990)).

Hence, two-electron dynamics is an active field of research to the present days. The persistent interest in the two–electron atomic three-body system lies in the fact that it is, indeed, complex enough for rather involved theoretical concepts (which we will review), yet it is simple enough to have accurate numerical and experimental data at our disposal to test the approximation – schemes. In this respect the two–electron resonances play a similar role among few-body quantum systems as atomic physics as a whole played among all fields of physics.

A. Scope of this review and related work

After a historical overview we will concentrate on the ideas on which our understanding of two-electron resonances is mainly based today. We distinguish here approximate quantum concepts

such as adiabatic and group-theoretical methods on the one hand and semiclassical methods on the other. We will use the unique opportunity provided by a review to compare these two groups of concepts and to work out their mutual relations. We are, however, by far not able to cover all aspects of two–electron systems. We take responsibility for our selection which is and must be subjective. The selection has been guided by our aim to catch the most relevant historical developments and to provide a perspective for future research directions. Thereby, we emphasize qualitative aspects and we only briefly summarize the progress in experimental and numerical techniques (which undoubtedly have made possible the present status of our understanding) in the first part of the review.

A second general restriction refers to the regime of energy: We will only review the quasi discrete spectrum, i.e. true bound states and resonances. Processes at energies above the three-particle break-up threshold will not be discussed. For accounts of this energy regime we refer the reader, e.g., to the work by Rau (1984), Fano and Rau (1986), Byron and Joachim (1989), and Rost (1998).

On a more technical level, we restrict ourselves to the non-relativistic problem of an infinitely heavy nucleus and two electrons. All three particles are assumed to be point-like. This constitutes a well-defined and widely accepted framework to study two–electron dynamics and allows to compare different theoretical approaches. Only for deeply bound states and high nuclear charges these restrictions lead to inaccurate approximations. In such cases relativistic and QED effects as well as the mass polarization terms accounting for the finite mass of the nucleus must be included in the theoretical treatment for a direct comparison with high-precision experimental results. Such calculations have been carried out by Drake and coworkers (1988, 1993). Although we will mostly refer to a nucleus with variable charge Z and two electrons, we will almost exclusively discuss helium (Z=2) and H^- (Z=1). Work on atoms with two active electrons and a structured core has been recently reviewed by Aymar et al. (1996). A detailed account of atomic negative-ion resonances has been given by Buckman and Clark (1994). Atomic and other Coulombic three-body systems have been reviewed by Lin (1995) within the framework of the hyperspherical approach.

Only within the restrictions stated it is possible to achieve a reasonable, coherent presentation of the overwhelming number of articles in this field and of the remarkable progress made on the understanding of two–electron atoms.

We note that, more recently, the correlation problem of few bound electrons has also become important in the context of so-called "artificial atoms". Heitmann and Kotthaus (1993) provide an overview over such systems where the electrons are confined by an electrostatic potential in semiconductor heterostructures to form, e.g. "quantum dot helium".

B. Content of the review

The review is structured as follows: In a first, mostly historical, part we will cover early attempts to quantize helium (starting from the classical mechanics) by Bohr and leading contemporary physicists. Those attempts were ended by the early quantum mechanical proof that helium has a stable ground state. Here, also the first refined semiclassical approaches for highly excited 'planetary atoms' will be discussed. We will briefly review the progress in complementary, quantum variational methods for the computation of two-electron states including resonances. We will summarize numerical methods mainly used today and will introduce in some detail the complex rotation method which is one of the most powerful contemporary techniques to compute resonances. Simultaneously, we will describe the state of the art concerning relevant experiments.

In the second part we will focus on theoretical concepts to understand the regularity in the resonance spectrum of helium: With group theoretical methods it has been possible to identify and predict multiplets of resonances which share common properties. Resonances play here a similar role as particles in group theoretical approaches in elementary particle physics. A second successful concept is based on the introduction of adiabatic variables. In the so called "molecular approximation" (MA) the interelectronic distance is treated as adiabatic variable. This approach is very similar to the Born Oppenheimer (BO) approximation for molecules. In a second adiabatic

approach, the so called "hyperspherical approximation" (HS), the average volume of the atom characterized by the hyperspherical radius $\mathcal{R} = \sqrt{r_1^2 + r_2^2}$, is the adiabatic variable. Here, the r_i are the electron-nucleus vectors. Both adiabatic approximations reveal similar key features of the two-electron system which have not been recognized in other theories. Most notably the surprising regularity in the decay pattern of two-electron resonances, the so called propensity rules, becomes transparent in the adiabatic approximation. Finally, some interesting 'non-mainstream' concepts will be discussed, in particular the extension of the two-electron problem from three to arbitrary spatial dimension.

In the third part of the review we will come to the renaissance of semiclassical methods. They offer a viewpoint of two-electron dynamics complementary to those discussed in the previous two parts. The broad interest in understanding the influence of classical chaos on quantum systems has led to a variety of new semiclassical techniques applicable also to non–integrable dynamics. This development will be reviewed here and the connection to traditional WKB–like methods useful for classical integrable systems is established. Structures in the quantum spectrum can now directly be related to structures of the classical phase space dynamics.

The semiclassical methods allow for a completely new approach towards two–electron atoms. Instead of trying to solve the Schrödiger equation explicitly, the focus lies now on the study of the classical three–body Coulomb problem and its influence on spectral features of the corresponding quantum system. The classical dynamics differs quite considerably in different phase space regions and ranges from near integrable behavior to complete chaos. Especially the collinear subspaces (where all particle move along the same line) turn out to be of great importance for the quantum spectrum which can be justified on semiclassical grounds.

The systematics of Rydberg resonance series can qualitatively be described by a small number of characteristic short periodic orbits of the electron pair in the classical three–body system. On a more sophisticated level, periodic orbit theory provides a new way to analyze the spectral density of (resonant) states by Fourier transformation. By exploiting the classical information in detail, periodic orbit trace formulae are moreover able to resolve quantitatively individual resonances and bound states from the ground state across the various two body fragmentation thresholds. Rydberg series converging to these thresholds can be obtained from a semiclassical quantum defect theory with purely classical coupling parameters.

The review will end with a conclusion and a brief outlook on open questions. They mostly concern the behavior of two-electron resonances for increasing energy in the nearly unexplored energy regime close to the complete fragmentation threshold where all three particles can be free.

We have written this review in the memory of Dieter Wintgen and his pioneering contributions to "quantum chaos" in atomic physics. His distinct knowledge both in atomic physics and in modern nonlinear dynamics triggered the revival of modern semiclassical methods in two–electron atoms. With two of the authors being former PhD–students of Dieter and the third one being a collaborator on several projects we all three shared with him interest, insight and esteem not only for the intricacy of the three-body Coulomb problem.

II. HELIUM-LIKE SYSTEMS: FROM OLD TO MODERN QUANTUM THEORY

Two-electron atoms share the intriguing property that, despite of the seemingly simple form of the underlying Hamiltonian, their spectral features get exceedingly more complicate with increasing (double) excitation. For a nucleus with charge Z and infinite mass the non-relativistic Hamiltonian reads (atomic units (a.u.) used, $e = m_e = 1$):

$$H = \frac{\mathbf{p}_1^2 + \mathbf{p}_2^2}{2} - \frac{Z}{r_1} - \frac{Z}{r_2} + \frac{1}{r_{12}} \,. \tag{1}$$

Here r_k $(k = 1, 2)$ denote the electron-nucleus distances and the distance between the electrons is r_{12}, see Fig. 1. The non-integrability of this three-body-Coulomb problem gives rise to a remarkably rich behavior both with respect to its quantum features and to its classical dynamics.

The helium atom does not only represent a prototype of an atom with complex spectral structure; moreover, it played a key role in the development of quantum mechanics until the end of the twenties of this century. At that time, the observation that atomic spectra display discrete levels called for the invention of a quantum theory. Hence, atomic systems served as most prominent test objects during the development of quantum mechanics in those days. A satisfying calculation of the ground state energy as well as of excited states of helium turned out to pose unsolvable problems to the first theoretical approaches which were based on a Bohr–Sommerfeld like quantization of classical electron pair motion. This method is usually nowadays refered to as the "old quantum theory". Its failure for helium led to a serious crisis of this original quantum approach to atoms which was finally superseded by the "new quantum theory" formulated by Schrödinger (1926) and Heisenberg (1925). The latter formalism was first applied to the helium atom by Heisenberg (1926), taking into account wave mechanics, the electron spin and the Pauli principle.

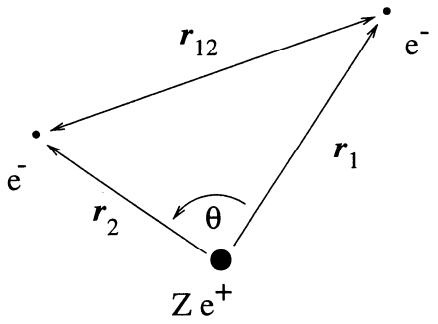

FIG. 1. The two electron atom and its basic coordinates.

The two complementary pictures — the (semi)classical approach to the helium spectrum on the one hand and the wave mechanical framework on the other hand — will guide us throughout the whole review and both (after significant refinement) complement one another in the present understanding of three-body Coulomb systems. We therefore describe in the following section in some detail the early semiclassical and quantum approaches to the helium atom, mainly refering to its ground state. In Sec. II.B we then turn to doubly excited states. We summarize their basic properties and review advanced quantum mechanical methods used today to take into account electron correlation effects. A corresponding novel approach in the spirit of the old quantum theory, a "new old quantum theory", i.e. a modern semiclassical theory, which adequately describes highly (doubly) excited two-electron atoms, is thoroughly presented in Sec. IV.

A. Early calculations of two-electron ground states

1. The failure of the "old quantum theory"

It is instructive, not only from a historical point of view, to reconsider the reasons for the failure of the "old quantum theory" when applied to helium. This approach, which is rather a collection of heuristic rules than a real theory, dates back to the early work on hydrogen by Bohr. Starting from his postulates on the quantization of the periodic Kepler motion, he presented a formula for the energy levels of hydrogen which showed remarkable agreement with measurements of that time. Hence, it was natural to apply the same approach to helium, the simplest atom with more than one electron. In Bohr's first model of helium (Bohr (1913)) the two electrons revolve, opposite to each other, on the same orbit about the nucleus as shown in Fig. 2(a). To obtain quantized energies he applied the condition

$$\oint p \, \mathrm{d}q = nh \,, \tag{2}$$

where (p, q) are generalized coordinates and momenta of the electron pair, h is Planck's constant and n is an integer. The result was discouraging: the ionization energy of the ground state was about 4 eV too high, compared with the then experimental value of 24.5 eV.

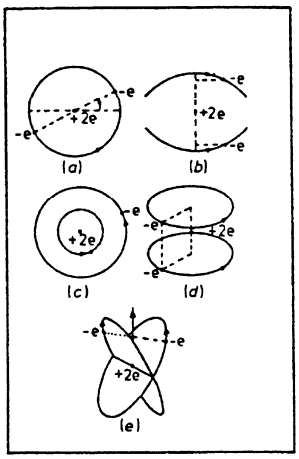

FIG. 2. Examples of periodic configurations of the electron pair in helium which served as classical models for the ground state: Bohr (1913) (a), Langmuir (1921) (b,d), Landé (1919) (c), Kemble (1921) and Kramers (1923) (e). (From Leopold and Percival (1980), see also van Vleck (1922).)

The following 10 years were characterized by a long sequence of attempts to find an appropriate classical periodic configuration for the electron pair motion in helium and to apply quantization conditions of the type of Eq. (2). A proper computation of the helium ground state energy became a challenge for leading theoretical physicists of that time, including Bohr, Born, Heisenberg, Kramers, Landé, Sommerfeld, and van Vleck, to name a few.

Some of the periodic orbits of paired electron dynamics proposed are depicted in Fig. 2. The corresponding ground state energies obtained are summarized in Tab. I. (For a thorough historical account of this long and tortuous chain of work see e.g. Mehra and Rechenberg (1982)). All models considered gave rather unsatisfactory results for the ground state of helium. For instance, in Langmuir's double circle model, Fig. 2(d), the ionization energy came out negative, i.e. the configuration was unstable. The approaches based on the models (a)–(d) in Fig. 2 were critically summarized by van Vleck (1922) who added another, no more successful three-dimensional model (not shown) which can be viewed as a hybrid of the configurations (b) and (d).

The failure of these early quantum approaches for helium was accompanied by a very unsatisfactory result obtained by Pauli (1922) in his PhD thesis on another three-body Coulomb system, namely the hydrogen molecule ion H_2^+: within the Born-Oppenheimer approximation this system is reduced to the (separable) problem of an electron moving in the field of two fixed Coulomb centers. By using a Bohr-Sommerfeld quantization condition he calculated the equilibrium internuclear distance to be nearly three times as large as the correct one ($\sim$ 2 a.u.). Moreover, he found the system to be metastable instead of being bound.

The approaches towards a description of the helium atom as presented above included all the principal problems of the "old quantum theory": the calculations were based only on a number of adhoc rules and postulates which were open for speculation. A rigorous theoretical framework, which could have been used as a guideline, was missing. Before presenting the principal shortcomings of this theory it is worth mentioning some of the common believes at that time. They led to the models for periodic electron pair motion shown in Fig. 2 and hindered a more rapid understanding of the helium problem. It was generally assumed that

(i) the ground state of helium is related to a single periodic orbit of the electron pair;

(ii) the electrons were supposed to move on symmetric orbits where their distance to the nucleus is equal at each instant;

(iii) orbits where the electrons hit the nucleus ("Pendelbahnen", Born (1925)) were excluded;

(iv) the quantum numbers in quantization conditions like Eq. (2) were supposed to be integers.

semiclassical			quantal/experimental		
year	method	$-E$	year	method	$-E$
1913	orbit Fig. 2(a), Bohr	3.06	1927	first order pert. Unsöld (1927)	2.75
1919	orbit Fig. 2(c), Landé (1919)		1927	molecular-like, Slater (1927)	2.895
1921	orbit Fig. 2(b), Langmuir (1921)	2.17	1927	variational, Kellner (1927)	2.873
1921	orbit Fig. 2(d), Langmuir (1921)	2.31	1928	variational, Hylleraas (1928)	2.895
1922	"hybrid orbit", van Vleck (1922)	2.765	1929	var., 38 param., Hylleraas (1929)	2.9037
1922	orbit Fig. 3, Heisenberg (1922)	2.904	1959	var., 38 param., Kinoshita (1959)	2.903722
1923	orbit Fig. 2(e), Kramers (1923)	2.762	1959	perimetric coord., Pekeris (1959)	2.903724376
1980	1. order pert., Leopold et al. (1980)	2.7410	1988	Hylleraas type basis,	2.903724377
1980	variational, Leopold et al. (1980)	2.8407		Drake (1988)	03415
1985	perturb. theory, Solov'ev (1985)	3.05	1995	perimetric coordiantes,	2.903724377
1991	as. stretch orbit, Ezra et al. (1991)	3.097		Bürgers et al. (1995)	034119589
1991	cycle expansion, Ezra et al. (1991)	2.932	1993	relativ. Drake (1993)	2.903700023
			1924	experimental, Lyman (1924)	2.9035
			1998	exp., Bergeson et al. (1998)	2.903693775

TABLE I. Semiclassical (left) and quantum mechanical as well as experimental (right) ground state energies (in a.u.) of the helium atom. The good agreement of the energy obtained from the Heisenberg-Sommerfeld model (see Fig. 3) must be considered as accidental (see text). The given result from Solov'ev's approach was extracted from Fig. 4 of Solov'ev (1985). The asymmetric stretch orbit (Ezra et al. (1991)) is shown in Fig. 20 (b), Sec. IV.B. The semiclassical cycle expansion is described in Sec. IV. The theoretical data do not include finite-mass-, relativistic and QED corrections, except the result by Drake (1993) which contains relativistic effects. The difference between the latter result and the latest experimental (Bergeson et al. (1998)) reflects QED effects. (Part of the data were taken from Leopold and Percival (1980), Table I.)

Two of the very few persons, who did not take these assumptions for granted, were Sommerfeld and his student Heisenberg. Although mainly being involved in problems of turbulence at that time, Heisenberg's interest in the helium problem was stimulated by Bohr in 1922. Sommerfeld and Heisenberg devised as a possible classical ground state configuration a model where both electrons move on two different Kepler ellipses of the same shape but oriented in opposite directions: one electron passes through the perihelion while the second is at its aphelion. Fig. 3 shows this configuration sketched by Heisenberg in a letter to Sommerfeld on the 28th of October 1922 (Heisenberg (1922)). In that letter, Heisenberg outlined a calculation of the ground state energy on the basis of this electron pair motion. As an important achievement from a todays point of view, he introduced, beside the quantization of the radial motion, a second quantization condition (Heisenberg (1922))

$$\oint p_\varphi \mathrm{d}\varphi = n_\varphi h \,, \tag{3}$$

for the motion of the angle φ between the major axises of the two orbits under the influence of the mutual electron interaction (see Fig. 3). Moreover, he introduced *half-integer* quantum numbers, e.g., $n_\varphi = 1/2$ for the ground state. Including the interaction in a perturbative manner, Heisenberg arrived at an ionization potential of 24.6 Volt, compared to the best experimental value of 24.5 Volt at that time! However, this approach was strongly criticized by Pauli and Bohr. They did not accept the concept of non-integer quantum numbers, but thought at that time that the classical laws of motion had to be modified in order to achieve agreement with experiment. Heisenberg, discouraged by Bohr, never published his calculations which may explain why the Heisenberg-Sommerfeld model, to the best of our knowledge, has never been mentioned in the atomic physics literature. Contrary to Bohr, Sommerfeld, encouraged by the results obtained by Heisenberg, wrote a paper (Sommerfeld (1923)), refering to Heisenberg's perturbative results where he suggested the underlying model of opposite electrons and half-integer quantum numbers as a possible classical ground state configuration.

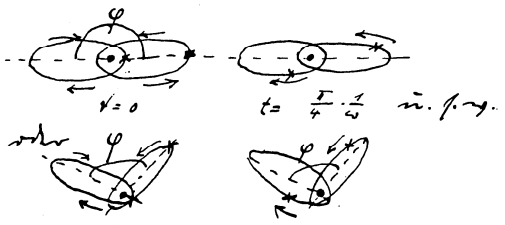

FIG. 3. Sketch of the periodic electron pair motion proposed by Heisenberg and Sommerfeld as a candidate for a classical ground state configuration of helium. The figure is copied from a letter of Heisenberg to Sommerfeld (Heisenberg (1922)). It was never published by Heisenberg.

Heisenberg, together with Born, went ahead and started to attack the more ambitious problem of excited states in helium. They considered different types of asymmetric electron configurations and developed an effective Hamiltonian based on a multipole expansion scheme for the potential of the outer electron in the combined field of the nucleus and the inner one. By that means they derived a Rydberg formula

$$H = \frac{(Z-1)^2}{(n+\delta)^2} \,, \tag{4}$$

where n is the principal quantum number of the outer electron. The quantum defect δ reflects non-Coulombic, short-ranged parts of the central potential and depends on the remaining quantum numbers and the configuration considered (Born and Heisenberg (1923)). However, the obtained energies of the excited states were unsatifying and led Heisenberg and Born to the conclusion that

"the result of our investigation is completely negative" (Born and Heisenberg (1923)).[1] For that reason Heisenberg also lost all confidence in his original ground state calculations. From then on he no longer followed the ideas of the "old quantum mechanics" but started to devise his "new" quantum theory based on conceptually new postulates.

The considerable agreement between the result of Heisenberg's first perturbative calculations of the helium ground state energy (see Tab. I) mentioned above and the experimental values must be considered as accidental: Heisenberg's perturbative scheme was not appropriate for the case of degenerate classical motion of the two electrons[2] and he did not know the role of Maslov indices (see Sec. IV.A) in quantization conditions. However, from a today's point of view the great virtue of the Heisenberg-Sommerfeld model for the helium ground state lies in two facts:

(i) the electrons move out of phase on perturbed Kepler ellipses opposite to each other. This type of classical motion comes rather close to the asymmetric stretch periodic orbit, a collinear out of phase motion of the electrons on opposite sides of the nucleus discussed in Sec. IV.B.2. This kind of electron pair motion turned out to be crucial for the structure of ground and symmetrically excited states (Ezra et al. (1991), Wintgen et al. (1992) as described in detail in Sec. IV.C and Sec. IV.D [3];

(ii) Heisenberg introduced ad-hoc half-integer quantum numbers, which simulate the effect of Maslov indices.

Due to these two facts the Heisenberg-Sommerfeld model and the related quantization condition (3) can be regarded as coming closest to a correct semiclassical description of the helium ground state compared to all other models employed in the "old quantum theory". We note, however, that in a rigrous semiclassical treatment the ground state is more precisely represented by a whole number of periodic orbits, as will be discussed in Secs. IV.A, IV.D.2.

The pessimistic mood in the early twenties concerning a semiclassical treatment of two-electron atoms, becomes apparent in a conclusion given by van Vleck (1922):

> "The conventional quantum theory of atomic structure does not appear to be able to account for the properties of even such a simple element as helium, and to escape from this dilemma some radical modification in the ordinary conceptions of the quantum theory or of the electron may be necessary."

The same negative point of view is expressed in the "Vorlesungen über Atommechanik" ("Lectures on the mechanics of the atom") by Born (1925). These conclusions, which mark the end of the "old quantum theory", address already the need of a completely different approach namely quantum wave mechanics. The essential shortcomings of the "old quantum theory" can be summarized as follows:

(i) the role of conjugate points along classical trajectories and their importance in a semiclassical approach to quantum states (via Maslov indices) were not properly accounted for;

(ii) the precise role of periodic orbits and their stability for systems with non-integrable or even chaotic classical dynamics was unknown.

The failure of the old methods on the one hand and the success of the "new quantum theory" on the other hand influenced the research for several decades. Still in 1941 the helium problem was

---

[1] Heisenberg's and Born's calculations of asymmetrically excited states are already based on schemes which later were re-considered by different authors (see e.g. Nikitin and Ostrovskii (1982), Belov and Khveshchenko (1985)).

[2] An appropriate semiclassical pertubative treatment was later performed by Solov'ev (1985) which will be briefly discussed in Sec. II.A.2.

[3] A periodic orbit of the Heisenberg-Sommerfeld type (Fig. 3) does not really exist as a solution of the classical Hamilton function, but only a quasiperiodic motion of that type, shown in Fig. 4.

considered as "raising unsolvable problems" (Bachelard (1941). We are not aware of any serious and successful attempts to attack the problem using a semiclassical framework until the 1980'ies.

For the separable H_2^+ problem only item (i) had to be accounted for. Strand and Reinhardt (1979) employed an Einstein-Brillouin-Keller (EBK) quantization procedure for H_2^+ (see Keller (1958) and Sec. IV.A.3.a for a short introduction), combined with a uniform treatment at potential barrier maxima. They obtained agreement with quantum results to within a fraction of a percent. As already pointed out by Einstein in 1917, such a quantization scheme being based on the existence of invariant tori cannot be applied to non-integrable systems (Einstein (1917)). It is therefore not an appropriate framework for the description of the helium atom.

Leopold and Percival (1980) and Solov'ev (1985) attacked the helium problem using improved variational and perturbative semiclassical methods, respectively. Although these approaches ignore item (ii) they represent important steps towards a rigorous semiclassical treatment of two-electron atoms. Thus, they will be briefly reviewed in the following subsection before we turn to quantum approaches for two electron atoms.

2. Semiclassical perturbative and variational approaches

a. *Planetary atoms*

More than 50 years after the first attempts to treat helium, Percival and coworkers were the first who re-considered the helium problem from a point of view of the "old quantum theory" (Leopold et al. (1980), Leopold and Percival (1980)). Percival had pointed out that in highly (doubly) excited atoms the electrons should carry features of classically moving particles. He thus coined these systems *planetary atoms* (Percival (1977)) due to their similarity with the gravitational three-body problem.[4] This picture is physically appealing, although one should keep in mind that a direct transfer of results from the celestical to the atomic three-body problem is generally not possible for two reasons: Firstly, in gravitational three-body systems the masses of the three bodies involved usually differ by orders of magnitude. This often allows for a perturbative treatment since the gravitational interaction depends on the masses (Arnold (1991)). Contrary, the mutual Coulomb interactions in two-electron atoms are of the same magnitude and perturbation theory is therefore not a priori applicable. Secondly, gravitational forces are always attractive, while the repulsive Coulomb interaction between the electrons usually leads to a destabilization of the two-electron atom. Depending on the initial conditions the *classical* two-electron atom generally autoionizes already after a few revolutions of the electrons around the nucleus. For a typical example of such a classical autoionizing configuration of equally excited electrons see Fig. 4. *Quantum mechanically*, the electrons cannot exchange an arbitrary amount of energy since the (remaining) He^+-ion has a minimum ground state energy. This allows for the existence of quantum bound states. Classically, the two–electron atom is an unbound system at all energies and the classical electrons escape on much faster time scales compared to quantum results.

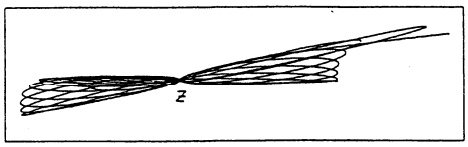

FIG. 4. Typical classical out-of-phase motion of the electron pair in helium obtained from a numerical integration of the full Hamilton equations of motion. The electrons evolve on perturbed Kepler ellipses around the nucleus until they autoionize after a few revolutions (from Richter (1991)).

---

[4]For a recent review on a celestical three-body problem, see for instance the work by Gutzwiller (1998) on the three-body system: moon, earth, sun.

b. Percival's treatment

Leopold and Percival (1980) could improve upon the results of the "old quantum theory" by introducing a variational semiclassical approach and, in particular, by pointing out the relevance of a correct inclusion of Maslov indices which lead to non-integer quantum numbers. They showed that the ideas of the "old quantum theory" were not intrinsically wrong. Moreover, they argued that semiclassical techniques should be powerful in dealing with highly doubly excited states where quantum approaches get more and more involved. Thereby, their work re-directed attention to semiclassical approaches for two-electron systems.

In a first paper, Leopold et al. (1980) used a first-order perturbative semiclassical scheme: without the electron – electron interaction the dynamics is integrable. The electrons evolve on tori and their motion can be described in terms of the respective action variables $\mathbf{I} = (I_r, I_\theta, I_\phi)$ where (r, θ, ϕ) represent the usual spherical coordinates. According to EBK quantization, the quantal states of the two unperturbed electrons ($k = 1, 2$) in helium correspond to those tori whose actions fulfill

$$I_{n_k} = n_k \hbar \; ; \quad I_{l_k} = \left(l_k + \frac{1}{2} \right) \hbar \; ; \quad I_{m_k} = m_k \hbar \tag{5}$$

with the corresponding quantum numbers n_k, l_k, m_k and actions $I_n = I_r + I_\theta + I_\phi; I_l = I_\theta + I_\phi$ and $I_m = I_\phi$, (see e.g. Goldstein (1980)).

First-order perturbative corrections to the independent electron energies were computed by taking the average $\langle 1/r_{12} \rangle$ over the six angle variables corresponding to the actions $I_{n_k}, I_{l_k}, I_{m_k}$. The resulting electron model obtained by Leopold et al. (1980) for the ground state is close to the configuration (e) in Fig. 2. The ionization potential is still about 4 eV lower than the experimental value (see Tab. I).

In a second paper, Leopold and Percival (1980) introduced a semiclassical variational treatment of the ground state and excited states of helium. To this end they introduced the ratio $z \equiv Z_{\text{eff}}/Z$ as a variational parameter, where Z_{eff} is a screened charge "seen" by each electron. The parameter z appears in the two-electron Hamiltonian as a scaling factor:

$$H_z = z^2 (T_1 + T_2) + z(U_1 + U_2) + \frac{z}{r_{12}} \; , \tag{6}$$

where T_k and U_k are the kinetic and potential energies of the independent electrons, respectively. Since the action integrals are invariant under this scaling, a variational principle can be formulated as follows (Leopold and Percival (1980)):

$$\frac{\partial}{\partial z} \left[\langle H_z \rangle - \sum_j \omega_j I_j \right] = \frac{\partial}{\partial z} \langle H_z \rangle \equiv 0 \; , \tag{7}$$

where the ω_j are the frequencies of the angle variables conjugate to the I_j. Employing the virial theorem $\langle U \rangle = -2\langle T \rangle = 2E_0 = -2(Z/2I_n)^2$ they found that $z_{\min} = 1 + \langle 1/r_{12} \rangle / (4E_0)$ minimizes the energy in Eq. (6). Using the expectation value of $\langle 1/r_{12} \rangle$ evaluated in their previous semiclassical pertubation theory Leopold and Percival found for the semiclassical variational ground state energy $E = -2.8407$a.u., compared to the exact ground state energy $E = -2.9037$a.u. (see, e.g. Tab. I).

c. Solov'ev's adiabatic perturbative treatment

In the following, we summarize a related semiclassical approach by Solov'ev (1985) which, to our belief, has not received the attention in the literature it deserves. Solov'ev argued that the unperturbed angular momentum eigenstates (or corresponding tori), used in the approach by Leopold et al. (1980) are inadequate as zero'th order reference states in a first order perturbative treatment

for the helium ground state and for symmetrically excited states. The occuring degeneracy in energy of these states, classically related to the commensurate periods of the motion along Kepler trajectories, has to be accounted for in an appropriate perturbation theory. Solov'ev starts from a configuration of two equivalent electrons moving out of phase on Kepler-like orbits similar to those shown in Fig. 4. As suitable coordinates he introduces the angle between the major axises of the two Kepler ellipses and the time difference τ between the passage of the first and second electron through the perihelion. He then establishes the separation of three time scales in the perturbative limit $1/Z \to 0$: the motion of an electron along the Kepler orbit is fast compared to the rate of change of τ. Its frequency is in turn by order $1/Z^{1/2}$ larger than that of the bending vibration of the perturbed Kepler ellipses.

By means of this separation of the frequency scales Solov'ev achieves an adiabatic decomposition of the full problem into one-dimensional effective potentials. Semiclassical quantization conditions for the resulting oscillatory motions gives rise to approximate quantum numbers. This method, which is in particular suited to describe highly symmetrically excited states, gives also a reasonable estimate $E \approx -3.05$a.u. for the helium ground state.

d. Discussion and summary of further approaches

It is by now well known (Richter and Wintgen (1990), Ezra et al. (1991), Wintgen et al. (1992)) that a considerable part of helium phase space is classically chaotic. Hence, an EBK approximation based on classical tori, as performed by Leopold et al. (1980), is in principle not adequate for a description of the full problem. The same is true for Solov'ev's treatment, applied to helium, since it assumes an effective decoupling of the different degrees of freedom.

We close this section by noting that the collinear configuration of two electrons being on opposite sides of the nucleus but moving symmetrically in phase ($r_1 = r_2$), known as the Wannier orbit, has been frequently proposed in the literature to be relevant for symmetrically doubly excited states (Miller (1972), Fano (1983), Harris et al. (1990), Sadeghpour (1991)). This type of motion and its importance for doubly excited states is critically reviewed in Sec. IV.

The periodic orbit originally proposed by Langmuir for the helium ground state (orbit (b) in Fig. 2) was reexamined by Dimitrijević and Grujić (1984) and Wesenberg et al. (1985). However, the latter authors overlooked that the Langmuir orbit is indeed stable (Richter and Wintgen (1990)), a fact which was not accounted for in their EBK type quantization. Finally, Klar (1986) re-considered the Langmuir double circle model (Fig. 2(d)) and showed that it is classically stable.

We will end the historical review of semiclassical approaches to two-electron atoms here in the mid eighties. We will return to semiclassical concepts in Sec. IV. There, we review more recent advances in the modern semiclassical theory for the non-integrable case and apply it to two-electron atoms taking into account that the corresponding classical system is chaotic. In particular, a generalized EBK scheme for excited states will be derived which leads in a natural way to the structure of perturbed Rydberg series and quantum defects. In the following we will summarize related pure quantum mechanical techniques to solve the Schrödinger equation directly.

3. Wavemechanical perturbative and variational results

It is physically elucidating to contrast the semiclassical perturbative and variational techniques with the corresponding early quantum mechanical methods. After Heisenberg's first application of the "new quantum theory" to the helium problem (Heisenberg (1926)), the quantum mechanically calculated ground state energy of helium was rapidly improved in a number of subsequent publications in the late twenties. The ground state energies obtained are summarized in Tab. I: Unsöld (1927), using first order quantum perturbation theory, obtained an energy with yet a rather large error. Slater (1927) treated helium by reducing it to the "molecular" problem of one electron in the presence of two fixed Coulomb centers of charge -e and Ze representing the nucleus and the

second electron. (Similar molecular models have been later employed to describe doubly excited states of two-electron atoms as will be reviewed in Secs. III.B.1, III.B.4.) Kellner (1927) was the first who used the Ritz variational principle and obtained already a rather precise ground state energy, $E = -2.895$ a.u. The above mentioned quantum results showed that the ground state of helium is indeed stable.

For variational calculations one chooses a physically plausible trial wavefunction in which a set of numerical parameters are left arbitrary, in helium typically screening constants and coefficients of polynomials involving the particle distances. These parameters are determined by finding the (absolute) minimum of the variational functional $E[\psi] = \langle\psi|H|\psi\rangle/\langle\psi|\psi\rangle$. As a most simple trial wavefunction for the ground state one may use

$$\psi(r_1, r_2, r_{12}) = e^{-(Z-\sigma)r_1}\ e^{-(Z-\sigma)r_2}\ , \tag{8}$$

where σ represents screening in a rather approximate way. The introduction of screening can equivalently be viewed as a change of the scale of the radial distances r_1, r_2. In helium, the variational principle for $E(\sigma)$ gives the minimum ground state energy for $\sigma = 5/16$ (Bethe and Salpeter (1977)). Hence, the energy is $E = -(Z - 5/16)^2$, i.e. $E = -2.85$ a.u. for helium. Given the simplicity ot the variational wavefunction, the error is small. In particular, it depends only weakly on Z. However, for the case of H^- a corresponding treatment does not yield a bounded ground state.

Historically, the first results by Kellner were improved through variational calculations performed by Hylleraas (1928,1929) who finally obtained $E = -2.9037$ a.u. using a trial wavefunction with 38 variational parameters. This method was again taken up with large-scale variational calculations by Kinoshita (1959), see Tab. I.

Quantum variational methods have proven most suitable to obtain precise results for the ground state or low-lying states of two-electron atoms and are superior to perturbative methods. As reported by Leopold et al. (1980), the same holds also for the perturbative and variational semi-classical treatment. The problem of quantum perturbation theory is related to the fact that the first-order result is too crude, at least for helium or H^-, while the calculation of second- and higher-order becomes already quite tedious.

First-order perturbation theory is already significantly improved upon by Hartree's method (see Bethe and Salpeter (1977)): The potential energy of the first electron is assumed to be the Coulomb potential of the nucleus plus the potential of the (unperturbed) charge distribution of the second electron and vice versa. Hence, the approximate effective potentials are furtheron related to central fields and the complete wavefunction is still of the form of a product of two single-particle wavefunctions. It turned out that Hartree-type wavefunctions are convenient and sufficient approximations to the ground state for many applications (where electron correlation effects need not be considered).

For a comprehensive and more detailed discussion of the different methods to obtain low-lying states of two-electron atoms, see e.g. Bethe and Salpeter (1977). A recent overview of ground state energies of general Coulombic three-body systems, including exotic two electron atoms, is for example given by Lin (1995). Most accurate ground state energies are nowadays achieved by diagonalization of the two-electron Hamiltonian matrix, Eq. (1), using large basis sets (see, e.g., Tab. I for the case of He). These methods, which had been introduced by Pekeris (1958, 1959) in his pioneering calculation of the helium ground state (see Tab. I), are presented in Sec. II.C.2.

B. Doubly-excited states: basic spectral structure and experimental developments

Since the famous experiment by Madden and Codling (1963) showed that doubly excited states of two electron atoms represent the paradigm for electron correlations in atomic systems, these states have attracted continuous interest of both theoreticians and experimentalists. We will approach these correlation effects stepwise: in this section we give a first preliminary overview of excited states of helium and H^-. Starting from singly excited states, we introduce doubly excited resonances on the traditional level of single particle quantum numbers. We then review in

Secs. II.B.2–II.B.4 progress in the understanding of doubly excited states from the experimental side by pointing out some of the key experiments which represent the variety of techniques used and the advances in the spectroscopic precision. Experimental results, as e.g. those by Madden and Codling, were incompatible with classification schemes based on the picture of two independent electrons and have triggered numerous theoretical work. In Secs. II.C.1 and II.C.2 we briefly review related computational advances and outline numerical techniques used at present for accurate quantum mechanical calculations of highly doubly excited states. Both the numerical and experimental facts provided here will act as starting and reference points for the physical pictures, classification schemes, and approximate methods which represent our understanding of correlation effects in doubly excited atoms up to day. They will be developed in detail in Secs. III and IV.

1. Basic spectral properties

The last section dealt exclusively with the computations of two-electron ground states, the main issue of early quantum theory. The question naturally arises how to characterize and calculate singly and doubly excited states. Certain exact symmetries of the three body Coulomb problem allow, at least partly, for a classification of these quantum states. The overall rotational symmetry, related to the conservation of the total angular momentum, $\mathbf{L}$, and its projection give rise to L and M as good quantum numbers. The quantum numbers of the total spin, S, and its z-component are linked to electron exchange $\mathbf{r}_1 \leftrightarrow \mathbf{r}_2$ through the antisymmetry of the total wavefunction. This leads to the distiction between singlet ($S=0$) and triplet ($S=1$) states. Furthermore, reflection symmetry infers that the wavefunctions of the electron pair are eigenfunctions of the parity operator P: $\mathbf{r}_1, \mathbf{r}_2 \rightarrow -\mathbf{r}_1, -\mathbf{r}_2$ with eigenvalue π describing even and odd states. These properties lead to the usual spectroscopic notation $^{2S+1}L^{\pi}$ (assuming LS-coupling).

It may appear appealing to treat, as a first step and similar to many-electron systems, two electron atoms in a mean field approach, possibly in a self-consistent way. As a result, the two electrons both evolve in an effective central potential which suggests their classification in terms of the usual hydrogenic principal quantum numbers, N, n, and angular momentum quantum numbers l_1, l_2. In such a conventional description, (excited) states, e.g. in helium, are organized in Rydberg series $(N, l_1; n \rightarrow \infty, l_2)$ which converge against one particle fragmentation thresholds, I_N, of the remaining $He^+(N)$-ion. Following the usual notation, N stands here for the principal quantum number of the inner electron. This model, being based on the individual quantum numbers, neglects electronic correlations completely but accounts at least qualitatively for certain general features of two-electron states.

In the following we will mainly use helium as an example to illustrate the general spectral characteristics emerging from the above model. The corresponding spectrum computed without approximations (see Fig. 9) will be discussed in Sec. II.C.3.

Roughly, the helium spectrum can be devided into three distinct parts: (i) the ground and singly excited bound states, (ii) doubly excited resonant states, and (iii) the continuum above the three-particle break-up threshold, 79 eV (or 2.9037 a.u.) above the ground state energy.

(i) For the discrete singly excited states ($N=1; n=1, \ldots, \infty$) singlet ($^1S, ^1P, ^1D, \ldots$) and triplet $^3S, ^3P, ^3D, \ldots$) configurations are usually distinguished. States of the two sub-systems with the same principal quantum numbers differ significantly in their quantum defects. Triplet levels lie noticeably higher in energy. This and the fact that singlet and triplet states do not combine optically with each other let early investigators think of two different kinds of helium, parahelium ($S=0$) and orthohelium ($S=1$) (see e.g. Bethe and Salpeter (1977)). Singly excited states converge to the first ionization threshold, I_1, which lies at $-Z^2/2$ a.u. This corresponds to an ionization energy of ~ 24.58 eV for helium.

(ii) Helium doubly excited states form a doubly infinite (in N and n) sequence of levels lying above the first ionization threshold. Their (perturbed) Rydberg series converge to ionization thresholds, I_N, at energies $-Z^2/(2N^2)$ (in a.u.) which are characterized by the remaining inner electron to be in an excited state N. Doubly excited states are therefore embedded into the continua above the fragmentation thresholds of energetically lower Rydberg series of singly or other doubly

excited states. Hence they form resonances which can decay by autoionization due to the electron-electron interaction via the coupling to the continua. This distinguishes them qualitatively from the stable singly excited states where the inner electron, being in its ground state, cannot further transfer energy to ionize the outer one. This picture of singly and doubly excited states and their difference is purely quantum mechanical and does not exist in classical two-electron atoms, see Sec. IV.B.

(iii) the three-body dynamics in the energy regime above the three-particle break-up threshold $E = 0$ has been probed by photo double ionization and collision experiments. Theoretical descriptions of electron impact ionization, often called $(e, 2e)$ reactions, are reviewed, e.g. by Byron and Joachim (1989). In particular the region close to the threshold has been studied extensively. In this region the energy dependence of the total cross section for three–particle breakup is strongly influenced by electron–electron correlation leading to the famous Wannier threshold law (Wannier (1953)). The physics in this energy region is somewhat beyond the scope of this review, see Rost (1998) for an extensive discussion.

As the probably most simple model to mimic the spectral structure of helium one may think of two independent electrons. The inner electron is bound in a state with principle quantum number N and energy $E_N = -Z^2/(2N^2)$, the outer electron is in a hydrogen-like orbital with energy $E_n = -(Z-1)^2/(2n^2)$ and $n \geq N$ assuming a screening of the nuclear charge. The total energy is simply the sum of the one-particle energies. The energy level diagram of singly and doubly excited states computed on the basis of this scheme is displayed in Fig. 5. The simple model reproduces, at least qualitatively, some of the most prominent spectral features. Fig. 5 shows one Rydberg series converging to each ionization threshold of the remaining $He^+(N)$ ion. Each Rydberg series shown represents a whole number of series which are energetically degenerate since the model is based on hydrogenic angular momentum quantum numbers l_1, l_2 and neglects the electron-electron interaction. For example, for ${}^1S^e$ states there are N different Rydberg series converging to I_N. Moreover, Fig. 5 indicates that the low-lying Rydberg series do not overlap. In the simple model neighboring Rydberg series begin to overlap for $N = 9$, compared to $N = 4$ in the real helium atom, see Fig. 9.

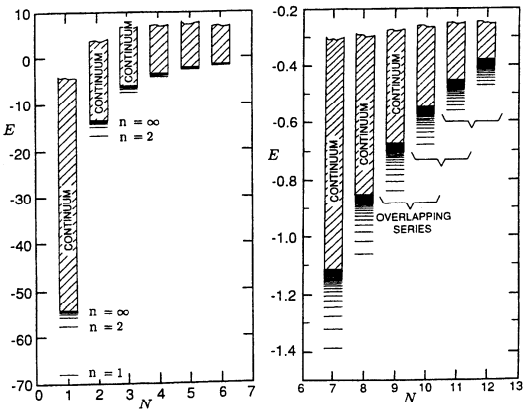

FIG. 5. Term scheme of the helium atom from an independent particle model where the outer electron (principle quantum number n) moves in the field of the charge $Z - 1$ screened by the inner one which is in a state with principle quantum number N (adapted from Blümel and Reinhardt (1992).)

2. Early experimental observation of electronic correlations

After the ground state and singly excited states of two- and more-electron atoms were fairly well understood, certainly the theory did not expect any surprises from doubly excited states.

Apart from the regime close to the double ionization threshold, where an increasing number of Rydberg series starts to overlap and to interact, the spectral structure in the energy regime of isolated, non-overlapping Rydberg series in Fig. 5 may suggest that the related doubly excited states behave similar to singly excited states. Hence, an improvement of the simple independent particle model introduced above along the lines of a Hartree-Fock description, which had proven very successful for multi-electron atoms, was appealing. Such an approach implies that two-electron states are more or less products of single particle configurations. Given the helium ground state as a dominant $1s^2$ configuration, the lowest doubly excited states were therefore expected to be roughly $2s^2, 2s2p, 2snp$ states and so on.

Although the existence of doubly excited resonant states has been known for about 60 years, the primary role of correlations in forming collective states of the electron pair became suddenly evident with the key experiment by Madden and Codling in 1963. It unveiled dramatic deviations from the expectations of Hartree-Fock-like models. Using synchrotron radiation and recording the absorption spectrum of helium they could observe a series of $^1P^o$ states converging to the $N = 2$ ionization threshold. $^1P^o$ states are strongly favoured due to dipol selection rules when probing the helium ground state $^1S^e$ by photo excitation. The original photoabsorption spectrum is reproduced in Fig. 6. Within the framework of the independent particle picture three series were expected: $2snp$, $2pns$ and $2pnd$. Instead, Madden and Codling observed one dominant, intense series. A second very faint series could only be guessed and the third series was not detected. The difference in the intensities was a clear indication that the electron-electron interaction leads to so far unknown selection or propensity rules for radiative excitation. Moreover, the position of the resonances in the strong and weak series did not match any of the expected combinations $2s2p, 2p2s$.

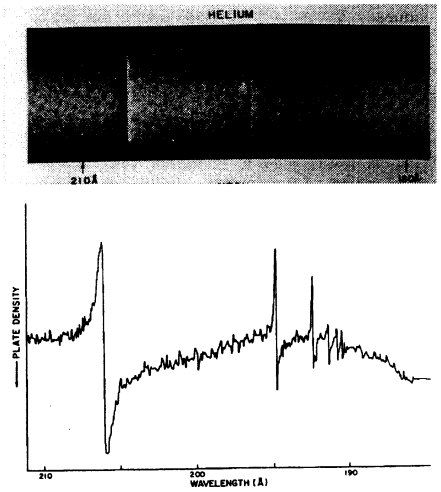

FIG. 6. Early photoabsorption spectrum of helium (in two different presentations) measured by Madden and Codling (1963) in the energy regime below the $He^+(N=2)$ limit (corresponding to 59-65 eV-photons). The spectrum is dominated by one intense series of doubly excited resonant states. A second very weak series is hardly visible.

In an early theoretical interpretation of the exerimental findings Cooper et al. (1963) proposed as explanation a strong configuration mixing of the $^1P^o(2l_1 2l_2)$ states due to their perfect degeneracy in the limit of vanishing electron interaction. For reasons of exchange symmetry they suggested to use combinations of the sum $(+)$ and the difference $(-)$ of the atomic product wavefunctions of the $2snp$ and $2pns$ states as an appropriate basis. Corresponding calculations showed that these linear combinations indeed shift the resonance positions towards the experimentally observed ones. This led to the original classification of these doubly excited states as $'+'$ and $'-'$ series. The $'+'$ labels were assigned to states of the intense series. The observed line widths, a measure of the

autoionization rates, were reflected in the photoionization yield: intense lines exhibit large widths.

It took more than twenty years before the early description of doubly excited atomic states could be backed by a deeper and consistent understanding of the astonishing symmetries of two electron atoms. The corresponding theoretical approaches will be discussed in Sec. III.

3. Overview over modern spectroscopical techniques

Until about ten years ago the existing experimental data for doubly excited two-electron atoms lagged considerably behind theoretical results. This was mainly due to the fact that appropriate monochromatic light sources, suitable for high-resolution spectroscopy, were missing which could bridge the rather large energy gap between the ground state and doubly excited states: in the case of helium the doubly excited $^1P^0$ resonances are lying approximately between 60 eV and 79 eV above the ground state. This problem was tackled experimentally along two main routes, either by direct double excitation using synchrotron radiation, see Sec. II.B.3.a, or by studying doubly-excited alkaline earth atoms with conventional dye lasers operating in the optical regime, see Sec. II.B.3.b. Further experimental efforts, partly based on non-photonic double excitation, will be summarized in Sec. II.B.4.

a. Double excitation of helium using synchrotron radiation

Until 1990 reliable measurements of resonant states in helium were limited to the $N = 2$ Rydberg series (Madden and Codling (1963), Morgan and Ederer (1984), Kossmann et al. (1988)) and to the lowest states of higher Rydberg series (Woodruff and Samson (1984), Kossmann et al. (1988), Zubek et al. (1989)). More recently the development of high-resolution monochromators for synchrotron radiation led to a striking improvement in precision of photo cross sections which will be discussed below. Complementary experiments based on emission spectroscopy even achieved the observation of *partial* decay widths. Due to the dipole selection rule for the single photon process from the $^1S^e$ ground state only final doubly excited states of $^1P^0$ symmetry can be detected with this technique. This restriction, however, facilitates the identification of the resonances.

Single photon double excitation with synchrotron radiation, combined with high-resolution monochromators as those at BESSY, Berlin (Domke et al. (1991,1992,1995,1996)) and even further improved monochromators at the "Advanced Light Source" in Berkley (Schulz et al. (1996)) made it possible to unveal for the first time several additional Rydberg series. Moreover, each Rydberg series could be followed up to higher excited states of the outer electron. In a first experimental breakthrough, Domke et al. (1992) could resolve for the first time the third Rydberg series, $2pnd$, below the $N = 2$ ionization threshold. This series was up to that time "missing" since the observation of the famous principal $(sp, 2n+)$ and secondary $(sp, 2n-)$ resonances by Madden and Codling (1963) (denoted in the original classification scheme).

Latest experiments on doubly excited helium using synchrotron radiation of the Advanced Light Source with further increased photon flux and a resolution of 1 meV (Schulz et al. (1996)) were able to measure all the three series converging to the $N = 2$ threshold with improved precision. The spectra of the three series of autoionizing states are shown in Fig. 7 which illustrates the experimental progress since the early measurements by Madden and Codling, Fig. 6. The most intense (principal, or $'+'$) series appears in panel (a) as a pure sequence of pronounced Beutler-Fano profiles (Fano (1961)). It is resolved up to $n=26$. The first secondary ($'-'$) series in Fig. 7(b), which is visible in panel (a) as a sequence of tiny peaks, is roughly 100 times less intense than the $'+'$ series. It is convenient to label the different series converging to the same threshold by the (Stark-type) quantum numbers K. This assignment, which is due to Herrick (1983), will not be justifed at this stage. (See Sec. III.C for details including the introduction of a further quantum number T.) The differences in the intensities observed will be explained in Sec. III.B.3.a, see also Fig. 13. The three observed series in Fig. 7(a)–(c) can then be classified according to $(N, K)_n$ with $K = 0, 1, -1$, respectively.

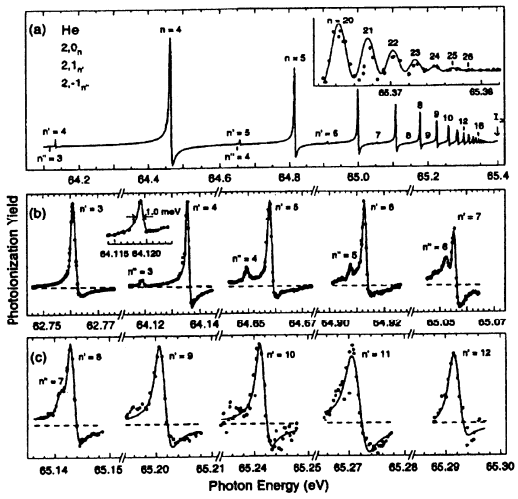

FIG. 7. Observed spectra of autoionizing resonances in helium after double excitation through synchrotron radiation. Panel (a) shows an overview spectrum of all three $^1P^o$ resonance series below the $N = 2$ ionization threshold, I_2, with the dominant, classic Beutler-Fano profiles of the intense principal series discovered by Madden and Codling (1963). Panels (b) and (c) depict the secondary series $(N, K)_n = (2, 1)_{n'}$ and $(2, -1)_{n''}$, see Sec. III.C for the notation. (From Schulz et al. (1996).)

Besides the detailed investigation of doubly excited states below the I_2 threshold Domke et al. (1996) could observe members of *all* strongest (principal) Rydberg series series up to the $N = 9$ ionization threshold as well as further secondary series with relatively weak intensities. The interesting regime of strongly overlapping and interacting Rydberg series is thus accessible today.

Fig. 8 shows as an example highly doubly excited resonances of helium in an energy region below the $N = 5$ threshold in order to illustrate the recent experimental achievements and to compare them with theoretical results. The dots mark measured cross sections (Domke et al. (1995)). The full line is *not* a fit but the numerical result from a complex rotation calculation (see Sec. II.C.2) by Wintgen (1994). The pronounced resonances are related to the principal (K=3 in Herrick's classification) Rydberg series with $(N = 5, n = 5, \ldots, 14)$. The tiny dips visible in between the pronounced states $n = 5, \ldots, 9$ reflect the lowest states of a secondary Rydberg series $(N, K)_n = (5, 1)_n$. Similar agreement between theory and experiment has been obtained by hyperspherical close coupling calculations (Tang and Shimamura (1994)).

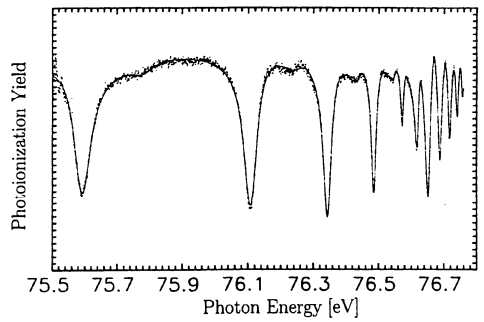

FIG. 8. Double excitation resonances $^1P^o$ of He in an energy regime below the $N = 5$ threshold. The dots denote experimental photo absorption cross sections from the helium grond state using synchrotron radiation (Domke et al. (1996)). The full line shows the theoretical prediction based on complex rotation (see Sec. II.C.2) by Wintgen (1994). The strong dips represent the principal Rydberg series with approximate quantum numbers $n = 5, \ldots, 14$ of the outer electron. The irregular structure at ~ 76.7 eV is due to interference of the $N = 5$ series with the lowest state in the $N = 6$ series.

The high-resolution experiments by Schulz et al. (1996) allowed furthermore for the first time to observe the secondary series $(N,K)_n = (3,2)_n$ and $(3,0)_n$. Recent comprehensive accounts of these fascinating experimental developments can be e.g. found in Domke et al. (1996) and Rost et al. (1997). They also include detailed comparisons between experiment and theory with respect to quantum defects, resonance widths, oscillator strengths and shape parameters.

The photoabsorption experiments described above have been recently complemented by *electron emission* measurements of *partial* photoionization cross sections and photoelectron angular distributions of helium in the energy region up to the I_5 threshold (Menzel et al. (1995, 1996)). These experiments also use the Advanced Light Source to study the resonant photoionization process $\mathrm{He}(1s^2) + h\nu \rightarrow \mathrm{He}^*(N,K_n) \rightarrow \mathrm{He}^+(j) + e^-$. The outgoing electrons are detected angular resolved which permits the determination of the corresponding photoelectron angular distribution parameters β_j (Menzel et al. (1995)). The energy dependence of the related partial cross section σ_j is obtained by simultaneously scanning the incident photon energy and the pass energy of the analyzers of the emitted electron. A thorough investigation of partial cross sections and angular distributions is given by Menzel et al. (1996) for a large variety of Rydberg series up to the I_5 threshold, including for instance the weak intensity series $(N,K)_n = (N,N-4)_n$. The measured spectra for σ_j and β_j are in considerable agreement with numerical results by Tang and Shimamura (1994) based on the hyperspherical close-coupling method (see Sec. II.C.1). Recently, the detection of long living neutral particles, which are generated through the decay of doubly excited states, was introduced (Sokell etal. (1996)). In this setup the observed strength of different series of doubly excited states is very different from the conventional findings by detecting charged fragments following the experiments by Madden Codling (1963).

b. Laser double excitation of alkaline earth atoms

Compared to helium, alkaline earth atoms exhibit the experimenal advantage having a total two-electron excitation energy of about 15 eV which can be reached by resonant multiphoton laser excitation, see Morita and Suzuki (1988) for calcium, Bloomfield et al. (1984), Camus et al. (1989), Eichmann et al. (1989, 1990), Roussel et al. (1990) and Jones and Gallagher (1990) for barium, and Eichmann et al. (1992), Hogervorst (1993) and Seng et al. (1995) in the case of strontium. Rydberg states in alkaline earth atoms are also thoroughly discussed in the book by Gallagher (1994). Compared to direct double excitation from the ground state by synchrotron excitation, the use of several lasers has the advantage that not only $^1P^o$ states but a variety of doubly excited states with different total angular momenta is accessible in a controlled way. While these facts render them favorite for experimental investigations, alkaline earth atoms differ from the pure three-body problem which is preferentially considered in theory. The difference arises from the spatial extension of the core which adds a non-Coulombic potential term and removes the l-degeneracy of valence electron states which penetrate the core. The corresponding non-degenerate single-electron configurations are therefore much less affected by the electron-electron interaction which renders the observation of related electron correlation effects rather difficult. Hence, elaborated multistep laser excitation techniques have been developed (Camus et al. (1989), Jones and Gallagher (1990), Eichmann et al. (1990)) involving up to six lasers, which allow for the controlled excitation of the two valence electrons into states with non-zero angular momenta and reduced overlap with the inner core. In particular, excited states with angular momenta $l > 3$ do not penetrate the core and should behave similar to helium. If the electrons are in addition asymmetrically excited, $\langle r_1 \rangle < \langle r_2 \rangle$, they are supposed to move in different regions of space, and these systems can be considered as experimental realizations of *planetary atoms* (Roussel et al. (1990), Eichmann et al. (1992), Seng et al. (1995)).

In two impressive experiments by the groups of Camus (Camus et al. (1989)) and Sandner (Eichmann et al. (1990)), the polarization of the inner electronic wavefunction by the outer electron could be observed. This can be interpreted as a correlation effect. Sandner and coworkers, for instance, used six lasers to bring the first valence electron to a highly excited nd-state ($60 \leq n \leq 100$) and then excited the second valence electron to $l = 4$ states with $N = 6$ using isolated core excitation.

The non-penetrating inner wavefunction is hydrogen-like and can therefore be polarized by the outer electron. This experiment, and in a similar way the experiment by Camus et al. (1989), showed a Stark-like energy splitting of the inner electronic states due to the electric field of the slow outer electron which can be assumed to be "frozen".

As will be discussed in Secs. III.B.4, IV.C.2.a, IV.D.1 similar highly correlated states have been predicted theoretically for helium by Richter and Wintgen (1990a, 1991). However, in those "frozen planet" states the outer electron is truely (dynamically) localized in space.

4. Further methods for double excitation

We briefly review further important experimental approaches here. They probably cannot compete with respect to precision with the high-resolution measurements using synchrotron radiation; however, they represent smart and elaborate alternative techniques to observe doubly excited states and are in particular suitable for other two-electron systems than helium.

a. Laser excitation of H^-

In a seminal experiment, Bryant and coworkers could reveal several series of doubly excited resonant states in a relativistic H^- beam (Harris et al. (1990)). The spectrum of the hydrogen negative ion, H^-, exhibits a similar overall structure as helium. However, the border between discrete and continuum levels, known as the detachment threshold in the case of H^-, is very low and lies at 0.75 eV. Furthermore, the series in H^- have dipole character at the ionisation thresholds steming from the long range potential formed by the polarized inner H subsystem which is in contrast to the typical Rydberg series found for all other two-electron atoms. Hence, only the H^- ground state is bound. In the experiments by Harris et al. H^- atoms, provided by a linear accelerator and moving with relativistic velocities, intercept a laser beam of laboratory photon energy E_0 at a variable angle α. The experiment made use of the relativistic Doppler shift leading to an angle dependent barycentric photon energy $E = E_0(1 + \beta\cos\alpha)/(1 - \beta^2)^{1/2}$ with $\beta = v/c$. This powerful tool allowed for a tuning of E over a large range from approximately 0.03 eV up to 21 eV covering the whole interesting regime of resonances in H^-, in particular high-lying states at energies of 10-14 eV. The work by Harris et al. (1990) contains a comprehensive account of measured resonance series converging to the $N = 4$ up to the $N = 8$ thresholds and gives a comparison with numerical results [5]. For a review with emphasis on atomic negative ion resonances we refer the reader for instance to the work by Buckman and Clark (1994).

b. Dielectronic recombination

Kilgus et al. (1990) made use of the time-reversed auto-ionization process (followed by the emission of a photon), namely *dielectronic recombination* of a positive ion and a free electron for the formation of doubly excited states. These experiments were performed in a heavy ion storage ring generating stored and cooled O^{7+} ions and an intense electron beam provided by an electron cooling device. The experiment allowed the observation of low lying doubly excited resonant states of the fairly exotic two-electron system $(O^{6+})^{**}$.

---

[5] The assignment by Harris et al. (1990) for the so-called + and − intrashell Feshbach resonances with symmetric and asymmetric stretch motion is incompatible with the present understanding of these resonances.

c. Electron impact experiments

By contrast to the rapid advances in photo-excitation spectroscopy of highly excited states, electron-impact measurements could reveal mainly doubly excited resonances below the $N = 2$ ionization limit in helium (Hicks and Comer (1975), van den Brink et al. (1989)) and, more recently, below the $N = 3$ threshold (Brotton et al. (1997)). Experiments by Buckmann et al. (1983, 1987) have reached doubly excited states up to $N = 9$, but with very limited energy resolution. However, the advantage of electron-impact spectroscopy lies in the fact that it allows for the observation of both the optically allowed *and* forbidden transitions. Hence, this method makes it possible to unveal the full spectral richness. For instance, in the experiment by Brotton et al. eleven states which are optically not accessible have been observed and relative cross sections have been measured.

A most recent alternative technique for double excitation was presented by Moretto-Capelle et al. (1997), who could measure double excitation cross sections of low-lying states in helium produced in collisions with 100-keV protons. The experimental information was extracted from electron emission spectra. In related experiments double excitation had been achieved previously by double electron capture processes in slow collisions of highly charged ions with atoms, see, e.g. Stolterfoth et al. (1986), Mack et al. (1989), and Sakaue et al. (1990).

Concluding, there exists a variety of different elaborated experimental techniques today to study properties of two-electron atoms. At present, spectra using synchrotron radiation exhibit the highest resolution which reach the accuracy of state-of-the-art numerical calculations reviewed in the following section.

C. Doubly-excited states: numerical approaches and spectra

1. Brief review of modern numerical methods

A huge number of numerical investigations have improved our understanding of electron–electron correlations in two-electron atoms. In recent years it has become possible to calculate cross sections of two-electron processes with a number of different numerical methods. Here, we can only mention a few of them which may be considered as representative examples for techniques currently in use. We refer the reader for further accounts on computational techniques to previous reviews on related topics, as for instance those by Fano (1983), Fano and Rau (1986), Lin (1986, 1995), Buckman and Clark (1994), Aymar et al. (1996).

a. Feshbach projection formalism

Among earlier methods which have been applied to obtain the resonance parameters (energies, widths, etc.) numerically, we mention those by Bathia and Temkin (1975, 1984) based on a *Feshbach projection formalism.* More recently, Martin and coworkers proposed an $\mathcal{L}^2$-method combined with the Feshbach formalism which takes into account interchannel coupling in an algebraic way (see Cortés and Martin (1993) for H^-, Sánchez and Martin (1993) for He).

b. Hyperspherical approaches

One of the most widely used theoretical approaches in the study of doubly excited states during the last three decades makes use of *hyperspherical coordinates* for the solution of the three particle Schrödinger equation (for reviews see e.g. Fano (1983), Starace (1988), Lin (1995)). The application of the adiabatic hyperspherical approach is twofold:

Starting with the work by Macek (1968) hyperspherical coordinates have built the framework for the (qualitative) understanding and classification (Lin (1984,1986)) of resonant states as will be reviewed in Sec. III.D.

Second, the hyperspherical treatment has been used for numerical computations of adiabatic energy curves, wavefunctions and transition amplitudes (see e.g. Park et al. (1991), Liu et. al (1991), Sadeghpour and Greene (1990), Sadeghpour (1991)) of doubly excited resonances. More recently, accurate numerical algorithms based on hyperspherical coordinates have been developed which will be sketched here briefly. The *hyperspherical close-coupling method* (HSCC) (Tang et al. (1992, 1992a), Tang and Shimamura (1994), Lin (1995)) circumvents typical difficulties which occur in the solution of coupled differential equations in an expansion through adiabatic basis functions. Problems can occur for instance at parameters where nonadiabatic couplings are strong. In the HSCC method, one first partitions the hyperradius $\mathcal{R} = \sqrt{r_1^2 + r_2^2}$ in small sectors. Within each sector one constructs a diabatic basis. At the boundary between two neighboring sectors a local basis transformation is calculated which propagates (the logarithmic derivative of) the wavefunctions along $\mathcal{R}$. After propagating the solutions to the asymptotic region, they are matched to asymptotic wavefunctions in terms of the usual independent-electron coordinates. For a detailed account of this method see e.g. the recent review by Lin (1995). The HSCC method has become one of the most powerful technique to obtain ab-initio results for cross sections. It allows to compute partial cross sections with high precision (about 1%) and has been recently extended to provide also angular distribution parameters and differential cross sections (Menzel et al. (1995, 1996)), as they are obtained in the electron emission experiments on helium described in Sec. II.B.3.a. We note that, besides the HSCC technique, conventional close-coupling methods have also been employed (Oza (1986)) to compute numerical cross sections for two-electron phenomena.

c. R-matrix method

A further important method, which is among the most widely used numerical techniques for atomic resonances and collision processes, is the *R-matrix method.* Cross sections are computed on a mesh of energies E and the resonance parameters such as resonance position, width and the shape parameter in photoabsorption are usually extracted subsequently by a fit. Here, we skip a more detailed account of the method in view of the recent review by Aymar et al. (1996) which includes a thorough description of the eigenchannel R-matrix method. The R-matrix approach has been applied to doubly excited resonances for instance by Hayes and Scott (1988), Hamacher and Hinze (1989), Sadeghpour et al. (1992), and Cheng-Pan et al. (1994), to name only a few.

d. Stabilization method

Different methods exist to compute resonance energies directly from diagonalizing the two-electron Hamiltonian using large $\mathcal{L}^2$ basis sets. Besides the *complex rotation technique* (see Sec. II.C.2) the *stabilization method* has been employed. The idea of this method is to repeatedly diagonalize the Hamiltonian in the basis sets of increasing extension (e.g. in a box of increasing size) from what is believed to cover the spatial region where resonance wavefunctions are located. Energies of (localized) resonant states can be extracted since they appear as rather unaffected with respect to changes of the box size. In addition, resonance widths can be extracted from the arising level diagrams. Müller et al. (1994), for instance, applied the stabilization method of Mandelshtam et al. (1993) to calculate $^1S^e$ states of helium.

e. Multi-configurational Hartree–Fock method

The *multi-configurational Hartree–Fock method* was extended to autoionizing states by Froese–Fischer and Indrees (1990). Nicolaides and coworkers have proposed a related method which they coined "state-specific solution of the complex-eigenvalue Schrödinger equation". They developed this approach to study in particular resonant states of negative ions like H^- ((Chrysos et al. (1990)) and He^- (Chrysos et al. (1992)). The idea is to decompose a resonance wavefunction into a

localized part and a contribution from continuum components. The former are represented by multi-configurational Hartree-Fock orbitals; the latter, the channel-dependent so-called "Gamow orbitals", are made square integrable by complexifying their radial parts (Chrysos et al. (1992) and references therein). This method allows for a calculation of partial decay widths, in contrast to the complex rotation method. The latter has turned out to be an efficient mean to compute resonance positions and widths and will be presented in the following. We will do this in some detail, since most of the numerical ab-initio results for two-electron atoms, which will be used throughout this work as reference data for approximate schemes, were obtained by using complex scaling.

2. Calculation by complex rotation

The complex rotation method (Balslev and Combes (1971), Junker (1982), Reinhardt (1982), Ho (1983)) allows to use elaborated bound state methods to calculate resonant energies, widths, cross sections, and wavefunctions of autoionizing states. Meanwhile it has become a standard approach to various atomic systems with states coupled to a continuum. Complex rotation has been applied to the hydrogen atom in a static (Reinhardt (1982)) and in an oscillatory (Buchleitner et al. (1994)) electric field and to the diamagnetic hydrogen atom (Main and Wunner (1992)), to name a few examples besides two-electron atoms.

Here, we briefly sketch the main physical ideas of complex scaling, for accounts of the mathematical backround see, e.g. Balslev and Combes (1971) and Ho (1983). Complex rotation is achieved by complex scaling of the radial coordinates and momenta according to $r \longrightarrow r\exp(\mathrm{i}\theta)$; $p \longrightarrow p\exp(-\mathrm{i}\theta)$ (Ho (1983)). The corresponding rotated Hamiltonian $H(\theta) = R(\theta)HR(-\theta)$ is then characterized by the following properties (Reinhardt (1982)):

(i) bound state energies of $H(\theta)$ are independent of θ, i.e. they are the same as those of H.

(ii) The (two-particle) fragmentation thresholds are independent of θ. The segments of the continua E_{frag} related to these thresholds are rotated by an angle 2θ into the lower energy half plane (around the branching points).

(iii) $H(\theta)$ is no longer hermitian. Complex eigenvalues $E_{n\theta}$ of $H(\theta)$, which appear in the lower half plane for rotations such that $0 \geq \arg(E_{n\theta} - E_{\mathrm{frag}}) \geq -2\theta$, can be associated with the resonance energies of H.

(iv) The non-integrable continuum wavefunctions are rotated in Hilbert space to square integrable eigenfunctions $|n_\theta\rangle$ of $H(\theta)$.

Numerical complex rotation procedures make use of the appealing property (iii). Resonance positions and widths are obtained from the complex eigenvalues

$$E_{n\theta} = E_n - \mathrm{i}\Gamma_n/2 \tag{9}$$

after diagonalizing $H(\theta)$ in a basis set of real square integrable wavefunctions. This means that continuum properties are represented by a discrete basis set.

This method was introduced by Doolen et al. (1974) for doubly excited two-electron atoms and then extensively employed by Ho and coworkers, see e.g. Ho and Callaway (1985), Ho (1986), Ho (1989) for helium, Ho (1990,1992) for H^-, and Ho and Bhatia (1992) for $^3P^e$ states in Ps^-.

While Ho has used a Hylleraas type basis set, Wintgen and coworkers have applied the complex rotation method within a Sturmian basis set using perimetric coordinates (James and Coolidge (1937), Pekeris (1958)); for details see Richter and Wintgen (1991), Richter et al. (1992), Bürgers et al. (1995). The perimetric coordinates, together with the Sturmian type basis set, have the great advantage that they lead to a matrix representation of the Hamiltonian in *algebraic* form. The matrix is moreover sparse and of banded structure which opens up the way for efficient

computations. In order to show the accuracy of this method the non-relativistic helium ground state has for instance been computed with a precision of up to 18 significant digits (see Tab. I)[6].

An extensive list of the energies and widths of ^1S and ^3S resonant states of helium has been presented by Bürgers et al. (1995) and for asymmetrically excited electrons (frozen planet states, see Sec. IV.C.2.a, IV.D.1) by Richter et al. (1992). An energy level diagram of $^1S^e$ states from such computations will be discussed at the end of this section. A listing of $^1P^o$ He resonances converging to the $N = 2 - 7$ thresholds is given by Rost et al. (1997). Results from the method outlined above will also be used as a check of the semiclassical calculations in Sec. IV.

Experimentally, resonant energies are usually not directly observed but indirectly deduced by excitation through electron impact or photo absorption. As reviewed in Sec. II.B.3.a high-precision photoabsorption spectra have been obtained in state-of-the-art experiments which challenge theory to calculate adequate cross sections for comparison. This is again possible by using complex rotation in terms of complex (dipole) matrix elements (Wintgen and Delande (1993), for a detailed discussion see Buchleitner et al. (1994)). The photo cross section then reads (Buchleitner et al. (1994), Rost et al. (1997))

$$\sigma(E) = \sigma_0(E) - \frac{1}{\pi}\mathrm{Im}\sum_n \frac{\langle i|D|n_\theta\rangle^2}{E - E_{n\theta}} \tag{10}$$

in terms of rotated wavefunctions $|n_\theta\rangle$ and complex energies $E_{n\theta}$ (Eq. (9)). In Eq. (10) $\sigma_0(E)$ is a smooth background coming from the continuum spectrum of the Hamiltonian. Note that in Eq. (10) the square of the dipole matrix element itself occurs and not the square of its modulus. Hence, *individual* resonance contributions can be positive or negative. In a diagonalization of $H(\theta)$ the (rotated) continua are replaced by a (dense) set of eigenvalues lying close to the half lines representing these continua (Wintgen and Delande (1993)). They mimic the true continua and yield a smooth backround of the photo cross section which leads to an overall positive value of $\sigma(E)$. An example of such a numerical calculation of the photoabsorption cross section in helium is given in Fig. 8. The good agreement between the numerical results, based on complex rotation, and the measured curves shows the high precision of state-of-the-art theoretical and experimental techniques.

The complex scaling method outlined above has been used in recent years for the calculation of photo excitation in helium by Wintgen and Delande (1993), Domke et al. (1995), and Rost et al. (1997). The most recent calculation by Grémaud and Delande (1997) covers the energy regime up to the $N = 9$ threshold where various resonances strongly overlap.

3. The helium $^1S^e$ energy level diagram

We close Sec. II by presenting in Fig. 9 the $^1S^e$ level diagram of helium as an example of a numerically calculated spectrum of doubly excited resonant states. The resonance energy positions shown were computed by complex rotation. The overall spectral structure appears to be similar to the spectrum in Fig. 5 which was obtained in the independent electron model. Nevertheless, there exist important differences already with respect to the positions of the resonances.

Fig. 9 shows that there are N different Rydberg resonance series converging to each ionization threshold, I_N. They can be labeled (see next section) by the Stark–type quantum number K which for ^1S-states runs from $K = -N + 1, -N + 3, \ldots, N - 3, N - 1$.

---

[6]One should, however, keep in mind that relativistic and finite mass corrections, which are not included in these calculations, become relevant on such a level of precision. Results including these effects were given by Drake (1993) (see Tab. I). They differ from the recent experimental results by Eikema et al. (1996) and Bergeson et al. (1998) (see Tab. I) due to the Lamb shift of the helium ground state.

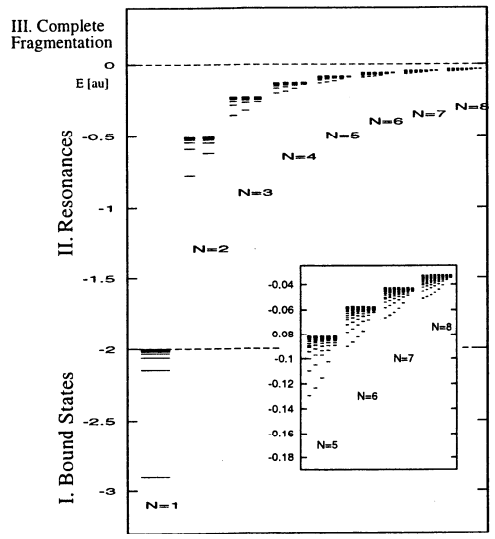

FIG. 9. Level diagram of the ${}^1S^e$ states of helium from the ground state to the $N = 8$ resonance series close to the three particle break-up threshold. There are N Rydberg series converging to each ionization threshold I_N. The inset shows the $N = 5 \quad 8$ levels on an enlarged scale.

Already the experiment by Madden and Codling (1963) revealed that the simple model of independent particle angular momentum quantum numbers l_1, l_2 (used in Fig. 5) proves inappropriate to characterize these series if the electrons can occupy a number of quasi-degenerate (individual electron) configurations. Depending on the degree of excitation, these configurations can be strongly mixed through the electron-electron interaction, such that there remains no dominant independent particle configuration (l_1, l_2) which could be assigned to a given resonance. In helium or H^- this mixing of independent particle states is in particular pronounced since, due to the absence of a core, each electron-nucleus sub-system possesses the high hydrogenic degeneracy of the energy levels (Eichmann et al. (1990)). Hence in such doubly excited atoms independent particle states are fragile and correlation effects should be strongest.

Approximate quantum numbers can be uniquely assigned for energies where Rydberg–series, converging to different ionization thresholds, do not overlap. Fig. 9 shows that Rydberg series converging to different I_N start to overlap for $N \geq 4$ (compared to $N = 9$ in the independent electron model). The mutual interaction of the Rydberg series in the energy regime shown in Fig. 9 can still be treated within quantum defect theory (Seaton (1983)), see e.g. Domke et al. (1991, 1995). This is only possible for moderate N, where individual perturbers can still be identified. However, the assignment of quantum numbers becomes increasingly difficult when more than two series of different N start to overlap (Bürgers et al. (1995)). The coupling between states belonging to different multiplets N depends on the labels K as will be explained in the preceding section.

The number of resonance series which interact simultanously increases further with N which renders the conventual description schemes, as e.g. approximate quantum numbers or quantum defect theory almost impossible.

In the next section, we present a thorough classification and interpretation of the resonances, given so far only numerically, in terms of approximate quantum numbers which account for the collective dynamics of the electron pair (Herrick (1983), Lin (1984), Feagin and Briggs (1986)). Furthermore, we will provide related propensity rules (Rost and Briggs (1991)) which govern the autoionization pattern and radiative transitions.

We will also discuss the limits of these approximate classification schemes (quantum numbers and propensity rules) when approaching the fragmentation threshold $E = 0$. This regime close to $E = 0$, which is characterized by a large number of strongly overlapping resonances, is far from being understood and is becoming a focus of current research activities.

III. APPROXIMATE QUANTUM MECHANICAL CONCEPTS FOR TWO-ELECTRON DYNAMICS

After the discovery of the effects of correlated electron motion by Madden and Codling (1963) and the first theoretical description by Cooper et al. (1963) in terms of configuration interaction, it took more than 25 years before a consistent picture and a fairly complete understanding of two-electron resonant dynamics emerged from the numerous attempts to approximate doubly-excited states. This is certainly a long time for a seemingly simple problem of three charged particles. However, as will be seen in this and the next chapter, surprisingly different, powerful and intellectually involved theoretical concepts, such as adiabatic approximations, group theoretical methods, and advanced semiclassical techniques, have been necessary to obtain the level of understanding of two-electron resonances we have achieved today. With this understanding we can answer the following crucial questions raised by the experimental and full numerical data, as summarized in Fig. 7 and Fig. 9.

1. The single particle picture is not applicable for two–electron atoms (see Sec. II) – why are two-electron resonances nevertheless organized in regular (Rydberg) series, and what distinguishes different Rydberg series quantitatively, i.e. can one calculate a quantum defect of the form Eq. (4)?

2. What is the common structure of the wavefunctions from states belonging to the same Rydberg series?

3. How can we understand the extreme selectivity in the photo–absorption cross section for different Rydberg series as can be seen for example in Fig. 6? What is the origin of the characteristic autoionization behaviour which leads to differences in the resonance widths of orders of magnitude for states belonging to different Rydberg series, see e.g. Fig. 7?

The last question addresses the possible existence of selection rules, or at least propensity rules, for transitions between two electron states, in analogy to, e.g., the well known angular momentum selection rules for dipole matrix elements between single electron states.

A. Overview

Among the many contributions towards answering the questions raised above three major theoretical concepts can be identified: the hyperspherical approach (HA), the algebraic approach (AA), and the molecular approximation (MA). These three qualitative and semi-quantitative descriptions could not have been developed without a continuously increasing set of two-electron resonance data, both from the experimental, as well as from the theoretical side through completely numerical, converged calculations.

The adiabatic hyperspherical approximation was introduced to the problem of two electrons by Macek (1968) and later on mainly pursued by Fano and coworkers (for reviews see Fano (1983), Fano and Rau (1986), Lin (1986, 1995)), however, also followed by collaborations around Matzsusawa and Watanabe in Japan (e. g. Atsumi et al. (1990), Tang et al. (1992), Tolstikhin et al. (1995)) and Klar (Klar and Klar (1980), Pelikan and Klar (1983)) in Europe. The separation of one variable, the hyperradius, leads to a set of adiabatic potential curves converging to each $He^+(N)$ threshold, similar to the Born-Oppenheimer approximation in molecules. Each of these potential curves carries an entire Rydberg series. The non-Coulombic short range form of the potential curves accounts naturally for a quantum defect which is different for each Rydberg series. Hence, already by construction, the hyperspherical adiabatic approximation provides a partial answer to question 1). Moreover, in days, when computers were not as powerful as today, the HA was a convenient way to lower the computational effort, since the calculation of adiabatic potential curves, still a substantial numerical task (see Section III.D), is not as involved as the numerical solution of the full problem. However, the structure underlying each potential curve, i.e. question 2) and therefore also 3) could not be answered. This goal was pursued by the algebraic approach.

The algebraic approximation was initiated by Wulfman (1968) who tried to use the well known dynamical SO(4) symmetry of hydrogen to understand the structure of two electrons from a coupled representation SO(4)×SO(4). The idea led Herrick and coworkers to an enlightening description of two-electron resonances which yielded for the first time an approximate but complete set of collective quantum numbers (for a review see Herrick (1983)). Various, also partly ad hoc assumed, coupling schemes of SO(4) led to the discovery of an astonishing degree of order in the two-electron resonance spectrum. In a series of papers, Lin (1983) succeeded in attaching approximative quantum numbers from the algebraic approach uniquely to hyperspherical potential curves. This was a great step forward and answered in addition to question 1) question 2) to a large extent: The existence of approximate quantum numbers per se revealed a common structure for each Rydberg series and Lin assigned the quantum numbers by following morphological similarities in the wavefunctions for the hyperspherical potential curves. Still, it was not known if the approximate quantum numbers correspond to a quasi separability of the problem in a suitable coordinate system. Such a coordinate system would automatically lead to an answer of the still open question 3). Can one find a quasi-separable approximation for two-electron states, which would explain possible selection rules? It was the third major concept of two-electron states which provided this separation.

The adiabatic molecular separation was introduced by Feagin and Briggs (1986), for a review see Rost and Briggs (1991). This approximation treats the two-electron atom literally as a molecule whereby the role of the adiabatic internuclear axis is taken over here by the interelectronic axis $\mathbf{r}_{12}$, see Fig. 1. The structure of the adiabatic potential curves is rather similar as in the HA with one major and important difference: the Hamiltonian for fixed interelectronic vector $\mathbf{r}_{12}$ is *separable* in elliptical coordinates providing a full set of quantum numbers (which are in one to one correspondence to the ones derived by Herrick within the (AA)). In addition the separability implies a coordinate system in which the wavefunction for the two electrons can be written approximately as a product of functions with a well defined number of nodes along each coordinate corresponding to the quantum numbers. Hence, the achievements of the HA and the AA could be combined in the MA, with the additional benefit of a set of coordinates in which the two-electron resonant wavefunctions are approximately separable. The separability permits the identification and formulation of propensity rules, and therefore, finally, in addition to question 1) and 2), also an answer to question 3).

The molecular description provides the most detailed information about two-electron resonances since it takes into account the rather special feature of the singular Coulomb potentials. Hence, it is probably difficult to transfer this approach to other (non-Coulombic) few-body systems.

The algebraic approach makes also heavily use of the SO(4) structure of the Coulomb problem. Nevertheless, constructing level multiplets from group theoretical considerations is a common technique in few-body dynamics and probably best known from the theory of quarks (Halzen and Martin (1984)). Therefore, the algebraic approach is much more 'transferable' between different few-body problems, in fact, it is the preferred theoretical concept if the interparticle forces are not known in detail.

The most general few-body concept is the adiabatic hyperspherical approximation, especially if the potentials are known. It produces in most cases good quantitative estimates for the energy levels and it has been used in nuclear physics as well as for the nuclear (non-Coulombic) motion in molecules containing a small number of atoms (see e.g. Hernandez and Clary (1996)).

We will discuss all three concepts in this chapter, and in addition a selection of interesting alternative approaches. However, for the sake of a pedagogical presentation we will not discuss the development in historical order. Instead, we present the MA first because it appears to provide the most complete qualitative description of doubly excited states within a single concept. In particular, the two limiting collinear cases with $\Theta \approx 180°$ (electrons on opposite sides of the nucleus) and with $\Theta \approx 0$ (electrons on the same side of the nucleus) will become clear: in the first case the interelectronic axis r_{12} is taken as adiabatic variable R, in the second case the distance $r_>$ from the nucleus to the outer electron is defined as the adiabatic R. The two collinear configurations persist as a structural element of doubly-excited states even for very high excitation of both electrons, where the approximate quantum numbers (to be derived in the present section)

loose their meaning. This fact is based on classical and semiclassical considerations which will be presented in Section IV.

B. The molecular adiabatic approximation

1. Symmetries and wavefunctions

Feagin and Briggs (1986, 1988) introduced and formulated the idea to view doubly excited atomic states in terms of 'molecular' potential curves known from H_2^+. This idea has the appealing consequence that each potential curve comes from a separable adiabatic two center Coulomb Hamiltonian (Slater (1977)) with well defined quantum numbers and carries naturally a (Rydberg) series of two-electron resonances.

In molecular Jacobi coordinates, with $\mathbf{R} = \mathbf{r}_{12}$ connecting the two electrons and $\mathbf{r} = (\rho, z, \phi)$ pointing from the middle of the two electrons to the nucleus, the two-electron Hamiltonian reads

$$H = -\nabla_R - \tfrac{1}{4}\nabla_r - \frac{Z}{|\mathbf{R}/2 - \mathbf{r}|} - \frac{Z}{|\mathbf{R}/2 + \mathbf{r}|} + \frac{1}{R}. \tag{11}$$

Treating the interelectronic axis $\mathbf{R}$ as a slow variable in analogy to the internuclear axis for H_2^+ does not seem to make sense on a first glance since the light electrons are expected to move *fast* compared to the heavy nucleus. However, firstly, the mass argument must refer to the reduced masses involved which are of comparable magnitude for the two electrons and the *center of mass* of the nucleus with respect to the electrons as can be seen from Eq. (11). Secondly, the success of adiabatic separations is not necessarily linked to slow and fast variables but can also originate in a quasiseparability of the system in the respective variables. Finally, an intuitive argument can be given in support of the interelectronic axis as an adiabatic variable for highly excited two-electron resonances, more specifically, if $N/Z \gg 1$. In this case, the effect of the attraction between an electron and the nucleus is much weaker than that of the repulsion between the electrons which is expected to dominate the structure of the resonant states. This is not the case for the ground state where $N/Z \leq 1$ and it is not too surprising that a molecular adiabatic separation leads to a binding energy for helium which is 20% too small (Hunter and Pritchard (1967, 1967a), Hunter et al. (1968)).

In a molecular expansion the spatial wavefunction is represented as a sum over products of rotational, $\mathcal{D}^{L,S,t}_{Mm}(\Psi, \vartheta, \phi)$, vibrational, $f^L_{im}(R)$ and molecular orbital (MO), $\psi^t_{im}(\rho, z; R)$, wavefunctions:

$$\Psi^{S,t}_{LM}(\mathbf{r}, \mathbf{R}) = \sum_{im} \mathcal{D}^{L,S,t}_{Mm}(\Psi, \vartheta, \phi) \frac{f^L_{im}(R)}{R} \psi^t_{im}(\rho, z; R). \tag{12}$$

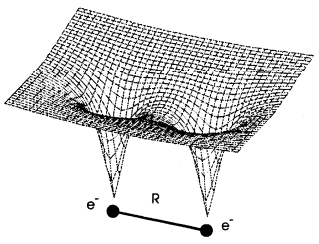

FIG. 10. The two-center Coulomb potential $-2/r_1 - 2/r_2$ at fixed interelectronic distance of $R = 2$ a.u. for two-electron motion in helium. The z-axis is parallel to R, the ρ-axis perpendicular to it, see also text. (From Rost et al. (1997).)

In the body-fixed frame, connected to the lab-fixed frame by the Euler angles Ψ, ϑ, ϕ, the interelectronic vector $\mathbf{R}$ is parallel to the z-axis. As in Rost et al. (1997) the azimuthal angular dependence on ϕ is described by the rotational wavefunction $\mathcal{D}^{L,S,t}_{Mm}(\Psi,\vartheta,\phi)$ and the MO $\psi^t_{im}(\rho,z;R)$ is a wavefunction for the center of mass motion of the nucleus in the coordinates ρ, z at fixed internuclear distance R and for a given quantized azimuthal motion m. The index i counts the quantized states in (ρ,z). The potential for this motion (with $m=0$) is shown in Fig. 10.

The wavefunction Eq. (12) has been constructed to respect all exact two-electron symmetries, see also Sec. II.B.1. In particular the rotational parts consist of a symmetry adapted linear combination of Wigner functions $D^L_{Mm}(\Psi,\vartheta,\phi)$ for the Euler angles (Feagin and Briggs (1988)),

$$\mathcal{D}^{L,S,t}_{Mm} = D^L_{Mm} + (-1)^{S+t+L+m} D^L_{M-m}. \tag{13}$$

Hence, the wavefunction Eq. (12) is eigenfunction of the permutation operator P_{12} for the (identical) electrons $P_{12} : \mathbf{R} \to -\mathbf{R}, \mathbf{r} \to \mathbf{r}$ with eigenvalue $(-1)^S$ where S is the spin of the electron pair, either singlet ($S=0$) or triplet ($S=1$). Furthermore, it is an eigenfunction of the parity operator $P : \mathbf{R} \to -\mathbf{R}, \mathbf{r} \to -\mathbf{r}$ with eigenvalues $p = \pm 1$. The product operator PP_{12} has thus eigenvalues $(-1)^S p = (-1)^t$ which defines the quantum number t in (12). The quantum number m is the eigenvalue of the projection operator l_z where $\mathbf{l} = -i\mathbf{r} \wedge \nabla_r$ and also of the body-fixed component L_z of the total angular momentum $\mathbf{L}$.

The solution of the eigenvalue equation $(H-E)\Psi^{S,t}_{LM} = 0$ reduces, after integration over $\mathbf{r}$ and the Euler angles, to the following set of coupled equations for the vibrational amplitudes:

$$\begin{aligned} -\left[\partial^2/\partial R^2 - 2(U^L_{im}(R) - E)\right] f^L_{im}(R) = \\ \textstyle\sum_{j\neq i} A^0_{ij}(R) f^L_{jm}(R) \\ + A^+_{ij}(R) f^L_{jm+1}(R) + A^-_{ij}(R) f^L_{jm-1}(R) \ , \end{aligned} \tag{14}$$

where we omitted the dependence on M, S, t to simplify the notation. The rotational coupling terms

$$A^{\pm}_{ij}(R) = [(L \mp m)(L \pm m + 1)]^{1/2} \langle \psi_{im} | l_{\pm}/R^2 | \psi_{jm\pm 1} \rangle \tag{15}$$

change the angular momentum quantum number m while the radial coupling term

$$A^0_{ij}(R) = \langle \psi_{im} | 2\partial/\partial R | \psi_{jm} \rangle \partial/\partial R \tag{16}$$

leaves m unchanged.

In the adiabatic approximation the sum in Eq. (12) is collapsed to one term im with the consequence that the r.h.s in Eq. (14) is zero, i.e. all couplings to channels $jm' \neq im$ are ignored, and Eq. (14) reduces to a conventional eigenvalue equation for $f^L_{im}(R)$. For fixed R the adiabatic molecular wavefunction $\psi^t_{im}(\rho,z;R)$ approximately diagonalizes the two-electron Hamiltonian if it is an eigenfunction of the two-center Hamiltonian ($Z=2$ for helium)

$$h_m(R) = -\frac{1}{2}\frac{\partial^2}{\partial z^2} - \frac{1}{2\sqrt{\rho}}\frac{\partial^2}{\partial \rho^2}\sqrt{\rho} - \frac{Z}{r_1} - \frac{Z}{r_2} + \frac{m^2}{2r^2} \tag{17}$$

which depends parametrically via r_1 and r_2 on the interelectronic distance R. In the adiabatic approximation the vibrational wavefunction $f^L_{im}(R)$ is an eigenstate of the adiabatic potential

$$U^L_{im}(R) = \mathcal{E}_{im}(R) + C^L_{im}(R) + 1/R, \tag{18}$$

where $\mathcal{E}_{im}(R)$ is an eigenvalue of $h_m(R)$ and $C^L_{im}(R) = \langle \psi_{im} | H - h_m | \psi_{im} \rangle$ is the expectation value of the part of the Hamiltonian which is not diagonalized by ψ_{im}.

Note that this is *not* the standard Born-Oppenheimer approach since we have left out parts of the kinetic energy in r to define the two-center Hamiltonian Eq. (17). Therefore, the residual kinetic energy $\frac{1}{4}\nabla^2_r$, not diagonalized in Eq. (17), is part of $C^L_{im}(R)$. This modified Born-Oppenheimer treatment acknowledges the fact that the reduced masses along both Jacobi coordinates to be separated adiabatically are of the same order of magnitude (Rost and Briggs (1991)). Using the kinetic energy as in Eq. (17) ensures by construction that the adiabatic correction term $C^L_{im}(R)$ is zero in the large R limit.

The most important feature of the molecular approximation is the fact that the two-center Hamiltonian Eq. (17) is separable in prolate spheroidal coordinates (Slater (1977))

$$\lambda = \frac{r_1 + r_2}{R}, \quad \mu = \frac{r_1 - r_2}{R} \tag{19}$$

with

$$r_{1/2} = \sqrt{\rho^2 + (z \pm R/2)^2}. \tag{20}$$

The separability implies a product form for the MO,

$$\psi_{im} = \Lambda^m_{n_\lambda}(\lambda) M^m_{n_\mu}(\mu) \,, \tag{21}$$

with quantum numbers n_λ, n_μ which count the nodes along the respective coordinates.

To summarize, in the molecular approximation individual resonances are obtained by computing vibrational eigenstates according to the Schrödinger equation

$$\left(-\frac{\partial^2}{\partial R^2} + U^L_{n_\lambda, n_\mu, m}(R) - E_{\bar{n}} \right) f_{\bar{n}}(R) = 0. \tag{22}$$

The vibrational quantum number $\bar{n}$ specifies the excitation of one electron along a Rydberg series. Physically, $\bar{n}$ counts the same states as n in Section II.B.1, and the relation between both quantum numbers is $\bar{n} = n - N$, where N is the principal quantum number of the $He^+(N)$ hydrogenic level for $\bar{n} \to \infty$. The exact quantum numbers L, M, S, M_S, π and the approximate quantum numbers $\bar{n}, n_\lambda, n_\mu, m$ constitute a complete classification of doubly-excited states. Moreover, they imply an approximate nodal structure of the wavefunctions which in turn leads to propensity rules for radiative transitions involving doubly excited states as well as autoionization. Fig. 11 illustrates schematically the calculation of a doubly-excited two-electron state with all its quantum numbers in the molecular approximation.

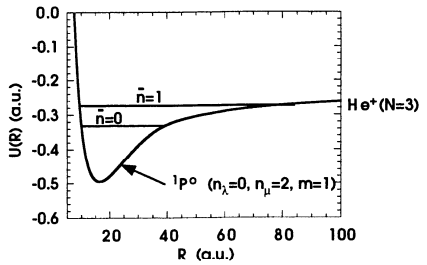

FIG. 11. Schematic representation of doubly-excited states in helium in an adiabatic approximation. The resonances appear as vibrational eigenstates (the first two are shown) in a potential curve which is constructed from an eigenfunction of all exact symmetries $^{2S+1}L^\pi$ and of the two-center Coulomb problem with the respective quantum numbers n_λ, n_μ, m, see text. The states $\bar{n}$ form a Rydberg series with the limiting energy of the excited $He^+(N)$ ion for $\bar{n} \to \infty$ (from Rost et al. (1997)).

As for other separable problems, the quantum numbers do not have to represent the actual number of nodes along some coordinates. Hydrogen itself is the best example, where only the azimuthal quantum number $m = n_\phi$ specifies directly the number of nodes of the wavefunction in the coordinate ϕ. The number of nodes in θ are given by $n_\theta = l - m$, and the radial nodes are counted by $n_r = N - l - 1$, see also Eq. (5). Moreover, the hydrogen problem separates in many other but the spherical coordinates (due to its high degree of degeneracy). Relevant for the two-electron problem is the separation of hydrogen in parabolic coordinates, where again two sets

of quantum numbers are used, the nodal quantum numbers $[N_1, N_2, m]$ with $N = N_1 + N_2 + m + 1$ and the 'Stark' quantum numbers (N, K, T) with $K = N_1 - N_2$ and $T = m$. While the nodal quantum numbers count the nodes of the wavefunction along the parabolic coordinates the Stark quantum numbers directly describe the energy eigenvalues in the presence of a static electric field (Stark effect).

To characterize the two-electron potential curves $U(R)$ from Eq. (18) one can also use the parabolic quantum numbers which classify each $U(R)$ uniquely in the 'separated atom' limit $R \to \infty$, when the outer electron has been removed to infinity and merely represents a static electric field for the inner one. Along an adiabatic MO curve the nodes of the wavefunctions do not change. Hence, numbers are in one-to-one correspondence:

parabolic	molecular	Herrick/Stark	
N_1	$= n_\lambda =$	$\frac{1}{2}(N - K - 1 - T)$	(23a)
N_2	$= [n_\mu/2] =$	$\frac{1}{2}(N + K - 1 - T)$	(23b)
$\lvert m \rvert$	$= m =$	T	(23c)
A	$= (-1)^{n_\mu} (=) A.$		(23d)

The notation $[x]$ stands for the closest lower integer to x. Herrick was the first to introduce the set of Stark quantum numbers N, K, T for two-electron states. They emerged from his algebraic approach (1983) to be discussed in Section III.C. Since the information of even and odd nodes n_μ is lost in the parabolic/Stark classification, an additional quantum number must be introduced, which has been given already by Herrick and Sinanoglu (1975), see Section III.C.1. Today it is commonly denoted by A, as coined by Lin (1983). He used A as a label to characterize hyperspherical potential curves for two-electron atoms with the values $A = +/-1$ for an antinodal/nodal line of the corresponding adiabatic wavefunctions at $r_1 = r_2$. Moreover, Lin (1983) introduced the label $A = 0$ for no apparent symmetry with respect to the line $r_1 = r_2$, see Section III.D. In the two-center adiabatic approach, A is the eigenvalue of the *body-fixed* electron exchange operator with values $A = \pm 1$ from $A = (-1)^{n_\mu}$. $A = 0$ does not occur in this description. This is the reason why we put the last equality of Eq. (23d) in parentheses. The correspondence to a hyperspherical potential curve with the empirical label $A = 0$ would be a linear combination of several molecular potential curves of different symmetry A.

3. Propensity rules for radiative and non-radiative transitions

a. *Autoionization*

The approximate constants of motion of Eq. (23) for correlated two-electron dynamics imply a nodal structure for the respective resonant states (Rost et al. (1991a)). In turn this nodal structure leads to preferences for autoionization (Rost and Briggs (1990)) and dipole transitions (Vollweiter et al. (1991)). They are easily understood in the molecular language of adiabatic potential curves identified by a set $[N_1 N_2 m]^A$ of quantum numbers. A small subset of such potential curves as a function of the adiabatic interelectronic distance R is shown in Fig. 12. The most obvious feature in Fig. 12 are avoided crossings between two potential curves, respectively. Their locus as a function of R, indicated by black squares in Fig. 12(b), follows closely the saddle point of the two-center Coulomb potential that plays a crucial role for the three-body Coulomb problem. The saddle point for fixed R (see Fig. 10) is defined by $\mathbf{r}_1 + \mathbf{r}_2 = 0$, where the $\mathbf{r}_i$ are the two electron-nucleus vectors. Moreover, this is exactly the definition for the configuration space occupied by the classical Wannier orbit which plays a prominent role for the classical understanding of two-electron dynamics, see Section IV.B.2.b.

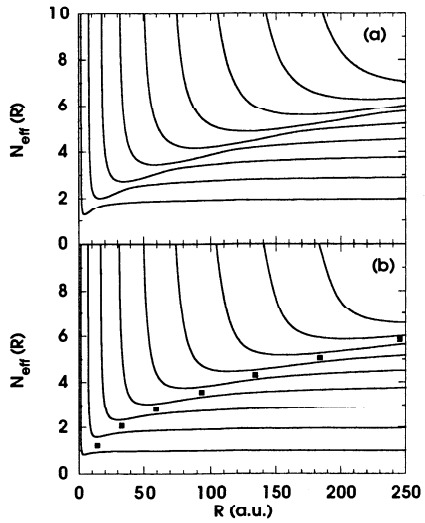

FIG. 12. Adiabatic molecular potential curves for two-electron doubly-excited states as a function of the interelectronic distance R. The resonances appear as vibrational eigenstates in the potential curves. The energy is plotted as effective quantum number $N_{eff}(R) = (-2/U(R))^{1/2}$ with $N_{eff}(R \to \infty) = 2, 3, 4, \ldots$ indicating directly the $He^+(N)$ ionization thresholds. Part (a) shows potential curves which carry the resonances of the principal series with quantum numbers $[N_1, N_2, m]^A = [0, N-1, 1]^+$, $N = 2, \ldots, 10$ from below. Part (b) shows resonances of $A = -1$ symmetry for $N = 1, \ldots, 9$ corresponding to the quantum numbers $[0, N-1, 0]^-$ from below. To guide the eye the black squares indicate the locus of the avoided crossing, see text (from Rost et al. (1997)).

The avoided crossings may be interpreted in the following way: To the right of such a crossing, the adiabatic two-electron wavefunction $\psi^m_{n_\lambda n_\mu}(R)$ has its main contribution in the Coulombic wells and the contributions in each well are separated from each other by a classically forbidden region with the probability density being small at the saddle point. To the left of the avoided crossing, the wavefunction has its main contribution at the saddle point. Hence, the avoided crossings separate two regions in R in which the wavefunction has different character. As can be seen in Fig. 12, potential curves whose quantum numbers differ by $\Delta N_2 = 1$ (i.e. $\Delta n_\mu = 2$) display avoided crossings, which are narrower for $A = +1$ states (whose wavefunctions have an antinode on the saddle, Fig. 12 (a)), than for $A = -1$ states (with a node on the saddle, Fig. 12 (b)). In the latter case the change in character of the wavefunction as a function of R passing an avoided crossing is not so dramatic, since for reasons of symmetry the wavefunction is zero exactly at the saddle point for all R.

The mechanism of autoionization relies on non-adiabatic transitions in this description, in full analogy to electronic transitions in molecules. *Radial* transitions via Eq. (16) are sensitive to the change of the wavefunction as a function of R. Hence, they occur preferentially through an avoided crossing of two potential curves. The second kind of non-adiabatic transition is due to *rotational* coupling $\Delta m = 1$ between potential curves according to Eq. (15). Finally, there is no explicit mechanism to change N_1 (n_λ). Hence, transitions with $\Delta N_1 \neq 0$ are strongly suppressed. From these observations one can extract three propensity rules for autoionization, which are labeled according to the relative efficiency of the underlying decay mechanism:

$$\text{(A)} \quad \Delta N_2 = -1 \quad \text{or} \quad \Delta N = -1, \Delta K = -1 \tag{24a}$$

$$\text{(B)} \quad \Delta m = -1 \quad \text{or} \quad \Delta T = -1 \tag{24b}$$

$$\text{(C)} \quad \Delta N_1 = -1 \quad \text{or} \quad \Delta N = -1, \Delta K = +1 \tag{24c}$$

In general, states with $A = +1$ have larger widths than those with $A = -1$. This can be expected following the discussion of Fig. 12 and it can be directly seen from the experiments, e.g. from

Fig. 7. As an example we show in Fig. 13 the decay systematics for the lowest resonance $n = N$ of ${}^1P^o$ symmetry in a series $[N_1N_2, m]_n$. Each box contains the width of the lowest resonance of the respective series with quantum numbers $[N_1N_2m]$. Simultaneously, the box represents the continuum $[N_1N_2m]$ into which a higher lying resonance may decay as indicated by the arrows and the respective mechanism (A), (B) or (C).

In the upper right triangle the states with $A = +1$ are located. Those of them, which can decay according to rule (A), have the largest widths (of the order of 10^2 meV). The arrows point to quantum numbers of the continuum into which these states decay according to rule (A). Close to the (dashed) diagonal separating $A = +1$ and $A = -1$ states we see those resonances that can not decay by (A). Instead, they decay according to (B) by changing their rotational quantum number. Since this change implies also a change of the quantum number A, the decay arrow has to cross the diagonal and points to a continuum state with $A = -1$. The rotational decay of these $A = +1$ states is only slightly less effective (by about a factor of 5) than the decay of the $A = +1$ states according to (A). Hence, we combine all $A = +1$ states located in the upper triangle to "I. class" states with the relatively largest widths.

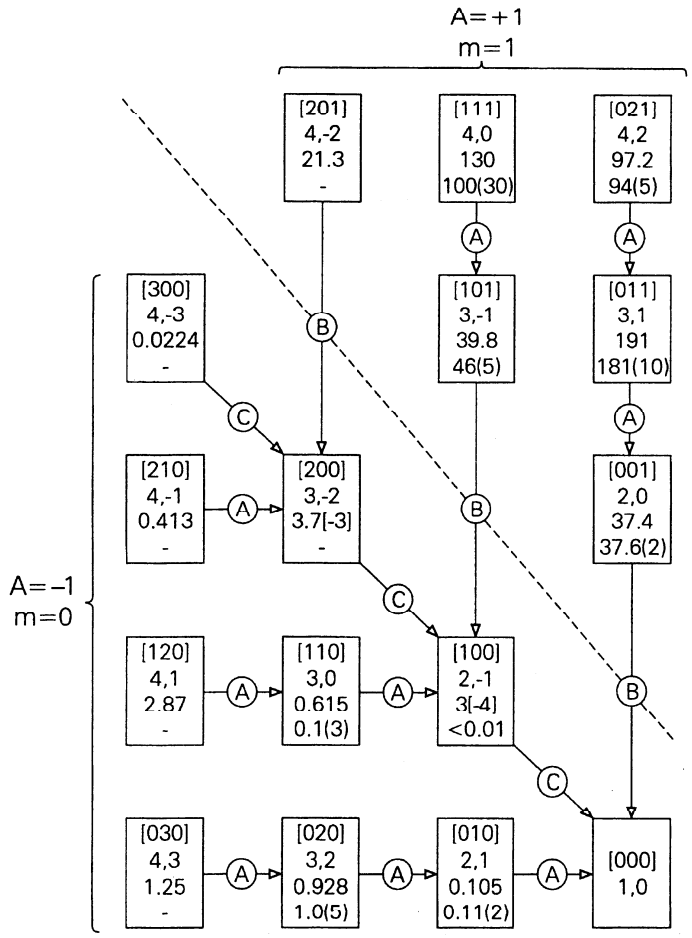

FIG. 13. Decay modes indicated by arrows with the respective rule from Eq. (24) for the lowest ${}^1P^o$ resonances in the manifolds $N = 2-4$. Each box stands for a continuum channel and the lowest resonance in this channel. The quantum numbers $[N_1N_2m]$ and N, K are given together with the theoretical and experimental width in meV from Rost et al. (1997) (uncertainty in parentheses). The diagonal (dashed) separates $A = +1$ and $A = -1$ states.

The $A = -1$ states below the diagonal that can decay according to (A) define the "II. class" states. Their widths (of the order of 10^0 meV) are one to two orders of magnitude smaller than the widths of the I. class states Among the $A = -1$ states are also "III. class" states located directly below the diagonal. They can only decay according to (C) along the diagonal and their widths ($10^{-4} - 10^{-2}$ meV) are more than two orders of magnitude smaller than those of II. class resonances, for more details see e.g. Rost et al. (1997), Rost and Briggs (1990).

To summarize, the three propensity rules (A), (B) and (C) group resonant two-electron states into three classes I-III. For helium, widths between members of two classes differ typically by at least two orders of magnitude, $\Gamma_I : \Gamma_{II} : \Gamma_{III} \approx 10^4 : 10^2 : 1$. For a semiclassical interpretation of the propensity rules discussed above see also Section IV.C.

b. Dipole transitions

Propensity rules for radiative transitions can be derived by analyzing the dipole matrix elements according to the nodal structure of the resonant wavefunctions, which is a simple analytical task on the potential saddle at $2\mathbf{r} \equiv \mathbf{r}_1 + \mathbf{r}_2 = 0$. This region in configuration space is most relevant for symmetrically excited electrons with $N \approx n$. It corresponds to the equilibrium geometry of a linear ABA molecule (Hunter and Berry (1987)). Not surprisingly, the relevant quantum number

$$v_2 = 2N_1 + m \tag{25}$$

for radiative propensities quantizes the two-fold degenerate bending motion of triatomic molecules and can be derived by normal mode analysis about the saddle point (Vollweiter et al. (1991)). Dipole matrix elements within the saddle approximation follow the selection rule

$$\text{(D)} \quad \Delta v_2 = 0, \pm 1 \tag{26}$$

that survives for the entire dynamics as a propensity rule. Rule (D) has been derived from properties of the doubly-excited state involved in the dipole transition. A preference among the possible transitions according to (D) can be induced by the second state of the dipole matrix element, see Rost et al. (1997). Such a preference has also been worked out by Gerasimovich et al. (1996), see Section III.E.3. The propensity rules are also confirmed by the latest measurements of partial ionization cross sections (Menzel et al. (1995, 1996)).

4. The molecular description of planetary states

For a long time the symmetrically excited states with $N \approx n$ were thought to be the most correlated states and they had been in the center of research activities, including the molecular description with the interelectronic axis r_{12} as adiabatic variable R.

After 1990 the development of sophisticated laser excitation schemes of alkaline earth atoms permitted to prepare non–core–penetrating doubly excited states and to examine helium–like three–body systems with high resolution laser spectroscopy (Eichmann et al. (1992)).

Many features of the experimental spectra for very asymmetrically doubly excited states (e.g. $N = 6, n > 25$) could be understood in the "frozen planet approximation" (Eichmann et al. (1990)) where the outer, very slow electron represents a static electric field for the inner electron, see also Section II.B.3.b.

a. Characteristics of planetary states

In 1990, Richter and Wintgen discovered a new class of strongly correlated but asymmetrically excited states. Their remarkable properties, discussed in detail in Richter et al. (1992), can be summarized as follows:

(i) distinct angular *and* radial correlations,

(ii) extremely small decay widths,

(iii) quasi–separability of the wavefunctions in collective semiclassical and molecular coordinates.

The strong radial and angular correlations of the electrons lead to the mixing of all single particle angular momenta l_i resulting in the formation of a molecular– (or Stark–) type inner electronic wavefunction and a vibrational, highly non–hydrogenic wavefunction for the outer electron. As will be discussed in section IV.B.2.a, the resonances are associated with a classical phase space region, where the three–body Coulomb system becomes nearly integrable.

The resonances exist for arbitrary *finite* nuclear charges $Z > 1$. Their existence is inherently tied to the repulsive electron–electron interaction. In particular, they do not possess a limiting independent–particle motion. Hence, standard perturbation theory in $1/Z$ starting from the independent–particle limit fails in describing these states. However, they can be described with an adiabatic approximation.

b. Structure of planetary states from the adiabatic approximation

The suitable adiabatic variable $\mathbf{R}$ for planetary states is the coordinate $\mathbf{r}_>$ of the slow outer electron. If the origin of the internal coordinate $\mathbf{r}$ describing the fast electron is taken as the geometrical midpoint of $\mathbf{R}$, i.e. $\mathbf{r} = \mathbf{r}_> - \mathbf{R}/2$ the Hamiltonian for fixed $\mathbf{R}$ is that of a two-center Coulomb problem where now one center, the nucleus, is attractive while the other center, the slow electron, is repulsive. The adiabatic wavefunction for fixed R is again separable in prolate spheroidal coordinates $\bar{\lambda}, \bar{\mu}$, however, they obviously have a different meaning compared to Eq. (19), namely

$$\bar{\lambda} = \frac{r_> + r_{12}}{R}, \qquad \bar{\mu} = \frac{r_> - r_{12}}{R}. \tag{27}$$

The adiabatic potential curves (Fig. 14) look also very different from e.g. Fig. 11. For each manifold N the uppermost curve, in which the fast inner electron is highly polarized towards the outer electron, develops a secondary potential well around $R \sim 100$ a.u.. These curves have $n_{\bar{\lambda}} = 0$ and the maximum number of nodes in $\bar{\mu}$, $n_{\bar{\mu}} = N - 1$. In helium, the minimum is for $N \geq 6$ deep enough for vibrational bound states with oscillator–like eigenfunctions for the outer electron.

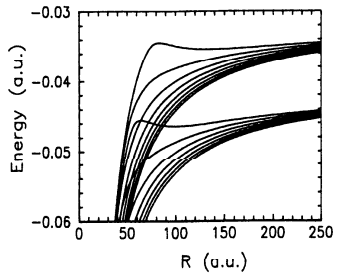

FIG. 14. Born-Oppenheimer potential curves for MO-states belonging to the manifolds $N = 6$ and $N = 7$ of helium, from Richter et al. (1992).

Applying the usual Coulombic scaling for energies and lengths of $1/N^2$ and N^2, respectively, leads for the adiabatic potential $U_{n_{\bar{\lambda}} n_{\bar{\mu}}}$ to the transformation

$$U_{0,N-1} \to \mathcal{U}_{0,N-1} = \frac{3N(N-1)}{4}\left(U_{0,N-1} + \frac{2}{N^2}\right)$$
$$R \to \mathcal{R} = \frac{4}{3N(N-1)} R, \tag{28}$$

(which is the special case for helium of a more general Z–dependent scaling technique discussed in Richter et al. (1992)). The shape of the scaled potentials is only weakly N–dependent with the maxima of the potential barriers becoming more pronounced with increasing N (see Fig. 5 in Richter et al. (1992)). This behavior reflects the increasing polarizability of the inner electron.

The occurrence of minima in the Born–Oppenheimer potentials is not restricted to MO states with $n_{\bar{\lambda}}$=0. If N is large enough (i.e. $N \geq 16$ in the case of helium), the polarization of an inner–electron state with one off–radial node ($n_{\bar{\lambda}}$=1) is strong enough to produce a potential well in the adiabatic potential. In Fig. 15 the probability densities of *ab initio* three-dimensional quantum wavefunctions for fixed distances R of the outer electron are shown for the state with $n_{\bar{\mu}} = 9$ and $n_{\bar{\lambda}} = 1$. The figure depicts the conditional probability for finding the inner electron in the coordinate space relative to $\mathbf{R}$ connecting the nucleus and the outer electron.

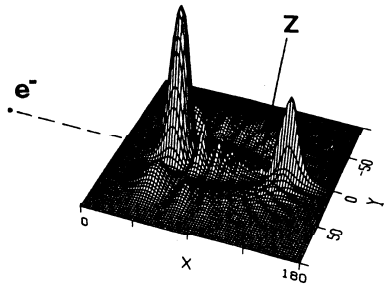

FIG. 15. Conditional probability density for the inner electron with respect to the fixed axis $\mathbf{R}$ between the nucleus (indicated by Z) and the outer electron. The $(n_{\bar{\mu}}, n_{\bar{\lambda}}, m) = (9, 1, 0)$ state of $^1S^e$ symmetry is shown in Cartesian coordinates. The distance R is chosen as the classical expectation value $\langle r_> \rangle_{cl}$ for the radial distance of the outer electron along the classical periodic orbit, see Fig. 20 (a) in Section IV.B.2.a (from Richter et al. (1992)).

The adiabatic picture not only describes the number of nodes in the wavefunctions correctly, but also predicts the shape of the nodal surfaces: In $\bar{\lambda}$ and $\bar{\mu}$ they appear as nearly straight lines (Richter et al. (1992)), which proves the approximate separability of the *ab initio* quantum wavefunctions in these coordinates (see also Richter and Wintgen (1992)).

Although the planetary atom resonances are separable in prolate spheroidal coordinates as the intrashell resonances are, one has to keep in mind the different meaning of the coordinates and the radically different character of these two sets of states which becomes also obvious in the decay characteristics.

c. Decay widths

While the adiabatic potential curves representing intrashell resonances show pronounced avoided crossings responsible for an efficient and characteristic decay mechanism (see Section III.B.3.a) such avoided crossings do not occur for potential curves representing the planetary states, see Fig. 14. Indeed, these states are oscillator like and they are so different from the hydrogenic like states into which they must decay that they have a remarkably long lifetime. Moreover, the lifetime increases exponentially with N such that for states starting from $N \approx 20$ radiative decay is more probable than autoionization (Richter and Wintgen (1991)). Their asymptotic stability for $N \to \infty$ is connected with the fact that the classical periodic orbit which supports these states is stable (see Section IV.B.2.a). This again is in sharp contrast to the intrashell states where the collinear subspace with electrons on different sides of the nucleus contains only unstable periodic orbits reflecting the larger instability of intrashell states.

5. Conclusions from the adiabatic molecular treatment

The insight into the structure of two-electron resonances gained from the adiabatic molecular treatment leads to the conclusion that there are two important limiting cases of collinear arrangement of the three particles: (i) In a H_2^+ like symmetric molecular approximation with the two electrons forming the adiabatic axis, a collinear configuration emerges for increasing N keeping the wavefunction nodeless in the λ coordinate of Eq. (19). Pronounced avoided crossings between the corresponding potential curves belonging to different N indicate the relative instability, i.e. large decay widths of these states. (ii) In a molecular adiabatic approximation, treating the vector of the outer electron as the slow variable, states without nodes along the $\bar{\mu}$ coordinate form for increasing N a collinear arrangement with both electrons on the same side of the nucleus ($\Theta \approx 0°$). These so called planetary states have very small decay widths. In Section IV.B.2.a we will see that these two collinear configurations emerge very naturally from a classical analysis. The difference in the decay properties of these two groups of resonances reflects the difference in the classical stability of representative periodic orbits belonging to the respective classical collinear configurations.

A comparison of the two adiabatic molecular descriptions reveals that the long living planetary correspond in the symmetric H_2^+ like description to states with the maximum bending excitation for a given N, $n_\lambda = N - 1$. The propensity rules Eq. (24), especially the forbidden transition (24c), also reflect the stability of planetary states. This shows, that the adiabatic molecular approximation with the interelectronic axis $\mathbf{r}_{12}$ as the adiabatic variable provides a good overall picture of the resonance properties. The quantitative representation for the states with maximal n_λ is, however, rather poor. The character of adiabatic wavefunctions changes quite drastically in this limit and the frozen planet states are quantitatively much better represented in the corresponding adiabatic molecular treatment with $\mathbf{R} = \mathbf{r}_>$ as the adiabatic variable.

C. The algebraic approach

The idea to understand the structure of the levels of doubly excited states in terms of group symmetries dates back to the work by Wulfman (1968). The real breakthrough of the algebraic approach, which is mainly based on properties of the SO(4) group, came with later work initiated by Wulfman (1973) and Sinanoglu and Herrick (1975) and completed by Herrick and coworkers in series of papers (Herrick and Sinanoglu (1975), Herrick (1975, 1975a), Herrick and Kellman (1980), Herrick et al. (1980)). A good overview is given by Herrick (1983).

1. Dynamical SO(4) representations for one and two electron atoms

For the dynamics of the hydrogen atom there is a second angular momentum type constant of motion, apart from the angular momentum $\mathbf{l}$, the Runge-Lenz vector (see e.g. Schiff (1968)),

$$\mathbf{A} = \tfrac{1}{2}(\mathbf{l} \times \mathbf{p} - \mathbf{p} \times \mathbf{l}) + \hat{\mathbf{r}}. \tag{29}$$

For bound states $\mathbf{l}$ and $\mathbf{b} = (-2H)^{-1/2}\mathbf{A}$ satisfy commutation relations which correspond to a SO(4)=SU(2)×SU(2) generating coupling scheme of angular momenta. Each irreducible representation of the dynamical $SO(4)$ group can be labeled by two indices $[p, q]$ (Herrick (1983)).

For two electrons indicated by indices $i = 1, 2$ Wulfman (1968) used initially coupled angular momenta $\mathbf{L} = \mathbf{l}_1 + \mathbf{l}_2$ and $\mathbf{B}' = \mathbf{b}_1 + \mathbf{b}_2$ to generate an SO(4) algebra. However, as he himself (Wulfman (1973)) and Sinanolgu and Herrick (1975) showed later, one should use $\mathbf{B} = \mathbf{b}_1 - \mathbf{b}_2$ instead of $\mathbf{B}'$ to describe doubly excited states. Coupled states within irreducible representations generated by $\mathbf{L}$ and $\mathbf{B}$ are defined by (Herrick (1983))

$$|PQLM\rangle = \sum_{l_1 l_2} |p_1 q_1 p_2 q_2 (l_1 l_2) LM\rangle (-1)^{l_2} \langle p_1 q_1 l_1, p_2 - q_2 l_2 | PQL\rangle. \tag{30}$$

Linear combinations of $\pm|Q|$ states can be constructed to be eigenfunctions of the parity operator. For convenience Herrick and Sinanoglu (1975) defined $T = |Q|$ and $K = P - n - 1$ where n is the principal quantum number of the outer electron, i.e. $n \geq N$. From configuration interaction (CI) calculations in the basis Eq. (30) Herrick and Sinanoglu found that the Hamilton matrix for intrashell states with $N = n$ is approximately block diagonal according to

$$\Delta|Q| = 0, \quad \Delta K = 0, \tag{31}$$

which means that K and Q are approximate quantum numbers for doubly excited states. This empirically found dynamical symmetry was a real surprise, in particular for the strongly coupled intrashell electrons with $n = N$. The existence of the approximate collective quantum numbers was rationalized as a consequence of angular correlation by looking at the operator $\cos\Theta$, where Θ is the interelectronic angle, (see Fig. 1). The evaluation of $\langle\cos\Theta\rangle$ is simplified in the absence of exchange of the electrons by the operator replacement $\cos\Theta \to \mathbf{b}_1\mathbf{b}_2/Nn$. In the SO(4) basis Eq. (30) this replacement leads to

$$\cos\Theta \to -\frac{K}{N} + \frac{N^2 - 1 + K^2 - T^2 + 2\mathbf{l}_1\mathbf{l}_2}{2Nn}. \tag{32}$$

The pictorial interpretation of Eq. (32) in the two limits $\cos\Theta \approx \pm 1$ is easily given in terms of two Kepler ellipses for the two electrons, oriented according to their Runge-Lenz vectors $\mathbf{b}_i$. If the two ellipses point into the same direction we have $\cos\Theta \approx 1$. The opposite case leads to $\cos\Theta \approx -1$. Note that for $\cos\Theta \approx 1$ complete degeneracy of the two single electron ellipses describing intrashell electrons will not be possible for finite nuclear charges Z because the electron–electron interaction would lead to infinite energy at the point where the two electrons meet each other. The observation suggests an non-trivial change in this type of configuration if the electron–electron repulsion is successively increased from the independent electron limit. The existence of so called planetary states is an interesting consequence, see Secs. III.B.4 and IV.C.2.a, IV.D.1.

For $n \gg N$, i.e. very asymmetrically excited states, Eq. (32) gives directly $\cos\Theta \approx -K/N$, while the operators $\mathbf{l}_i$ in the second part leads for smaller n to an admixture of other SO(4) channels. Hence, the explanation in terms of $\cos\Theta$ is at least for intrashell states $N = n$, where the assignment in terms of K, T quantum numbers works very well, not complete. We have already seen that the separability of the two center Coulomb problem supplies the 'missing link' to understand why the algebraic scheme of the coupled SO(4) representation works so well for intrashell states. In fact the derived quantum numbers are in one-to-one correspondence as can be seen from Eq. (23). We have so far not mentioned the molecular quantum number A which can be interpreted as the body-fixed electron exchange operator. The algebraic approach has with $T = m$ basically the same projection onto a (body-fixed) quantization axis as the MA with the interelectronic axis $\mathbf{R}$, here defined by $\mathbf{B} \propto \mathbf{R}$. Herrick and Sinanoglu (1975) already noticed the existence of A which they called ν (see also Herrick (1983)). The difference between the two groups of states distinguished by the two possibilities for A are most evident for states with total angular momentum $L = 0$. Then $N = n$, i.e. intrashell states, are forbidden by the Pauli principle for $A = -1$. Basically, $A = \pm 1$ is a generalization of the original classification $(2s, np) \pm (2p, ns)$ by Fano and Cooper (1965).

2. The energy level multiplets for intrashell doubly-excited states

We can now try to find an ordering of the energy levels according to similar correlation patterns defined by the quantum numbers K, T, A. We note that $L = T$ defines the lowest possible total angular momentum for a given T. If we plot within a manifold for fixed N and A the lowest resonance energies as a function of T we obtain Fig. 16. It shows a typical 'diamond' pattern where the energy axis can be identified with the scale for the quantum number K to a remarkable degree of accuracy. From Fig. 16 we can draw several conclusions: (i) Since the diagram for $A = -1$ (not shown here, see Fig. 6 in Herrick (1983)) is almost identical to the one for $A = +1$ the situation is reminiscent of the Λ-doubling phenomenon in molecules (Schutte (1976)). Indeed,

in the adiabatic molecular approximation in Sec. III.B.1 these states are exactly degenerate. (ii) The K,T quantum numbers mainly determine the correlation energy of the doubly excited states. Different angular momenta and discrete symmetries (spin, parity) have subdominant influence on the spectral ordering.

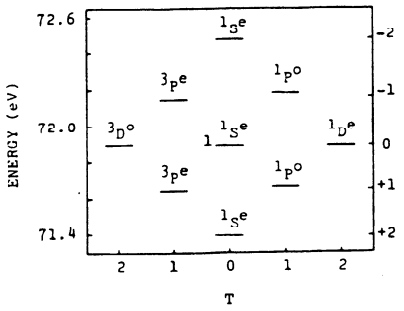

FIG. 16. Energy levels of different symmetries with $L = T$ and $A = +1$ in the $N = 3$ manifold for helium doubly-excited states (from Herrick (1983)). The energy scale on the left is in eV above the ground state, on the right the K quantum number is given.

The multiplet of Fig. 16 corresponds to the SU(2)×SU(2) decomposition of the SO(4) group in the basis of Eq. (30). The SU(2)×SU(2) decomposition with its characteristic diamond pattern for the energy levels is the basic multiplet for two-electron resonant states. Herrick and coworkers have investigated other coupling schemes and additional quantum labels leading to 'supermultiplets' which uncover even more similarities between certain groups of resonances (Herrick (1983)).

3. Supermultiplets for two-electron states

To account for the 'external' degrees of freedom, such as total angular momentum L, Herrick invented another, so called supermultiplet scheme characterized by the label $I = L - T$. It turns out that the level diagrams for fixed I look all very similar, i.e. the characteristic diamond pattern of Fig. 16 is always found. We refer to the literature (Herrick and Kellman (1980), Herrick et al. (1980)) for more details.

Another supermultiplet structure emerges, when the two-electron SO(4) group is decomposed into a series of SO(3) representations. In fact we deal with $[SO(4)]_1 \times [SO(4)]_2 = SU(2) \times SU(2) \times SU(2) \times SU(2)$. The SO(3) representations of this product group are irreducible under the operator $\mathbf{d}_>^2$, where $\mathbf{d}_>$ is the angular momentum with the larger eigenvalue $d = max(C, D)$ of $\frac{1}{2}(\mathbf{L}^2 + \mathbf{B}^2) = D(D+1)$ and $\frac{1}{2}(\mathbf{L}^2 - \mathbf{B}^2) = C(C+1)$. In terms of the coupled basis Eq. (30) the quantum number for $\mathbf{d}_>$ is

$$d = \frac{P+Q}{2} = \frac{1}{2}(N - 1 + K + T), \tag{33}$$

where the last identity follows from the definition of K and T for intrashell states $N = n$. The coupling induces the quantum number hierarchy

$$\begin{aligned} N &= 1, 2, 3, \ldots \\ d &= N-1, N-2, \ldots, 0 \ldots \\ T &= d, d-1, \ldots, 0 \\ L &= T, T+1, \ldots \\ M &= 0, \pm 1, \ldots, \pm L. \end{aligned} \tag{34}$$

According to this coupling the two-electron SO(4) product group decouples into representations

with fixed $\{d\}$. Each of these representations defines one supermultiplet $d \leq N-1$ which contains the multiplets $[K,T]$ according to the decomposition

$$\{d\} = [2d,0] + [2d-1,1] + \ldots + [d,d]. \tag{35}$$

An example of a d-supermultiplet is shown in Fig. 17.

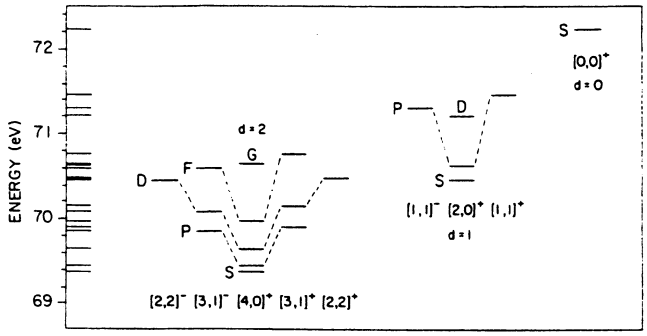

FIG. 17. Supermultiplet for $N = 3$ doubly excited states of helium (from Herrick (1983)).The energy is in eV above the ground state, the capital letters indicate total angular momentum.

The quantum number d cannot be related to the dynamics of a physical coordinate directly within the group theoretical approach. However, the comparison with the molecular approximation (Eq. (23)) reveals that d is nothing else but the number of nodes along the elliptical coordinate λ.

In this context we should also mention that Kellman and Herrick (1980) as well as Yuh et al. (1981) have formulated a model for doubly-excited states as the normal mode vibrations about the equilibrium of a linear triatomic molecule $X-Y-X$. Without going into details it is clear that the molecular approximation justifies directly this model and the interpretation of certain features in the two-electron resonances as a rovibrational structure.

D. The hyperspherical adiabatic approximation

In 1968 Macek proposed an adiabatic separation of the 'slow' radial variable $\mathcal{R} = \sqrt{r_1^2 + r_2^2}$ to describe doubly-excited states. A full set of hyperspherical coordinates for two electrons includes the hyperradius $\mathcal{R}$, the hyperangle α defined by $\tan\alpha = r_1/r_2$ and a set of four geometrical angles $\omega = (\theta_1, \phi_1, \theta_2, \phi_2)$ as usual to describe the position of the vectors $\mathbf{r}_i$ in the physical space. Hyperspherical coordinates had been used in nuclear physics before, and a coordinates has been given, e.g, by Fano and Rau (1986). The two-electron Hamiltonian reads in these coordinates

$$H = -\mathcal{R}^{-5/2}\frac{\partial^2}{\partial\mathcal{R}^2}\mathcal{R}^{5/2} + H_{\mathcal{R}} \tag{36}$$

with

$$H_{\mathcal{R}} = \frac{\mathbf{\Lambda}^2 + 15/4}{\mathcal{R}^2} + \frac{C(\alpha,\Theta)}{\mathcal{R}}, \tag{37}$$

where Λ is the grand angular momentum operator in 6 dimensions (see Fano and Rau (1986)). The three-body Coulomb potential in Eq. (37) may be interpreted as having an angular dependent charge $C(\alpha,\Theta)$ where Θ is the angle between the two electron-nucleus vectors $\mathbf{r}_1$ and $\mathbf{r}_2$, see Fig. 1. The 'grand angular momentum' operator can be expressed in terms of the two individual angular momentum operators $\mathbf{l}_i$ and the hyperangle α, see e.g. Fano and Rau (1986).

1. Potential curves and channel functions

The hyperspherical two-electron wavefunction is constructed to be an eigenfunction of the same exact symmetries as Eq. (12) with quantum numbers L, M, π, S and reads

$$\Psi^{S,t}_{L,M}(\mathcal{R},\omega) = \sum_{\mu} \mathcal{R}^{-5/2} F_\mu(\mathcal{R}) \Phi_\mu(\omega;\mathcal{R}), \tag{38}$$

where the adiabatic channel function $\Phi_\mu(\omega;\mathcal{R})$ is an eigenfunction of $H_\mathcal{R}$ from Eq. (37) with eigenvalues $\mathcal{E}(\mathcal{R})$. The expansion Eq. (37) leads to a similar set of coupled differential equations for the $F_\mu(\mathcal{R})$ as in the molecular case for the $f_i(R)$ in Eq. (14). The adiabatic approximation is invoked by truncating the expansion in μ to a single term which leads to the vibrational eigenvalue equation

$$\left(-\frac{\partial^2}{\partial\mathcal{R}^2} - \langle\Phi_\mu|\frac{\partial^2}{\partial\mathcal{R}^2}|\Phi_\mu\rangle + \mathcal{E}(\mathcal{R}) - E\right) F_\mu(\mathcal{R}) = 0. \tag{39}$$

The eigenenergies E approximate two electron energies in the adiabatic potential curves as shown in Fig. 18.

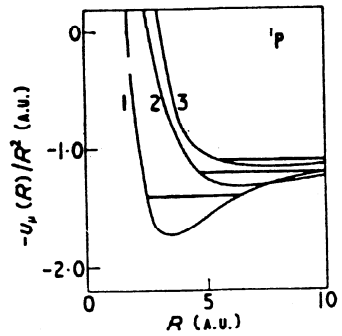

FIG. 18. Adiabatic molecular potentials $U(\mathcal{R})_\mu$ and energy levels of $^1P^o$ symmetry below He^+ ($N = 2$). (From Macek (1968)). Note that μ only counts the potential curves here and has nothing in common with the elliptical coordinate μ defined in Eq. (19).

In many respects the adiabatic hyperspherical representation is similar to the molecular representation of Eq. (12), a comparison can be found in Abramov et al. (1997). Without an apriori justification of the adiabatic separation the Rydberg series of doubly-excited states can be naturally explained as quantized states in different adiabatic hyperspherical potentials $U(\mathcal{R})$ (see Fig. 18). The difference between the molecular and the hyperspherical approximation is twofold. Firstly, in the MA the interelectronic *vector* $\mathbf{R}$ is separated, leaving for fixed $\mathbf{R}$ the solution of a three-dimensional problem, the so called two-center Coulomb problem. This separation includes the definition of a body-fixed frame (along the vector $\mathbf{R}$) which has turned out to be an important structural property of doubly excited states. (The approximate quantum number m as well as the body-fixed exchange quantum number A result from this property which is built into the algebraic approach by taking $\mathbf{B} = \mathbf{b}_1 - \mathbf{b}_2 \propto \mathbf{R}$ as an SO(4) generator, see Sec. III.C.1.) The HA separates only the scalar hyperradius $\mathcal{R}$, leaving for fixed $\mathcal{R}$ a five-dimensional problem to be solved numerically. Clearly, this requires much more numerical effort and different methods have been developed to solve this problem (see Sec. II.C.1.b). The effort is rewarded by the much better quantitative prediction of doubly-excited resonance energies compared to the MA (see e.g. Koyama et al. (1986, 1989), Fukuda et al. (1987)). However, the qualitative interpretation is difficult. The numerically solved five-dimensional Hamiltonian is not separable. Hence, the approximate separability of the body-fixed dynamics, built into the MA and in the AA from the beginning, must be reconstructed from the adiabatic potential curves. There, it can be recognized in extremely narrow avoided

crossings. A diabatic passage corresponds to a conservation of the quantum number m. Without knowing this molecular symmetry, Lin worked out in a series of papers how the algebraic quantum numbers K, T, A could be uniquely assigned to hyperspherical potential curves (Lin (1982, 1982a, 1983a), Lin and Macek (1984)). He gave rules to identify which curves had to be diabatically connected by comparing patterns of adiabatic hyperspherical wavefunctions. A new feature emerged through the introduction of the value $A = 0$ for potential curves which did not have the exchange symmetry $A = \mp 1$ in their eigenfunctions. Such potential curves have been interpreted to have dominant 'single particle' character. However, as it has been discussed in Sec. III.B.4 there exist highly correlated planetary states with another adiabatic axis $\mathbf{R} = \mathbf{r}_>$. The connection between Lin's $A = 0$ states and the planetary states has never been worked out. Nevertheless, it is clear that the planetary states can be considered as those with maximum λ–excitation $n_\lambda = N - 1$, and therefore, they can be regarded at least as a subset of Lin's $A = 0$ states. For a review of the hyperspherical work up to the mid eighties see Fano (1983) and Lin (1986).

In 1986 Watanabe and Lin re-analyzed the hyperspherical potential curves under the assumption that T or m, respectively, was the quantized projection of the total angular momentum onto a body-fixed axis, a more detailed investigation followed later (Chen et al. (1992)). Around the same time Feagin and Briggs (1986) published the adiabatic molecular formulation and the close relation between both concepts became clear (Feagin and Briggs (1988)).

2. Nodal pattern of wavefunctions and propensity rules

A second major difference between the hyperspherical and the molecular adiabatic separation lies in the fact that the three-dimensional two-center Coulomb problem is separable providing naturally a full set of quantum numbers to classify the potential curves (see Sec. III.B.1). If this quasi-separability is true it must also show up in adiabatic hyperspherical wavefunctions. Based on their beautifully regular nodal pattern Sadeghpour and Greene (1990) recognized the importance of the quantum number v_2 of Eq. (25) and deduced the propensity rule $\Delta v_2 = 0$ for photoabsorption in H^-. This propensity rule was also verified for other two-electron systems (Sadeghpour (1991), Atsumi et al. (1990), Gou et al. (1991)). It is a special case of the general propensity rule Eq. (26). Moreover, the nodal pattern of the hyperspherical wavefunctions in Fig. 19 follows indeed the spheroidal coordinates λ, μ (Eq. (19)) as predicted by the molecular approximation and pointed out by Rost et al. (1991).

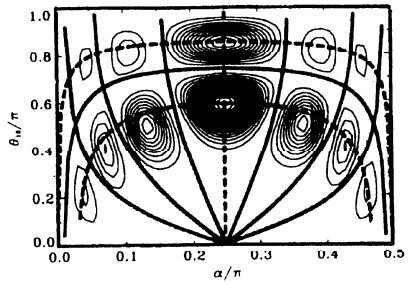

FIG. 19. Two-electron density for the $n_1 = 1, n_2 = 3, m = 1$ state of $^1P^o$ symmetry of H^- from an adiabatic hyperspherical calculation (Sadeghpour and Greene (1990)). Overlaid are the spheroidal nodal lines according to Eq. (19) from Rost et al. (1991).

To summarize the comparison of the molecular and hyperspherical adiabatic treatments, the hyperspherical approach provides a better quantitative and the molecular approximation provides a better qualitative representation of two-electron resonances. With today's computing power it is possible to determine two-electron resonances fully numerically, making adiabatic approximations for quantitative predictions unnecessary. One of the fully numerical concepts, the hyperspherical

coupled channel method (Tang et al. (1992, 1992a), Abrashkevich et al. (1995), see Sec. II.C.1.b), has evolved from the adiabatic hyperspherical approximation and has been very successful in predicting two-electron resonance phenomena, in particular photoabsorption spectra which are in impressive agreement with the experiment (see Section II.B.3.a).

Recently, a hybrid formulation has been proposed which unifies the advantage of the hyperspherical and the molecular description (Tolstikhin et al. (1995)).

E. Other quantum mechanical concepts for two-electron resonances

1. Dimensional scaling

One of the intellectually most intriguing concepts to reveal the hidden symmetries of doubly-excited states is the idea to consider the two-electron Hamiltonian as a function of the dimension D with $D = 3$ representing reality. Early work dates back to Herrick (1975a) and Herrick and Stillinger (1975). More recently Herschbach and coworkers have worked intensively on D-dimensional scaling in the context of atomic and molecular problems, for overviews see Herschbach et al. (1993), Herschbach (1993), and Witten (1980).

We sketch only briefly the idea of dimensional scaling using the simple one-electron case. General results for two-electron atoms are presented without going into details but emphasizing the insight which this concept has added to the understanding of doubly-excited states on top of the results already described.

The one-electron problem is separable in D dimensions into an angular part (depending on $D-1$ angles) and the radial part for which the Schrödinger equation reads

$$\left(-\frac{1}{2}\frac{\partial^2}{\partial R^2} + \frac{L(D)(L(D)+1)}{2R^2} - \frac{Z}{R} - E\right)\Phi(R) = 0\,. \tag{40}$$

Here, $L(D) = L_3 + \frac{1}{2}(D-3)$ is the angular momentum eigenvalue in D dimensions with L_3 being the orbital angular momentum in $D = 3$ (Herschbach (1986)). The function $L(D)$ constitutes the so called 'dimensional link', i.e.

$$(D, L) \leftrightarrow (D-2i, L+i), \quad i = 0, 1, 2, \ldots \tag{41}$$

which means, that e.g. the radial wavefunction for a spherically symmetric system of $L = 2$ in $D = 3$ is the same as the one for $L = 0$ in $D = 7$. The two-electron Hamiltonian does not have spherical symmetry. However, in the molecular adiabatic approximation it turns out that the body–fixed adiabatic wavefunction ψ from Eq. (21) remains the same in different dimensions D if its azimuthal quantum number $m(D) = m_3 + \frac{1}{2}(D-3)$ is kept the same, where m_3 is the azimuthal quantum number for $D = 3$. This demonstrates once again the strong influence of the spheroidal nodal structure of the wavefunction on two-electron states. This structure is preserved, even in arbitrary dimension D. The adiabatic vibrational motion for the D-dimensional two electron state is determined by the potential

$$V(R) = V_{im}(R) + \frac{L(D)(L(D)+1) - m(D)^2}{R^2} + \frac{(D-3)(D-5)}{4R^2}, \tag{42}$$

where the first two terms are the adiabatic potential $U^L_{im}(R)$ in $D = 3$ from Eq. (18) and V_{im} does not depend on $L(D)$. The form of Eq. (42) confirms certain exact interdimensional degeneracies as already found by Herrick and Stillinger (1975) between $(D = 3, L = 1)$ and $(D = 5, L = 0)$ where the additional centrifugal barrier, the last term in Eq. (42), vanishes.

For higher angular momenta L, the interdimensional degeneracies according to the dimensional link, Eq. (41), for $L(D)$ and $m(D)$ are only approximate. Nevertheless, the similarity between certain sets of adiabatic hyperspherical potential curves of different symmetries, noticed already by Lin (1984), can easily be explained with the dimensional link Eq. (42). Moreover, one can define so called generator states which are ground states of $^1S^e$ symmetry in some dimension $D > 3$ and

generate by virtue of the dimensional link states of different symmetry in $D = 3$ (Rost et al. (1992)).

In a more general context perturbation theory about the infinite dimensional limit $1/D = 0$ (which provides a simple but non-separable approximation) has been used to determine zeroth order normal modes for correlated dynamics (Herschbach (1986)). This approach also provided hints for the existence of approximate quantum numbers if the evolution of the normal modes is followed from $1/D = 0$ to the physical case of $D = 3$.

2. The grandparent model and the double Rydberg formula

In analogy to the Rydberg formula for singly excited states (Friedrich (1990)) it seems to be tempting to look for a similar concept for doubly excited states. Indeed, as argued semi-empirically and subsequently confirmed by numerical and experimental evidence (Read (1977, 1982), Buckman et al. (1983, 1987), Wang (1986), Lin and Watanabe (1987), Lin (1989), Molina (1989), Read (1990)), the energies of the lowest intrashell resonances $n = N$ in each manifold N can be very well described by a 'double Rydberg' formula

$$E_{N,N} = -\frac{(Z-\sigma)^2}{(N-\mu)^2}, \tag{43}$$

where $Z - \sigma$ is the screened charge of the core and μ is a two-electron quantum defect.

Rau (1983) was the first to motivate the existence of Eq. (43) theoretically with a concept that treats the highly correlated electron pair as a single particle with internal degrees of freedom (see also Rau (1984)). Over the years it turned out that this point of view leads to a kind of diabatic zeroth order approximation (see e.g. Rost and Briggs (1988, 1989), Heim et al. (1997)). However, a diabatic approximation is, in contrast to an adiabatic one, not uniquely defined. This may be one reason, why the concept of electron pairs, as appealing as it is, never really succeeded, despite the fact that the double Rydberg formula itself has been refined continuously to describe asymmetrically excited resonances as well (e.g. Sadeghpour and Greene (1990), Burgdörfer et al. (1995)).

The most natural explanation for Eq. (43) and in general for double Rydberg formulae (see Eqs. (77) and (79)) of correlated two-electron dynamics is provided by a semiclassical treatment, see Sec. IV.C. A nice quantum mechanical motivation including a generalization of Eq. (43) has emerged from analytical work in the high Z-limit which will be discussed briefly in the next section.

3. Work in the limit of large nuclear charge Z

Apart from the well known algebraic approach discussed in Section III.C there is a substantial number of papers where doubly excited states have been approached from the independent electron limit $Z \to \infty$. Numerical results have been reported e.g., by Bachau (1984, 1988), Macias and Riera (1986, 1986a) and Martin et al. (1988). An analytical method has been developed by Dmitrieva and Plindov (1988, 1988a, 1989, 1990, 1991) to determine from a perturbative quantum treatment for high Z the behavior of symmetrically excited two-electron states at, what they call, the 'lower edge' and the 'upper edge' of each manifold N. These are exactly the two collinear symmetries with $\Theta \approx 180°$ and $\Theta \approx 0°$. In accordance with the existence of the double Rydberg formula they find for the lower edge an analytical screening constant $\sigma = N^2\langle 1/r_{12}\rangle/2$ with the constant value $\sigma = 1 - 2/\pi$ and for the upper edge a screening which increases logarithmically with N, $\sigma \propto \ln N$ (Dmitrieva and Plindov (1988)). The results are only weakly dependent on the total angular momentum L of the two electrons (Dmitrieva and Plindov (1990)), an observation which is again consistent with the classical considerations to be discussed in the following. More recently, the same group generalized their work to calculate propensity rules in the high Z limit which compare favorably with the rules stated in Eq. (26) (Gerasimovich et al. (1996)).

IV. SEMICLASSICAL THEORY FOR TWO-ELECTRON ATOMS

The previous section was devoted to understand the structure of two–electron spectra as well as to describe the decay widths and propensity rules for transitions between different Rydberg series. The various methods developed so far are based solely on a possible quasi–separability of the 3–body Coulomb Schrödinger equation in suitable coordinate systems and/or the underlying group theoretical structure of the problem. Hence, the concepts introduced in the last section are purely based on quantum mechanics (even so the separability conditions might be guided by classical considerations).

In this section we will analyze the complex structure of quantum spectra of two-electron atoms in terms of the dynamics of the classical problem, i.e. two electrons moving in the Coulomb potential of a positively charged nucleus. At first sight this effort might sound contradictory, the helium atom is certainly a quantum object. However, modern developments in semiclassical theory have proven the existence of an intimate connection between the structure of quantum spectra and the dynamics of the corresponding classical system. Quantum spectra for classically integrable problems tend to be ordered and a set of quantum numbers can be assigned to each level. Wavefunctions are localized on classical tori and there is no interaction between levels corresponding to series with different 'good' quantum numbers. Quite the opposite is true for classically chaotic systems. The quantum spectra have no obvious structure, and wavefunctions are extended over the whole phase space. Energy level statistics for quantum spectra are again very different for systems with an integrable or a chaotic classical counterpart, see e.g. Bohigas (1991) or Gutzwiller et al. (1998).

The classical two–electron atom is neither integrable nor fully chaotic. The apparently regular structure in the spectrum as well as the breakdown of approximate quantum numbers for high doubly-excited states and the enormous variation in the decay widths for resonances can be understood by studying the classical dynamics in detail. Qualitative results can be obtained by exploiting semiclassical periodic orbit theory.

Modern semiclassical theory provides a link between the quantum and classical world for non–integrable systems and will be introduced in detail in Section IV.A. The analysis of the classical phase space structure for two–electron atoms will be presented in IV.B. A *qualitative* description of the quantum spectrum in terms of only a few fundamental classical periodic orbits will emerge which is discussed in Section IV.C. A more refined picture allows to calculate resonances belonging to various Rydberg series *quantitatively* from the ground state to the single ionisation thresholds in Section IV.D.

A. Introduction to modern semiclassical theory

Semiclassical theories combine classical concepts, e.g. discrete trajectories, actions and phase space probabilities with the wave mechanical nature of quantum mechanics. This offers a viewpoint which is in many respects closer to our day–to–day experience in the classical world surrounding us. However, it is far from obvious how classical, in general nonlinear, dynamics might be reflected in an inherently linear quantum theory. In this section, we will review semiclassical concepts which have been developed over the past twenty years in order to understand the influence of classical chaos on quantum mechanics. The techniques have been especially useful to broaden our understanding of two–electron atoms.

The formulation of quantum mechanics which is most semiclassical in nature is the Feynman path integral formalism. Being equivalent to the Schrödinger equation, it describes the quantum propagator as sum over possible 'events' (Feynman and Hibbs (1965)). In coordinate representation, the exact propagator $U(\mathbf{q}, \mathbf{q}'; t)$ can be written as a sum over all possible (not necessarily classical) paths from $\mathbf{q}$ to $\mathbf{q}'$ in the time t.

The crucial step leading form the quantum into the semiclassical world is performed by replacing the sum over all paths by the sum over the classical trajectories from $\mathbf{q}$ to $\mathbf{q}'$ in the time t only. Formally derived via a stationary phase approximation of the path integral this leads to the van Vleck – Gutzwiller formula (Gutzwiller (1967), see also Gutzwiller (1990)),

$$U_{sc}(\mathbf{q},\mathbf{q}';t) = \sum_{\substack{cl.tr \\ \mathbf{q}\to\mathbf{q}'}} \frac{1}{(2\pi i\hbar)^{f/2}}\sqrt{|C(\mathbf{q},\mathbf{q}';t)|}\exp\left[\frac{i}{\hbar}W(\mathbf{q},\mathbf{q}';t) - i\nu\frac{\pi}{2}\right] . \tag{44}$$

Here, $W(\mathbf{q},\mathbf{q}';t)$ is the classical action and f denotes the number of degrees of freedom. The amplitude

$$C(\mathbf{q},\mathbf{q}';t) = \det\left(\frac{\partial^2 W}{\partial q_i \partial q_j'}\right) = \det\left(-\frac{\partial p_j}{\partial q_i'}\right), \qquad i,j-1,\ldots,f \tag{45}$$

can be identified as the classical probability density of finding a trajectory going form $\mathbf{q}$ to $\mathbf{q}'$ in the time t (Gutzwiller (1990)). The integer Morse index ν is determined by the singularities in the amplitude $C(\mathbf{q},\mathbf{q}';t)$ when integrating along the path from $\mathbf{q}$ to $\mathbf{q}'$ and it corresponds to the number of caustics along the trajectory. Eq. (44) was essentially derived by van Vleck in the early days of quantum mechanics (van Vleck (1928)) long before Feynman's ingenious formalism was established. The original formula did, however, not include the Morse phases which were obtained later by Gutzwiller (1967) starting from the path integral.

The van Vleck – Gutzwiller formula (44) can be seen as the starting point of all semiclassical theories. Classical paths build the skeleton along which quantum mechanics propagates. The 'quantum flesh' originating from the non-classical contributions leads to fluctuations, which are suppressed by a factor of $\hbar$ due to destructive interference. Hence, the stationary phase approximation of the propagator is the leading term in an expansion in powers of $\hbar$. The full power series is in general an asymptotic expansion, i.e. convergence of the resulting sums is not guaranteed (Berry and Howls (1994)). The applicability of the stationary phase approximation is in itself limited due to the presence of non–smooth boundaries or classically forbidden regions leading to diffraction or tunneling corrections.

Proper error bounds for semiclassical approximations are in general difficult to obtain. In many applications, however, semiclassical techniques turn out to be surprisingly successful offering unique tools with both, diagnostic and predictive power.

1. The semiclassical Green function

For time independent Hamiltonians it is useful to go from the time domain to the energy domain, and we will concentrate on this regime from now on. The transition is established by a Laplace transformation of Eq. (44) which leads to the energy dependent Green function

$$G(\mathbf{q},\mathbf{q}';E) = -\frac{i}{\hbar}\lim_{\epsilon\to 0^+}\int_0^\infty \mathrm{d}t\, U(\mathbf{q},\mathbf{q}';t)\, \exp\left[\frac{i}{\hbar}(E+i\epsilon)t\right] .$$

The Green function exhibits poles at the eigenenergies or resonances of the system with residuals determined by the corresponding eigenfunctions at $\mathbf{q}$ and $\mathbf{q}'$. Semiclassically, the Green function $G(\mathbf{q},\mathbf{q}';E)$ can be written as sum over all classical paths from $\mathbf{q}\to\mathbf{q}'$ on the energy manifold, i.e.

$$G_{sc}(\mathbf{q},\mathbf{q}';E) = \frac{2\pi}{(2\pi i\hbar)^{(f+1)/2}}\sum_{\substack{cl.tr \\ \mathbf{q}\to\mathbf{q}'}}\sqrt{|D|}\exp\left[\frac{i}{\hbar}S(\mathbf{q},\mathbf{q}';E) - i\mu\frac{\pi}{2}\right] . \tag{46}$$

The action $S(\mathbf{q},\mathbf{q}';E) = \int_{\mathbf{q}}^{\mathbf{q}'}\mathbf{p}\,\mathrm{d}\mathbf{q}$ is taken along the classical path and we have $S(\mathbf{q},\mathbf{q}';E) = W(\mathbf{q},\mathbf{q}';t) + Et$ for trajectories on the energy manifold E. The amplitude

$$D(\mathbf{q},\mathbf{q}';E) = \frac{1}{|\dot{\mathbf{q}}||\dot{\mathbf{q}}'|}\det\left(\frac{\partial^2 S}{\partial\tilde{q}_i\partial\tilde{q}_j'}\right) , \tag{47}$$

contains the velocities $\dot{\mathbf{q}}$, $\dot{\mathbf{q}}'$ at the starting and ending points of the trajectory and $\tilde{\mathbf{q}}$ denotes an $(f-1)$ dimensional coordinate system perpendicular to the classical path (here in coordinate space)

(Gutzwiller (1971), see also Gutzwiller (1990)). The integer index μ counts the caustics along the classical path on the energy manifold (and may differ from ν in Eq. (44) only by ± 1). The validity of the semiclassical formula (46) is so far independent of the type of the underlying classical dynamics, e.g. chaotic, integrable or mixed behavior. The deviations of the semiclassical formulae (44), (46) from the exact quantum Green functions are most prominent at classical caustics corresponding to the singularities in the amplitudes $C(\mathbf{q},\mathbf{q}';t)$, $D(\mathbf{q},\mathbf{q}';E)$.

2. From classical paths to periodic orbits: trace formulae and semiclassical zeta functions

The information about the energy spectrum $\{E_n\}$ is already contained in the trace of the Green function having poles at the same positions as the full Green function, i.e. [7]

$$g(E) = \mathrm{Tr}G(E) = \int \mathrm{d}^f q\, G(\mathbf{q},\mathbf{q};E) \sim \sum_n \frac{1}{E-E_n}. \tag{48}$$

In scattering systems, the trace is defined only after subtracting the asymptotic behavior in the separable limit, i.e. $g(E) = \mathrm{Tr}[G(E) - G_0(E)]$ with $G_0 = (E - H_0)^{-1}$ and H_0 is the Hamiltonian for non–interacting particles far from the interaction zone. For bound systems, the density of states is related to the trace of the Green function by

$$d(E) = -\frac{1}{\pi}\mathrm{Im}\; g(E) := \lim_{\epsilon\to 0+} \frac{i}{2\pi}[g(E+i\epsilon) - g(E-i\epsilon)] = \sum_n \delta(E-E_n). \tag{49}$$

Closed semiclassical expressions for the trace can be given only for very restricted classes of dynamical problems. These are the two extreme cases, integrable systems on the one hand and completely chaotic systems on the other hand. In both cases, the trace can be written as a sum over classical periodic orbits of the system. The formulae are, however, very different in nature.

In integrable problems, the phase space is foliated by invariant tori, and periodic orbits occur as continuous families on tori with rational winding numbers. Here, the integration in Eq. (48) along the families can be done analytically (Berry and Tabor (1976, 1977)) and the resulting periodic orbit formula coincides essentially with the semiclassical Einstein–Brillouin–Keller (EBK) – quantization, the multidimensional generalization of the WKB - approximation (Berry and Tabor (1976), Gutzwiller (1990)). The other extreme case, hard chaos, is characterized by ergodic motion with uniform exponential separation of neighboring trajectories. All periodic orbits are unstable and isolated forming a dense set of measure zero in phase space. Both types of classical dynamics are present in two–electron atoms, a fact which has profound influence on the interpretation and semiclassical calculation of two-electron spectra.

We will present here only the trace formula for the classically chaotic case. A semiclassical treatment for integrable or near integrable dynamics can be performed within the usual EBK – formalism, see Sections IV.A.3.a, IV.D.1 and the semiclassical approximation for the trace of the Green function is not needed here.

a. *Semiclassical trace formula for chaotic systems*

Inserting the semiclassical expression (46) into Eq. (48), only those trajectories contribute which close in coordinate space. The main contributions to the trace integral come from the stationary phase points. The action along a trajectory closing in coordinate space, $S(\mathbf{q};E) = S(\mathbf{q},\mathbf{q}';E)|_{\mathbf{q}=\mathbf{q}'}$, is stationary along periodic orbits of the classical system, i.e.

---

[7] The sum over the eigenvalues in (48) is in general not convergent. This merely reflects the fact, that the Green function is not trace class; the divergence is, however, trivial and can be regularised by considering $g(E) = \mathrm{Tr}[G(E) - G(E_0)]$ for a fixed energy E_0 (Voros (1987), Keating and Sieber (1994)).

$$\frac{\partial S(\mathbf{q})}{\partial \mathbf{q}} = \frac{1}{2}\left(\frac{\partial S(\mathbf{q},\mathbf{q}')}{\partial \mathbf{q}'} + \frac{\partial S(\mathbf{q},\mathbf{q}')}{\partial \mathbf{q}}\right)|_{\mathbf{q}=\mathbf{q}'} = \mathbf{p}' - \mathbf{p}|_{\mathbf{q}=\mathbf{q}'} \stackrel{!}{=} 0. \tag{50}$$

A stationary phase approximation of the trace integral (48) may be carried out for isolated stationary phase points, a condition which requires chaotic behavior in the dynamics of the underlying classical system.[8] The trace can then be written as sum over (unstable) periodic orbits which leads to the Gutzwiller trace formula for chaotic systems (see e.g. Gutzwiller (1990)), [9]

$$g_{sc}(E) = \overline{g}(E) - \frac{i}{\hbar}\sum_{po} T_{po} \sum_{r=1}^{\infty} \frac{1}{\sqrt{|\det(\mathbf{M}_{po}^r - \mathbf{1})|}} \exp\left[ir\frac{S_{po}(E)}{\hbar} - ir\sigma_{po}\frac{\pi}{2}\right]. \tag{51}$$

The first sum is taken over all periodic orbits (po) of the classical system, where the sum over r accounts for the repetitions. The action S is taken along the orbit and T represents the period. The Monodromy or stability matrix $\mathbf{M}$ is the Jacoby matrix of the full phase space flow in a reduced local phase space coordinate system perpendicular to the trajectory and on the energy manifold. It describes the linearized dynamics in the neighborhood of the orbit after one revolution. The stability of a periodic orbit is characterized by the eigenvalues Λ of $\mathbf{M}$. The denominator $\det(\mathbf{M}_{po}^r - \mathbf{1})$ in Eq. (51) arises in a non–trivial way when merging the amplitude (47) and the second derivative of $S(\mathbf{q};E)$ at the stationary phase point Eq. (50), (see e.g. Gutzwiller 1990). Note that both the amplitude $D(\mathbf{q};E)$ and $\det(\partial^2 S(\mathbf{q})/\partial^2\mathbf{q})$ are representation dependent (here given in q – representation), the final term $\det(\mathbf{M}_{po}^r - \mathbf{1})$ as well as the actions S_{po} and the indices σ_{po} are coordinate independent as they should be in being part of a trace!

The integer index σ, also called the Maslov index, is closely related to the number of caustics μ in Eq. (46). It is equivalent to a winding number counting twice the number of revolutions of the stable or unstable eigenvectors of $\mathbf{M}$ around the periodic trajectories (Creagh et al. (1990), Robbins (1991)).

The smooth Thomas–Fermi part $\overline{g}(E)$ stems from the limit $\overline{g}(E) = \lim_{\mathbf{q}\to\mathbf{q}'} G(\mathbf{q},\mathbf{q}')$ for direct paths $\mathbf{q} \to \mathbf{q}'$ of zero length. It is connected to the mean level density via

$$\overline{d}(E) = -\frac{1}{\pi}\mathrm{Im}\,\overline{g}(E) = \frac{1}{(2\pi\hbar)^f}\int\int \mathrm{d}q^f\,\mathrm{d}p^f\;\delta(E - H(\mathbf{p},\mathbf{q})) \tag{52}$$

being proportional to the classical phase space volume on the energy manifold, (see e.g. Gutzwiller (1990)). The oscillating part in Eq. (51) containing the periodic orbit contributions is of order $\hbar^{-1}$ and is such of lower order as compared to integrable systems where the leading term of a periodic orbit expansion is of order $\hbar^{-(f+1)/2}$, see Berry and Tabor (1977).

For uniformly chaotic systems, the largest eigenvalue of the Monodromy matrix increases typically as $\Lambda_{po} \approx \exp(T_{po}\,\lambda_0)$. Here, $\lambda_0 > 0$ denotes the total Liapunov exponent of the classical dynamics corresponding to the mean separation per unit time, (see e.g. Schuster (1989)). The

---

[8] To be more precise, the stationary phase approximation requires, that the stationary phase points, here the periodic orbits, are isolated in the sense that the distance between neighboring stationary points is of the order

$$\left|\det\left(\frac{\partial^2 S(\mathbf{q})}{\partial^2\mathbf{q}}\right)\right|/\hbar \gg 1\,.$$

Note that $S(\mathbf{q})$ is a multi–valued function, and the trace integration is performed over each "action sheet" (corresponding to trajectories of comparable length) separately. The above condition requires uniform hyperbolicity of the dynamics and it is violated near marginally stable points in phase space. Hence, the applicability of the stationary phase approximation depends on local properties of the dynamics as well as on the quantum scale $\hbar$ itself (Ozorio de Almeida and Hannay (1987), Tanner (1997)).

[9] The trace formula is exact in its domain of convergence for a certain class of billiards on spaces of constant negative curvature which was proven by Selberg in 1956, see also Balazs and Voros (1986).

amplitudes in Eq. (51) behave thus like $|\det(\mathbf{M}_{po} - \mathbf{1})|^{-1/2} \approx \exp(-T_{po}\lambda_0/2)$. The number $N(T)$ of orbits with period less than T increases on the other hand exponentially with T, i.e. $N(T) \approx \exp(h_t T)$ where h_t is called the topological entropy; for uniformly chaotic and bound systems we find typically $h_t \approx \lambda_0$ (Eckhardt and Aurell (1989)).

The above consideration shows that the Gutzwiller periodic orbit sum (51) is not absolutely convergent for real energies (Eckhardt and Aurell (1989)). In mathematical terms one has to find a meromorphic extension of the trace $g_{sc}(E)$ in Eq. (51) as function of the complex energy from the region of convergence onto (or below) the real energy axis.

Such a procedure is simplified in scaling systems, where the dynamics is up to a scaling transformation independent of the energy. The energy dependence of the actions is then of the form $S(E) = f(E)S_0$, and $f(E)$ is a universal scaling function; the amplitudes are energy independent. The trace g_{sc} can then be written as a function of the complex variable $z = f(E)/\hbar$. The three body Coulomb problem is such a scaling system as will be shown in Section IV.B.1.

When constructing analytic continuations of semiclassical expressions, it is advantageous to consider the semiclassical spectral determinant introduced below.

b. The spectral determinant and semiclassical zeta functions

The convergence problem mentioned above can be overcome by choosing a suitable expansion of the semiclassical spectral determinant $D_{sc}(E)$ which is the semiclassical approximation of

$$D(E) = \det(E - \hat{H}) = \prod_n (E - E_n).$$

The spectral determinant can be expressed in terms of the trace of the Green function via $D(E) = \exp\left[\int \mathrm{d}E' g(E')\right]$. Inserting the semiclassical expression (51) leads to

$$\begin{aligned} D_{sc}(E) &= A(E)e^{-i\pi\overline{N}(E)} \prod_{po} \exp\left[-\sum_{r=1}^{\infty} \frac{\exp\left[ir(S_{po}(E)/\hbar - \sigma_{po}\pi/2)\right)}{r\sqrt{|\det(\mathbf{M}_{po}^r - \mathbf{1})|}}\right] \\ &= A(E)e^{-i\pi\overline{N}(E)}\zeta_{sc}^{-1}(E). \end{aligned} \tag{53}$$

The energy integration is carried out by using the relation $T_{po} = \partial S_{po}/\partial E$ and $\overline{N}(E)$ denotes the integrated mean level density Eq. (52), (or mean level staircase function). The function $A(E)$ originates from the (regularised) real part of $\overline{g}$ and contributes as smooth background non–zero everywhere. The last equality defines the semiclassical zeta function [10] $\zeta_{sc}^{-1}(E)$.

For two dimensional systems, the amplitude $|\det(\mathbf{M}_{po}^r - \mathbf{1})|^{-1/2}$ may be expanded in terms of the eigenvalues of $\mathbf{M}$. The sum over the repetitions is then equivalent to the Taylor series of the logarithm. We may thus finally write the zeta function as (Miller (1975), Voros (1988))

$$\zeta_{sc}^{-1}(E) = \prod_{po}\prod_{l=0}^{\infty}(1 - t_{po}^{(l)}) \qquad \text{with} \quad t_{po}^{(l)} = \frac{\exp[i(S_{po}(E)/\hbar - (l + 1/2)\sigma_{po}\pi)]}{|\Lambda_{po}|^{l+1/2}}. \tag{54}$$

The products (53), (54) are again not absolutely convergent. The zeros of the single factors in Eq. (54) are therefore not the true zeros of the zeta function corresponding to the quantum eigenvalues. However, the determinant structure of $D(E)$ allows one to expand the product in a

---

[10] The name originates from the similarity of Eqs. (53), (54) with the Riemann zeta function. Its representation both, as a sum over the natural numbers, $\zeta_R(s) = \sum_n n^{-s}$ or as a product over the prime numbers $\zeta_R(s) = \prod_p (1 - p^{-s})^{-1}$, is also not absolutely convergent for Im $s \leq 1$. An analytic continuation of the Riemann zeta function can, however, be given explicitly (Titchmarsh (1986)).

controlled way guided by the cumulant expansion for infinite matrices. These expansions can be shown to lead to convergent expressions being analytic in a strip containing the real axis. The zeros of these functions are then the approximate eigenvalues of the corresponding quantum problems. Details will be presented in Section IV.A.3 and when applying this formalism to two-electron atoms in Section IV.D.

c. The S–matrix and periodic orbits

The periodic orbit formulae discussed in the previous sections are valid also for scattering systems provided the Green function has been appropriately regularised before taking the trace. However, for scattering systems, it might be more useful to work with the scattering matrix directly. A direct connection between the S–matrix and the trace of the Green function, (and thus periodic orbit formulae), is provided by Krein's formula (Krein (1953)) [11]

$$\lim_{\epsilon\to 0} \mathrm{Im}\mathrm{Tr}\,[G(E+i\epsilon) - G_0(E+i\epsilon)] = \frac{i}{2}\frac{\mathrm{d}}{\mathrm{d}E}\log\det \mathbf{S}(E). \tag{55}$$

In the semiclassical approximation, the periodic orbit contributions are contained in the trace of the full Green function. The reference Green function G_0 is needed to regularize the zero–length term.

We obtain the determinant of the S–matrix in terms of semiclassical zeta functions after formally integrating and exponentiating Eq. (55) on both sides. After splitting up the imaginary part into a contribution from the upper and the lower complex energy half plane, we obtain (Wirzba (1997))

$$\det \mathbf{S}(E) = e^{-2\pi i\tilde{N}(E)}\frac{\zeta_{sc}^{-1}(E^*)^*}{\zeta_{sc}^{-1}(E)}\,. \tag{56}$$

The zeta function $\zeta_{sc}^{-1}(E)$ introduced here is defined in Eq. (54), the product runs now over all classical periodic orbits of the scattering system. The phase $\tilde{N}(E)$ is the effective phase space volume of the scatterer (Smilansky and Ussishkin (1996)); its derivative with respect to energy is directly related to the mean delay time caused through the scattering process. The representation (56) is very similar to the form of the S–matrix in quasi one–dimensional partial wave scattering problems written as fractions of Jost–functions, see Taylor (1972). It reveals the connection between the zeros of the zeta function and the poles of the S–matrix. The resonances of a scattering system (as, e.g. two electron atoms) are thus intimately connected to the classical periodic orbits, which indeed form the backbone of the bounded part of the classical dynamics.

The trace formula (51) and the determinants (53) and (56) connect two at first instant very distinct sets characterizing classical and quantum systems. These are the periodic orbits and the quantum eigenvalues or resonances. The classical ingredients, e.g. the actions, stabilities and winding numbers of periodic orbits as well as the quantum eigenvalues, are invariant under coordinate transformation and so are the quantum and semiclassical traces. The connection between these two different sets is, however, intriguing. Both for classically chaotic as well as for integrable systems, it is the sum over all periodic orbits which gives rise to the poles at the eigenenergies. There is in general no direct relation between single periodic orbits and individual eigenstates. To the contrary, a quantization of single periodic orbits must be regarded as the exception rather than the rule, a fact which is often confused in the literature. Single periodic orbit quantization is possible e.g. for one dimensional systems, where all orbits are periodic. Other examples are the harmonic oscillator and the Coulomb–problem, which are special in having constant frequency ratios for the

---

[11] Strictly speaking, Eq. (55) is applicable only after putting the whole system in a large box to obtain a discrete spectrum for both G and G_0. The imaginary part of the traces is (up to a factor of π) the level density Eq. (49); it is properly defined only by setting $\mathrm{Im}\,\mathrm{Tr}G(E+i\epsilon) := -\frac{i}{2}[\mathrm{Tr}G(E+i\epsilon) - \mathrm{Tr}G(E-i\epsilon)]$. Letting the box radius go to infinity before taking ϵ to zero provides the finite, nontrivial result.

dynamics along the various degrees of freedoms. The hierarchical structure of the periodic orbit sum allows, however, for approximate quantizations schemes using a few periodic orbits only, which will be described in the next section.

3. Semiclassical quantization for integrable and chaotic dynamics: EBK–quantization and periodic orbit expansions

In the following, we will describe how to use periodic orbit information efficiently to obtain semiclassical estimates for individual eigenvalues. We will first review the integrable case and discuss then the semiclassical quantization for chaotic systems.

a. Einstein Brioullin Keller (EBK) quantization

A semiclassical quantization for integrable dynamics leads to the well known Einstein–Brioullin–Keller (EBK) quantization, the multidimensional generalization of WKB–quantization in one dimension. It can be derived directly by constructing WKB–type wavefunctions in action–angle variables. The boundary conditions on the torus then lead to the usual Bohr–Sommerfeld quantization conditions for the actions $\mathbf{I}$, (see e.g. Gutzwiller (1990)),

$$I_j(k_j) = 2\pi\hbar(k_j + \frac{\sigma_j}{4}), \qquad \text{with } k_j \text{ positive integer}, \quad j = 1, \ldots, f. \tag{57}$$

The integer Maslov index σ_j labels the number of caustics within a full 2π rotation in the angle ϕ_j conjugated to I_j.

The integrability condition ensures that the classical Hamiltonian can be written as a function of the actions alone and the semiclassical eigenenergies are then given by

$$E_{\mathbf{k}} = H\left(I_1(k_1), \ldots, I_f(k_f)\right). \tag{58}$$

A quantum eigenvalue corresponds thus to a torus characterized by actions $\mathbf{I}$ being integer multiples of $\hbar$ (up to the topological phases). The corresponding wavefunction (in Wigner representation, see Gutzwiller (1990) for details) is localized on this torus (Berry (1977), Ozorio de Almeida and Hannay (1983)). Note that the trajectories on tori characterized by these conditions are in general not periodic; the periodic orbit condition is

$$\omega(\mathbf{I_N})\, T_{\mathbf{N}} = 2\pi\mathbf{N}, \tag{59}$$

where $T_{\mathbf{N}}$ is the period of that orbit and $\mathbf{N}$ denotes a f–dimensional integer vector. The frequencies ω are given by $\omega(\mathbf{I}) = \nabla_I H(\mathbf{I})$, which is not equivalent to Eq. (57).

The EBK–formalism was used by Leopold and Percival (1980) in an early attempt to quantize helium assuming an integrable phase space structure, see Section II.A.2. It will also play a fundamental role when quantizing the so-called collinear frozen planet configuration in Section IV.C.2.a, IV.D.1.

b. Periodic orbit quantization for chaotic systems

The periodic orbit formula (51) for chaotic systems is not absolutely convergent for real energy E and the sum depends thus on the order of summation. A natural ordering parameter for periodic orbit sums is the action or equivalently the period of the orbits. The minimal period needed to resolve structures on the scale of the mean level spacing $1/\bar{d}(E)$ is given by the so–called Heisenberg time,

$$T_H = 2\pi\hbar\bar{d}(E). \tag{60}$$

T_H is also the time scale which it takes for a smooth wavepacket centered at energy E to develop structures of the size of a Planck–cell.

Convergence of the trace (51) can be achieved by Gaussian smoothing (Aurich et. al (1988), Sieber and Steiner (1990)) which is equivalent to an effective cut–off in the summation. Inspired by the Riemann–Siegel relation for the Riemann zeta function (Titchmarsh (1986)), Berry and Keating (1990) expanded the semiclassical spectral determinant (53) by multiplying out the various factors in Eq. (54). The terms in the resulting sum are then ordered with increasing period of orbits and so-called composite orbits up to half the Heisenberg time. Similar methods have been reported by Sieber and Steiner (1991).

The techniques mentioned above are suitable for bound quantum systems only. In the following we will introduce a slightly different concept based on quantum and classical Poincaré maps and their associated symbolic dynamics. This leads us to the well controlled theory of spectral determinants for infinite matrices. These determinants are calculated in terms of so-called cumulant expansions, which provide a guide for periodic orbit expansions of semiclassical zeta functions valid both for bound spectra and resonances and hence is appropriate for two-electron atoms.

The classical Poincaré map is a discretisation of the phase space flow acting on a $2n-2$ dimensional sub-manifold of the full phase space defined by the condition $f(\mathbf{q},\mathbf{p})=0$; $H(\mathbf{q},\mathbf{p})-E=0$; the mapping is given by subsequent crossings of a trajectory with the Poincaré surface of section. Choosing, e.g. $f=q_f$, (which may be achieved after an appropriate coordinate transformation), one may define in analogy a quantum Poincaré map acting as a discrete quantum propagator on wave functions in an $f-1$ dimensional space $\mathbf{q}=(q_1,\dots q_{f-1})$,

$$\psi_{n+1}(\mathbf{q}') = \int \mathrm{d}q^{f-1}\; T(\mathbf{q},\mathbf{q}';E)\;\psi_n(\mathbf{q}).$$

The so–called transfer operator $T(\mathbf{q},\mathbf{q}';E)$ is unitary for bound systems reflecting the phase space conservation of the classical map. Neither the classical Poincaré map nor the corresponding quantum transfer operators can in general be given analytically. The classical map is usually obtained by solving the equations of motion numerically. Explicit constructions of corresponding quantum maps is a much more elaborate task even so there are quite general methods available today (Doron and Smilansky (1992), Dietz and Smilansky (1993), Prosen (1994, 1995, 1996), Rouvinez and Smilansky (1995)). The quantum Poincaré map contains the whole information about the quantum spectrum. The quantum eigenvalues correspond to energies E for which a fixed point of the quantum map exists, i.e. $\psi = T(E)\,\psi$. Hence, the quantization condition can be cast into the form

$$\det[1-T(E)]=0. \tag{61}$$

This connection was first established in the semiclassical context by Bogomolny (1992) and independently by Doron and Smilansky (1992). The semiclassical expression for the transfer operator is

$$T_{sc}(\mathbf{q},\mathbf{q}';E) = \frac{1}{(2\pi i\hbar)^{(f-1)/2}} \sum_{\substack{cl.tr\\ \mathbf{q}\to\mathbf{q}'}} \sqrt{\left|\det\left(\frac{\partial^2 S}{\partial q\partial q'}\right)\right|}\;\exp\left(\frac{i}{\hbar}S(\mathbf{q},\mathbf{q}';E)-i\mu\frac{\pi}{2}\right), \tag{62}$$

where the $f-1$ dimensional vectors $\mathbf{q}$, $\mathbf{q}'$ lie on the Poincaré surface of section. The structure of the operator is similar to the energy dependent Green function (46) but the sum is taken now over all classical paths from $\mathbf{q}$ to $\mathbf{q}'$ crossing the Poincaré surface only once. In stationary phase approximation the trace of the transfer operator T^n is linked to the periodic orbits of the n-th return of the classical Poincaré map, i.c.

$$\mathrm{Tr}\;T^n_{sc}(E) = \sum_{po}^{(n)} \frac{\exp(\frac{i}{\hbar}S_{po}(E)-i\sigma_{po}\frac{\pi}{2})}{\sqrt{|\det(\mathbf{M}_{po}-\mathbf{1})|}}. \tag{63}$$

By using the basic relation

$$\det(1-T) = \exp[\mathrm{Tr}\log(1-T)] = \exp\left(-\sum_{n=1}^{\infty}\frac{1}{n}\mathrm{Tr}\,T^n\right), \tag{64}$$

one obtains again the semiclassical zeta function Eqs. (53), (54) as products over periodic orbits. The representation (64) suffers obviously from the same deficit as the periodic orbit zeta function. However, the computation of determinants and traces of infinite dimensional operators is well understood, see e.g. Reed and Simon (1972), Wirzba (1997). Provided the operator T has the so called trace class property, (which essentially means, that the trace exists and converges), the determinant can be written as

$$\zeta^{-1}(E) = \det[1-T(E)] = \sum_{m=0}^{\infty} c_m(E), \tag{65}$$

where the cumulant or curvature terms c_m are defined recursively as

$$c_m = -\frac{1}{m}\sum_{k=0}^{m-1}\mathrm{Tr}\,T^{m-k}\,c_k; \qquad c_0 = 1. \tag{66}$$

The trace class condition ensures that the sum converges faster than exponential for large m. [12] Writing out the first few terms in the expansion, we obtain

$$\zeta^{-1}(E) = 1 - \mathrm{Tr}T - \frac{1}{2}\left(\mathrm{Tr}T^2 - (\mathrm{Tr}T)^2\right) - \frac{1}{3}\left(\mathrm{Tr}T^3 - \frac{3}{2}\mathrm{Tr}T^2\mathrm{Tr}T + \frac{1}{2}(\mathrm{Tr}T)^3\right) - \frac{1}{4}\ldots . \tag{67}$$

The convergence of the cumulant expansion (65) originates from cancelations between the various traces. This means in terms of periodic orbits that an exponentially increasing number of orbits contained in Tr T^m is balanced in a delicate way by products of shorter orbits to make the total curvature term c_m decrease exponentially with m. The classical dynamics represented by the periodic orbits must obviously carry a lot of redundant information.

The cancelation mechanism is indeed an effect caused by the self-similarity of the phase space dynamics in chaotic systems. It can be understood on the basis of individual orbits when introducing the concept of symbolic dynamics. We can not go into the details of coding theory for deterministic, fully chaotic systems, here. We just note that chaotic dynamics can often be mapped onto a symbolic code of say n–symbols in the sense that there is a one–to–one correspondence between trajectories in phase space and all possible infinitely long symbol sequences. For details see e.g. Schuster (1989) or Cvitanović (1998) and references therein. The symbolic dynamics is in general linked to a Poincaré surface of sections and the length of the code marks the iterates of the map. The (collinear) three-body Coulomb problem is a prototype of a physical system where such a symbolic dynamics exists, see Section IV.B.2.

With the help of a symbolic code the expansion (67) can be rewritten on the basis of individual orbits in terms of a so-called cycle expansion (Cvitanović (1988), Artuso et al. (1990)). For a binary code denoted by the symbols {0,1} (as e.g. in the collinear three body Coulomb problem) the cycle expansion for ζ^{-1} reads

$$\zeta_{sc}^{-1} = 1 - t_0 - t_1 - [t_{01} - t_0 t_1] - [t_{001} - t_0 t_{01} + t_{011} - t_{01} t_1] - \ldots \tag{68}$$

with

$$t_{po} = \frac{1}{\prod_{j=1}^{f-1}\sqrt{\Lambda_{po,j}}}\exp\left(i\frac{S_{po}(E)}{\hbar} - i\sigma_{po}\frac{\pi}{2}\right) \tag{69}$$

---

[12] The trace class property can in general be relaxed by introducing a suitable regularisation mechanism, see Reed and Simon (1972), Voros (1987).

and $\Lambda_{po,j} > 1$ being the $f-1$ leading eigenvalues of the Monodromy matrix $\mathbf{M}_{po}$. (The denominator in Eq. (53) is here approximated using $|\det(\mathbf{M}_{po} - \mathbf{1})| \approx \prod_{j=1}^{f-1} \Lambda_{po,j}$, see Artuso et al. (1990); this is equivalent to considering only the $l = 0$ – term in Eq. (54).) The cycle expansion provides a very detailed insight into the structure of the zeta function and the cancelation mechanism between the various periodic orbit contributions. The expansion has the form of a perturbation series. The zeta function is dominated by short periodic orbits; the contributions of long orbits become negligible due to increasing cancelations between orbits and composite orbits. The cancelation mechanism is energy dependent; the minimal number of terms c_m to be included in the expansion can be estimated with the help of the mean level density (being the mean density of zeros of $\zeta^{-1}(E)$ on the real energy axis), i.e.

$$m_{min} = \frac{T_H}{T_0} = \frac{2\pi\hbar\bar{d}(E)}{T_0},$$

where T_0 is the average return time for the Poincaré map. The cycle expansion has been tested successfully for both bound and scattering problems (Cvitanović and Eckhardt (1989), Tanner et al. (1991), Wirzba (1992)).

Periodic orbit theory provided also the missing link for the long outstanding semiclassical quantization of the helium atom; the cycle expansion technique allowed for the first time to calculate bound states (including the ground state) and resonances in helium semiclassically in a consistent way (Ezra et al. (1991)). Still the essential requirement for a semiclassical treatment is the understanding of the classical dynamics of this three–body Coulomb problem which will be summarized below.

B. Two-electron atoms: a classical analysis

In this section we discuss the classical phase space dynamics of two–electron atoms with an emphasis on helium. We first give a general characterization of the problem and describe the treatment of the various singularities present in the equations of motion. We will then concentrate on total angular momentum $L = 0$ and identify three lower dimensional invariant subspaces of the full phase space. They are of special importance for doubly excited states and will be studied in detail.

1. General overview: Integrals of motion, scaling properties and regularisation techniques

a. The Hamiltonian and scaling properties

The classical three–body system can be reduced to four degrees of freedom after eliminating the center of mass motion and incorporating the conservation of the total angular momentum. In the special case of zero angular momentum, the motion of the three particles is confined to a plane fixed in configuration space (Pars (1965)) and the problem reduces to three degrees of freedom. We will as usual work in the infinite nucleus mass approximation. The classical Hamiltonian for a two-electron atom is then given by Eq. (1); the Hamiltonian including finite nucleus mass terms and after elimination of the center of mass coordinates can be found in Richter et al. (1993).

The energy dependence of the classical dynamics is equivalent to a scaling transformation of the classical motion in phase space, since the potential energy in Eq. (1) is a homogeneous function of the coordinates. Choosing the canonical transformation

$$\mathbf{r}_i \to \frac{1}{\alpha}\,\mathbf{r}_i, \quad \mathbf{p}_i \to \sqrt{\alpha}\,\mathbf{p}_i, \quad i = 1, 2 \tag{70}$$

and introducing a time transformation $t \to \alpha^{-3/2}\ t$ eliminates the energy dependence in the classical Hamiltonian, i.e.

$$H = \frac{\mathbf{p}_1^2}{2} + \frac{\mathbf{p}_2^2}{2} - \frac{Z}{r_1} - \frac{Z}{r_2} + \frac{1}{r_{12}} = \begin{cases} +1 : E > 0 \\ 0 : E = 0 \\ -1 : E < 0 \end{cases} \tag{71}$$

with $\alpha = \pm E > 0$, respectively. The scaling property simplifies classical calculations considerably. The classical dynamics has to be studied only for $H = \pm 1, 0$; its behavior for other energies is then obtained by the scaling transformation (70).

The $H = +1$ regime corresponds to the energy region where three body breakup is possible. There exist no periodic orbits of the electron pair and at least one electron always escapes to infinity. The classical dynamics for $E > 0$ is important when studying the energy dependence of the total quantum cross section for three particle fragmentation. The cross section can be deduced from purely classical considerations by studying the classical three particle breakup along the so–called Wannier orbit (see e.g. Wannier (1953), Eckhardt (1991)). The resulting threshold law was first derived by Wannier (1953) for small energies above $E = 0$ and later extended to $E > 0$ (Rost (1994)). A detailed discussion of this energy regime can be found in Rost (1995, 1998).

The classical dynamics for $H = -1$ is linked to the quantum energy regime $E < 0$ where the bound and resonance spectrum of two electron atoms can be found, see Fig. 9. Only one electron can escape classically and it will do so for most starting conditions. The remaining classical one electron system has no lower bound for the energy, and there is in turn no upper limit on the kinetic energy carried away by the ionizing electron. We will discuss the classical aspects of this energy regime in Section IV.B.2.

The classical action S and the (conserved) total angular momentum $\mathbf{L}$ scale like

$$S \to \frac{1}{\sqrt{\pm E}}\, S, \quad \mathbf{L} \to \frac{1}{\sqrt{\pm E}}\, \mathbf{L}. \tag{72}$$

Note that the angular momentum in the scaled coordinates converges to zero with increasing electronic excitation ($E \to 0$) and fixed unscaled $\mathbf{L}$. The dynamics of *high* doubly–excited quantum states with moderate total angular momentum are thus semiclassically connected to a quantization of the planar configuration $\mathbf{L} = 0$ in the scaled variables. This fact is exploited when considering the influence of the classical dynamics at $\mathbf{L} = 0$ on quantum states with angular momentum $\mathbf{L} \neq 0$, see IV.C.3. It also plays an important role when studying the cross section at the three particle break–up threshold $E = 0$ (Rost (1998)).

The scaled action S for a trajectory from $\mathbf{q}$ to $\mathbf{q}'$ (with $\mathbf{q} = (\mathbf{r}_1, \mathbf{r}_2)$) is related to the scaled time t along the path, i.e.

$$\frac{1}{2} S(\mathbf{q}, \mathbf{q}') = t(\mathbf{q}, \mathbf{q}') + (\mathbf{p}'\mathbf{q}' - \mathbf{p}\mathbf{q}) \,, \tag{73}$$

where $\mathbf{p}$, $\mathbf{p}'$ denote the momenta at the start and ending point. We obtain $T_{po} = \frac{1}{2} S_{po}$ for periodic orbits.

b. Regularisation of the two–body collisions

The equations of motion for the three body Coulomb problem diverge whenever two of the three particles collide, i.e. an inter–particle distance vanishes. In order to integrate the classical trajectories it is essential to regularize the dynamics near these collisions. There is a fundamental difference between the two–body collisions $r_1 = 0$, $r_2 = 0$ or $r_{12} = 0$ and the triple collision $r_1 = r_2 = r_{12} = 0$. The two–body collisions can be regularised, i.e. solutions of the classical equations of motion can be uniquely continued through the singular points. This can be done by introducing a so-called Kustaanheimo–Stiefel (KS) – transformation (Kustaanheimo and Stiefel (1965), Aarseth and Zare (1974)). The technique was originally developed in celestial mechanics to obtain numerically stable solutions for planetary motion. It consists of a coordinate-dependent time transformation which stretches the time scale near the origin and a suitable canonical transformation in the coordinates. The application of the technique to the planar three body Coulomb configuration is outlined in detail in Richter et al. (1993).

The singularity at the triple collision is essential and can not be regularised. A trajectory, which hits the singularity has indeed no future, i.e. there is no way to tell, how the trajectory will leave the singular point again. A trajectory starting in the singularity has no past in the same sense. The dynamics near the triple collision is extremely sensitive to small changes in the initial conditions and dynamics in this regime is very unstable. The triple collision singularity is the source for strong chaos in the three–body Coulomb problem, see Sec. IV.B.2.

c. Symmetries and invariant subspaces

The Hamiltonian for two-electron atoms, Eq. (1), has certain discrete symmetries. The equations of motion are invariant under parity transformation $(\mathbf{r}_1, \mathbf{r}_2) \rightarrow (-\mathbf{r}_1, -\mathbf{r}_2)$ as well as particle exchange transformation $(\mathbf{r}_1, \mathbf{r}_2) \rightarrow (\mathbf{r}_2, \mathbf{r}_1)$. The latter symmetry is quantum mechanically linked to the total spin quantum number due to the antisymmetry of the full wave function (when neglecting spin orbit coupling, see Sections II.B.1, III.B.1).

The symmetries give rise to invariant subspaces in the full phase space. Trajectories which start in such a subspace will remain there for all times thus reducing the relevant degrees of freedom of the dynamics. Invariant subspaces are an extremely useful tool to study classical dynamics in a high dimensional phase space. They serve as a low dimensional window into the full dynamics; access to the full phase space in the vicinity of the symmetry plane can be obtained by studying the linearized dynamics in all degrees of freedom for trajectories in the symmetry plane.

The symmetry planes which exist for $L = 0$ turn out to be crucial for an understanding of two–electron spectra and will be discussed in detail in the following section. The three existing invariant subspaces are:

(i) the *Wannier ridge*
$r_1 \equiv r_2$; $p_{r_1} \equiv p_{r_2}$.

(ii) the collinear eZe configuration
$\Theta \equiv \pi$; $p_\Theta \equiv 0$.

(iii) the collinear Zee configuration
$\Theta \equiv 0$; $p_\Theta \equiv 0$.

The particle exchange symmetry allows to reduce the configuration space for the collinear configurations to the domain $r_1 \geq r_2$, i.e. we can (and will henceforth) always assume $r_1 \geq r_2$ and treat an encounter with the symmetry line $r_1 = r_2$ as hard wall reflection (Wintgen et al. (1992)); the Wannier ridge lies exactly in this symmetry plane $r_1 = r_2$.

2. Invariant subspaces: collinear configurations and the Wannier ridge

In the following, we will discuss the three invariant subspaces mentioned above for $H = -1$. We concentrate first on the collinear configurations which form the backbone of the semiclassical quantization of helium introduced in Section IV.D.

a. Collinear Helium: the Hamiltonian and general properties

The collinear configurations are 4–dimensional invariant subspaces of the 6–dimensional phase space $\mathbf{L} = 0$; the three particles move along a common axis and the two degrees of freedom are the electron–nucleus distances r_1 and r_2. We may further distinguish between the situation, where both electrons are on the same side of the nucleus (Zee or $\Theta = 0$ – configuration) or on opposite sides of the nucleus (eZe or $\Theta = \pi$ – configuration). Collinear two-electron atoms attracted attention only recently after their fundamental role for the semiclassical quantization of the helium spectrum was discovered (Ezra et al. (1991)). The classical dynamics of the collinear subspaces has been

investigated in detail by Kim and Ezra (1991), Ezra et al. (1991), Blümel and Reinhardt (1991), Richter (1991), Richter et al. (1993), and Gaspard and Rice (1994). Collinear collision dynamics has also been studied by Gu and Yuan (1993) and Tang et. al (1996) and has been used to develop the classical S-matrix theory for reactive scattering in molecular problems by Miller (1974) and others.

Handke et al. (1993) and Dräger et al. (1994) studied the so–called s–wave helium which is similar to the eZe classical collinear dynamics even so the quantum arguments motivating the model are quite different in nature. The model treats the electrons as pure s–waves, i.e. the classical dynamics of both electrons takes place only in radial direction. Electron-electron repulsion is included through an effective screening of the nucleus by the actual inner electron as seen by the then outer electron. The screening is assumed to change abruptly whenever the electrons change places i.e. the inner electron becomes the outer one and vice versa which makes the classical dynamics non-trivial.

Classical calculations for collinear three particle Coulomb problems with mass ratios different from those found in two-electron atoms have been performed recently by Duan et al. (1998).

The collinear Hamiltonian is given by

$$H^{\pm} = \frac{p_1^2}{2} + \frac{p_2^2}{2} - \frac{Z}{r_1} - \frac{Z}{r_2} + \frac{1}{|r_1 \pm r_2|} = -1. \tag{74}$$

The $\pm$ sign corresponds to the two possible configurations. The potential together with the shortest periodic orbits are displayed in Fig. 20.

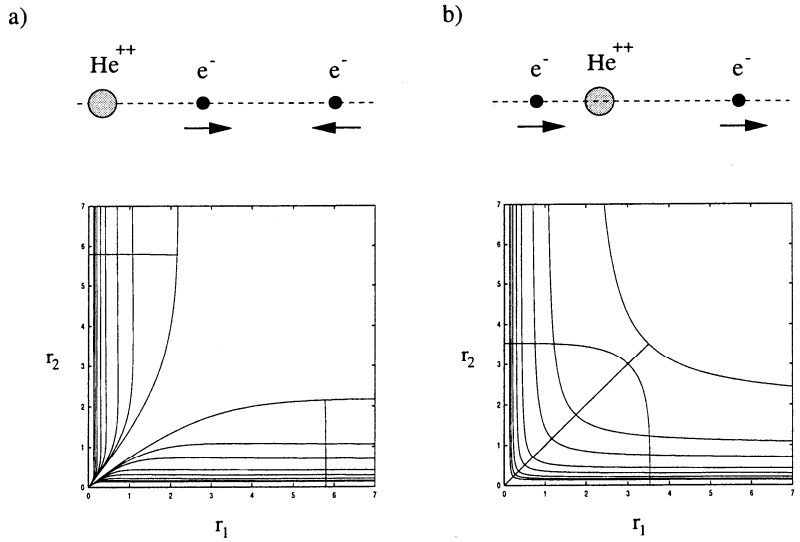

FIG. 20. The potential $V(r_1, r_2) = -\frac{Z}{r_1} - \frac{Z}{r_2} + \frac{1}{|r_1 \pm r_2|}$ in the classically allowed regime $V \leq E$ together with the shortest periodic orbits; a) the Zee–configuration with both electrons on one side of the nucleus together with the stable frozen planet orbit (FP); b) the eZe–configuration with electrons on different sides of the nucleus together with the unstable asymmetric stretch orbit (AS).

In the Zee – case, surprisingly, the electron–electron repulsion leads to a stabilization of the dynamics for $Z > 1$. The electrons cannot penetrate each other, and there is a well defined inner and outer electron for all times. The inner electron bounces back and forth into the nucleus while the outer electron performs an oscillation at a finite distance from the nucleus, which is in turn driven by the motion of the inner electron. The shortest periodic orbit (shown in Fig. 20(a)) corresponds to a configuration where the outer electron is almost frozen at a finite distance from the nucleus. The orbit resembles the situation of a planetary system where the outer planet is fixed in a position

far from the origin (Richter and Wintgen (1990a), Richter et al. (1992)). [13] The frozen planet orbit (FP) is indeed stable and is surrounded by a stable island which dominates the whole phase space, see Fig. 21(a) (Richter (1991), Wintgen et al. (1994)); the Poincaré section in Fig. 21(a) corresponds to $r_2 = 0$, i.e. we plot the momentum and position of the outer electron, whenever the inner electron hits the nucleus. The frozen planet orbit is also stable with respect to the Θ–degree of freedom perpendicular to the symmetry plane thus forming the center of a stable island in all six phase space coordinates. This behavior persists over a wide range of Z–values (Richter (1991)) and even for angular momentum $L \neq 0$ (Yamamoto and Kaneko (1993)). The frozen planet orbit proves in particular that the dynamics of two–electron atoms is *not* ergodic.

This is in contrast to the eZe – configuration where the energy transfer between the electrons depends sensitively on how the particles approach the origin. The fundamental difference of the dynamics in both cases can be seen in the Poincaré surface of sections in Fig. 21. No stable islands are visible in the eZe – configuration and especially the region near the origin in the Poincaré plane is completely structure less. In the following, we list some basic properties of the dynamics for the collinear subspaces (for further details see Richter et al. (1993) and Blümel and Reinhardt (1997) as well as Handke et al. (1993) for the related s-wave helium):

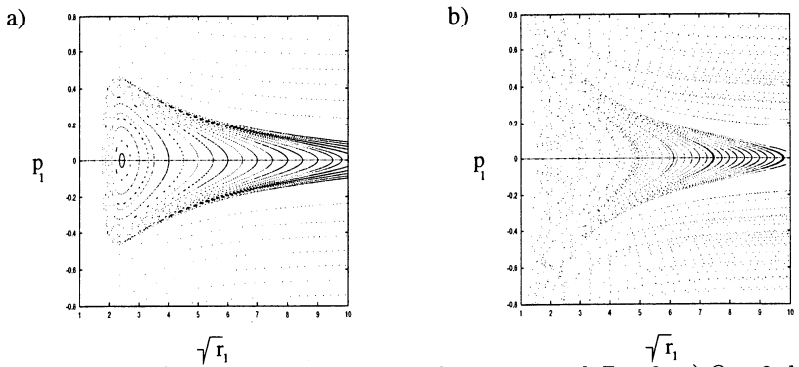

FIG. 21. Poincaré map (r_2=0) for the two collinear configurations and $Z = 2$: a) $\Theta = 0$; b) $\Theta = \pi$. The FP-orbit is at the center of the stable island in a).

- Both collinear configurations are unbound in the sense that one electron (say electron 1) can escape, i.e. ionize classically, with an arbitrary amount of kinetic energy. The other electron then remains in a Kepler motion with total energy in the range $[-\infty, -1]$. There is no energy barrier in coordinate space which allows to distinguish between bound and unbound motion. However, from general kinetic arguments it is easy to deduce that the outer electron will never return when $p_1 > 0$, $r_2 \leq Z$ at the turning point of the inner electron $p_2 = 0$.

- In the limit $r_1 \to \infty$ the Hamiltonian (74) takes on the form of two non–interacting Kepler problems, i.e.

$$H \underset{r_1 \to \infty}{\longrightarrow} \left(\frac{p_2^2}{2} - \frac{Z}{r_2}\right) + \left(\frac{p_1^2}{2} - \frac{Z-1}{r_1}\right) . \tag{75}$$

  The dynamics in both configurations is equivalent in this limit which is also reflected in the torus–like structure for large r_1 in both Fig. 21 (a) and (b). Note, however, that the tori are not closed in the eZe – configuration when the outer electron returns to the nucleus. A typical trajectory alternates between chaotic motion near the nucleus and time intervals with

[13] The extreme localization of the outer electron justifies the use of r_1 as an adiabatic parameter in the molecular treatment of the corresponding quantum states, see Sec. III.B.4.

regular dynamics for $r_1 \gg r_2$ until the outer electron eventually escapes to infinity without returning to the nucleus. The 'periodic orbit' at $r_1 \equiv \infty$, $p_1 \equiv 0$ is special in the sense that it corresponds to the limiting case of an electron escaping with zero kinetic energy.

- There exists a symbolic dynamics for the chaotic eZe – configuration which maps each trajectory one–to–one onto a binary symbol string. The symbols are obtained from the rules

  1 if a trajectory hits the line $r_1 = r_2$ between two collisions with the nucleus, (i.e. $r_2 = 0$);

  0 otherwise.

  The symbolic dynamics is generated by the triple collision orbits, i.e. those trajectories starting in or ending at the singular point $r_1 = r_2 = 0$.

- Periodic orbits in the eZe-subspace can be characterized by a periodic symbol string $\overline{a} = \ldots aaaa \ldots$ and a is a finite symbol string of length n; there are infinitely many periodic orbits and they are all unstable with respect to the dynamics in the collinear plane. Their number increases exponentially with the code length and thus with the period of the orbits. The asymmetric stretch orbit $\overline{1}$ is the shortest orbit in this subspace, see Fig. 20(b). The marginally stable orbit $r_1 \equiv \infty$, $p_1 \equiv 0$ discussed above would have the notation $\overline{0}$ in our code. Some periodic orbits together with their code are displayed in Fig. 22.

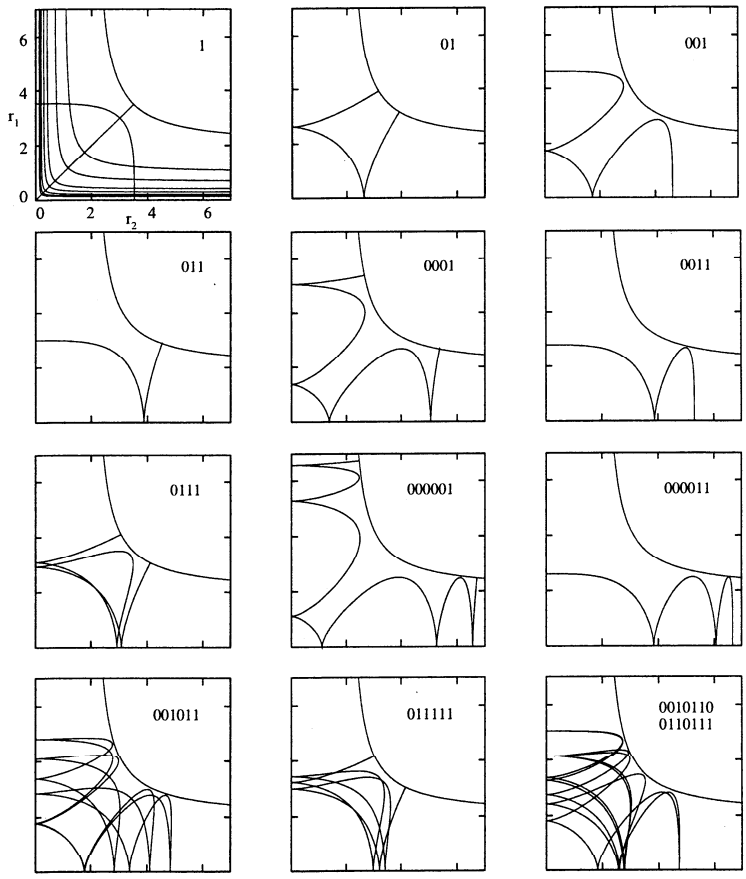

FIG. 22. Some unstable periodic orbits in the chaotic collinear eZe – configuration together with their binary code.

- Strong chaos and electron escape originates from the triple collision. Large energy and momentum transfer between the electrons which leads to subsequent ionisation can happen only, if the particles come close to the triple collision. The triple–collision is always approached along the so–called Wannier orbit running on the line $r_1 = r_2$. There is strong evidence that the Wannier orbit itself is infinitely unstable in the collinear subspace, i.e. for angular momentum $\mathbf{L} = 0$ (Richter and Wintgen (1990), Kim and Ezra (1991)), see also the discussion in IV.B.2.b and IV.C.3.

- Both collinear configurations are stable with respect to linear perturbation perpendicular to the collinear phase space; the Zee – configuration is at the center of a 6–dimensional stable island of the $L = 0$ – phase space. The eZe – configuration is stable in the bending motion corresponding to the dynamics in the Θ–degree of freedom.

The last point is maybe the most important in the quantum context. *The collinear dynamics is disconnected from the rest of the $L = 0$ – phase space due to the stability in the Θ degree of freedom.* Two-electron atom eigenstates are localized along the collinear axis because there is an enhanced classical probability to remain close to the collinear configuration (Wintgen et al. (1994)). The quantum and semiclassical consequences of this observation are discussed in Secs. IV.C and IV.D.

b. The symmetry plane of the Wannier ridge

The symmetry plane of symmetric collective electron motion $r_1 \equiv r_2 = r$, $p_{r_1} \equiv p_{r_2} = p_r$ is known as the Wannier ridge (Fano (1983)). The electron pair motion in the phase space region near the symmetry plane $r_1 = r_2$ plays an important role in Wannier's classical description of the three–particle break–up at small energies $E > 0$ (Wannier (1953), Eckhardt (1991)). The classical dynamics for $E < 0$ is, however, bound and ionisation is prevented classically. The Wannier ridge was proposed to be of importance for quantum resonances below the three particle breakup threshold $E = 0$, especially for symmetrically excited resonances (Fano (1983), Harris et al. (1990)). Classical considerations together with semiclassical arguments indicate, however, that there is no special influence of the Wannier ridge dynamics on the spectrum (apart form the Langmuir orbit discussed below). The main arguments leading to this conclusion will be presented here. Further evidence is given by spectral Fourier analysis, see Section IV.C.3.

The dynamics in the Wannier ridge subspace is of mixed behavior, i.e. classical chaotic regions and regular motion within stable islands coexist. The phase space dynamics follows the typical KAM scenario (Arnold (1979)) from regular to chaotic dynamics when changing the nuclear charge from $Z = 1/4$ to $Z = \infty$ (Richter (1991), Richter et al. (1993)). In Figs. 23 (a) – (h), the phase space structure is shown for various Z – values in the Poincaré surface of section $\Theta = \pi$. The coordinates X, P_X correspond to r, p_r, respectively, after suitable rescaling, (see Richter et al. (1993) for details). The phase space for $Z \to 1/4$, Fig. 23 (a), is filled by invariant tori grouped around the so-called Langmuir orbit (Langmuir (1921)). It is a periodic mode of the electron pair exhibiting strong bending vibration as shown in Fig. 2(b). An additional constant of motion giving rise to the torus structure in the limit $Z \to 1/4$ could indeed be found by Richter et al. (1993).

An increasing number of (resonant) tori is destroyed when Z becomes larger, see Figs. 23 (b) – (h). Chains of elliptic and hyperbolic fixed points appear and chaotic bands are formed along the hyperbolic fixed points expanding with increasing Z.

The physically relevant cases $Z = 1$ (H^-) and $Z = 2$ (helium), Figs. 23 (d),(e), exhibit a mixed regular and chaotic phase space. The elliptic island around the Langmuir orbit is preserved and clearly dominates the Poincaré section. The Langmuir orbit becomes unstable at $Z \approx 5.6$ and a new orbit born at the bifurcation point converges to a collinear Zee - configuration in the limit $Z \to \infty$ (Richter (1991), Müller and Burgdörfer (1993)).

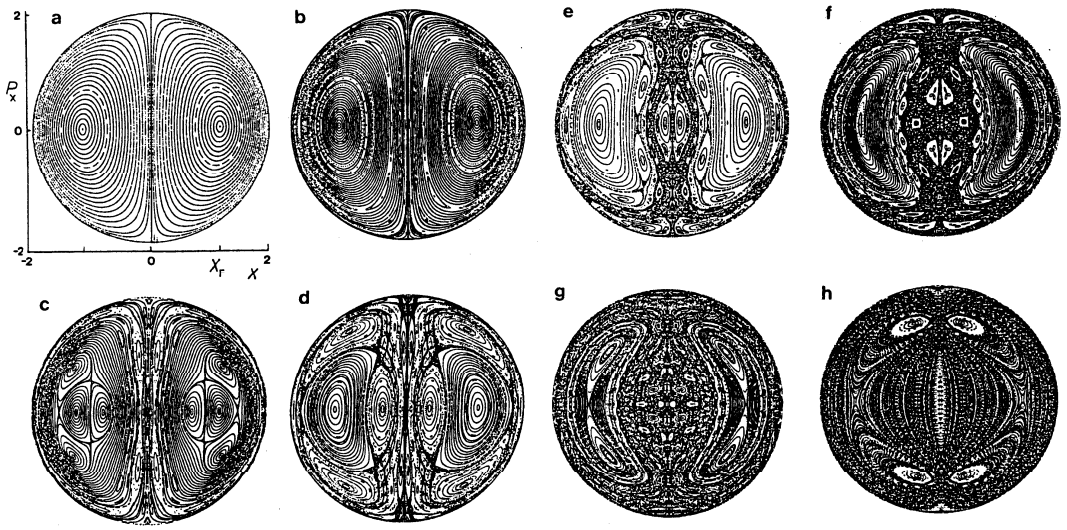

FIG. 23. Poincaré surface of section $\Theta = \pi$ in the Wannier ridge configuration for varying Z – values; (a) $Z = 0.26$, (b) $Z = 0.43$, (c) $Z = 0.75$, (d) $Z = 1$, (e) $Z = 2$, (f) $Z = 5$, (g) $Z = 10$, (h) $Z = 100$. (From Richter et al. (1993).)

The limit of large nuclear charge $Z = 100$ is depicted in Fig. 23 (h). The phase space is now mainly covered with remnants of tori or so–called Can–tori (MacKay et al. (1984)). The independent particle limit $1/Z \to 0$ cannot be handled by means of the KAM theory due to the degeneracy of the classical dynamics in this limit, see also the discussion in Section II.A.2.

The Wannier ridge is, in contrast to the collinear subspaces, mostly unstable with respect to perturbations away from the symmetry plane. This is intuitively clear, a small asymmetry in the electron dynamics tends to get amplified due to the electron–electron repulsion and the trajectory 'falls off' the Wannier–ridge. The stability of trajectories with respect to the degree perpendicular to the symmetry plane (often measured in terms of the hyperangle $\alpha = \arctan(r_1/r_2)$) can be studied with the help of linear stability analysis by calculating the full Monodromy matrix along periodic orbits including the α – degree of freedom. Numerical calculations for helium show that the 25 shortest periodic orbits on the Wannier–ridge (apart from the Langmuir orbit) are all extremely unstable with respect to α (Richter (1991)); the dynamics on the Wannier–ridge is thus strongly coupled to the rest of the phase space due to the instability in α. Localization of quantum states on the Wannier–ridge can therefore not be expected semiclassically.

There is, however, one exception; the Langmuir orbit is only moderately unstable in α for most Z–values and even stable for helium, i.e. $Z = 2$ (Richter and Wintgen (1990)). The Langmuir orbit in helium is thus surrounded by a full 6–dimensional stable island in the classical phase space $L = 0$. The Wannier ridge is therefore strictly speaking not globally unstable in the α coordinate as e.g. conjectured by Wesenberg et al. (1985) and Fano and Rau (1986). The stable island indicates the existence of sharp resonances in helium associated with a quantization of the Langmuir orbit, see also the discussion in Sec. IV.C.2.b.

Another 'fundamental' mode on the Wannier ridge is the Wannier orbit $\Theta = \pi$, $p_\Theta = 0$. It is the only orbit which exists in both the collinear subspace eZe and on the Wannier ridge. (The Wannier orbit forms the boundary of the Poincaré surface in Fig. 23). The orbit has attracted particular attention in the past to model the electron dynamics in symmetrically double–excited states in H^- and helium (Miller (1972), Fano (1983), Harris et al. (1990), Sadeghpour (1991)). Studies by Richter and Wintgen (1990) indicate, however, that the Wannier orbit is infinitely unstable for $L = 0$ reflecting the non–regularizability of the dynamics at the triple collision. The influence of the Wannier orbit on the quantum spectrum can thus be dismissed on semiclassical grounds. The semiclassical prediction has been confirmed by quantum calculations. Wavefunctions

of symmetrically excited states tend to be localized perpendicular to the Wannier orbit (Kim and Ezra (1991), Ezra et al. (1991), Richter and Wintgen (1993)). The Wannier orbit is also absent in a spectral Fourier analysis (Richter (1991), Blümel and Reinhard (1992), Qiu et al. (1996)) even for angular momentum $\mathbf{L} \neq 0$ (Grémaud and Gaspard (1998)). A detailed discussion is given in Section IV.C.3.

C. Qualitative semiclassical analysis of the two-electron spectrum from fundamental periodic modes

1. Classical interpretation of the spectral structure of two–electron atoms

The structure of the classical dynamics presented in the last section explains many details of the quantum spectrum qualitatively including propensity rules and widths of resonances from a purely classical point of view (even without referring to explicit semiclassical calculations).

In the following and henceforth we will restrict ourself to $L = 0$, i.e. we will analyze the ${}^1S^e$ or ${}^3S^e$ spectrum of two electron atoms, especially of helium as e.g. shown in Fig. 9. Considering total angular momentum $L = 0$ implies $M = 0$ and also $T = 0$ (in Herrick's notation, see Eq. (23)). We are thus dealing with states below the diagonal in Fig. 13; the transition (B), i.e. $\Delta m = -1$, in Eq. (24) does not occur.

The two collinear invariant subspaces discussed in Sec. IV.B.2 are stable with respect to perturbation in the angle Θ; this implies an enhanced probability to stay close to the collinear configuration both classically as well as quantum mechanically and localization of quantum states (resonances) on these configurations takes place. The approximate quantum numbers associated with the collinear configurations can be identified by exploiting Herrick's relation (32) for the expectation value of the inter–electronic angle Θ, which for large excitation of the outer electron $n \to \infty$ reads

$$< \cos\Theta > \underset{n\to\infty}{\longrightarrow} -\frac{K}{N} = -\frac{N_1 - N_2}{N_1 + N_2 + 1} \; ; \tag{76}$$

(the above quantum numbers are introduced in Sec. III.B.1, see also Eqs. (23)). The Rydberg–series with maximum $K = N - 1$ and $< \cos\Theta > \approx -1$ are linked to the eZe – configuration $\Theta = \pi$, (the corresponding series in Fig. 13 are those in the bottom row). The series with minimal $K = 1 - N$ and $< \cos\Theta > \approx 1$ are the states associated with the Zee – subspace and $\Theta = 0$. These are the series directly below the diagonal in Fig. 13.

The existence of distinct non-interacting Rydberg series for fixed N can semiclassically be understood in terms of the stability in the Θ–degree of freedom. We infer from classical dynamical localization on the collinear subspaces, that the Rydberg series with maximal/minimal K interact least with the rest of the spectrum. The dynamics in the eZe – configuration is, however, strongly chaotic. We thus expect a mixing between series with different N but maximal K, i.e. $\Delta N = -1$, $\Delta K = -1$, which is exactly the propensity rule (A), i.e. $\Delta N_1 = -1$ listed in Eq. (24). The Zee – configuration is fully stable in all degrees of freedom. Interaction between series localized in this collinear subspace, i.e. having minimal K but different N quantum numbers, are exponentially suppressed. This in turn corresponds to the suppression of the transition (C) in Eq. (24), i.e. $\Delta N = -1$, $\Delta K = 1$, or equivalently $\Delta N_2 = -1$, as discussed in a completely different context in Section III.B.3.a.

The difference in the resonance widths can be understood along the same lines. The states associated with the Zee – configuration can only decay via (dynamical) tunneling (semiclassically described by complex classical paths) and have thus extremely small decay widths and very long life times. The quantum states as well as the classical dynamics is trapped in the classically stable island and autoionisation is exponentially suppressed (Richter and Wintgen (1991)). In the eZe – subspace, classical escape is fast along the collinear axis due to the chaotic dynamics. The typical resonance widths are thus orders of magnitude larger than in the stable collinear configuration. Classical escape happens when the two electrons approach the nucleus almost symmetrically along the Wannier orbit allowing for large momentum transfer between the particles, see also Section IV.B.2.a. The Wannier orbit being the link between the collinear eZe – configuration and the

unstable Wannier – ridge subspace Sec. IV.B.2.b is thus an effective escape channel in agreement with the findings in the molecular adiabatic picture, see Section III.B.3.a and Fig. 12. More detailed studies of resonance widths in this K - regime have been undertaken by Blümel and Reinhardt (1992, 1997) and Burgdörfer et. al (1997); especially the transition from regular behavior into the Ericson regime of overlapping and strongly interacting resonances (Ericson (1960)), where an assignment of quantum numbers looses its meaning, has been investigated.

The picture is less clear for intermediate K – values in a given N – manifold. The classical phase space has not been studied systematically in this region, i.e. for $\Theta \approx \pi/2$, but the dynamics is supposed to be mixing here in all degrees of freedom. Numerical studies of the quantum spectrum indicate increasing interference between all Rydberg series. A breakdown of any approximate scheme of quantum numbers in the regime $K \approx 0$ and $N \geq 9$ is indeed observed (Bürgers et al. (1995), Rost and Tanner (1997)). The largest resonance widths are typically found in this intermediate K – regime; classical escape can occur here along two degrees of freedom.

2. Single periodic orbit quantization

In order to get quantitative semiclassical approximations for two–electron resonance positions, a detailed knowledge of the periodic orbits of the system is essential to apply the semiclassical methods introduced in Section IV.A. We cannot hope to obtain the full spectrum including all the Rydberg series in each N-manifold, even when restricting ourselves to S – states; the high dimensionality of the classical phase space makes a systematic study of the full set of periodic orbits almost impossible. However, a description of Rydberg series which correspond to classical configurations centered on the collinear subspaces is feasible in the light of the previous paragraph. Especially symmetrically excited intra–shell states with $< r_1 > \approx < r_2 >$ and wavefunctions concentrated near the origin can be semiclassically reached by considering the fundamental short periodic orbits only. A full semiclassical treatment of asymmetrically excited states including complete Rydberg series up to the various single ionisation thresholds will be presented in section IV.D.

a. *The frozen planet orbit*

The two–electron states corresponding to the Zee – configuration can be treated within an EBK–quantization as outlined in Section IV.A.3.a. The center of the classical stability island, see Fig. 21(a), is dominated by the behavior around the fixed point, the frozen planet periodic orbit (FP). The dynamics in the vicinity of this central orbit can be well described in harmonic approximation. The winding numbers, i.e. the frequency ratios ω_1/ω_2 for the motion on and perpendicular to the FP, are approximately constant for tori close to the central fixed point. This makes it possible to perform a harmonic oscillator quantization of the core region of the stable island by considering the FP and its normal modes only; the corresponding quantum states are called the frozen planet states. Richter and Wintgen (1990a, 1991) could give a simple double Rydberg formula for collinear Zee – resonance states,

$$E_{m,k,\bar{n}} = -\frac{(S_{\mathrm{FP}}/2\pi)^2}{[(m+\frac{1}{2}) + 2(k+\frac{1}{2})\sigma_1 + (\bar{n}+\frac{1}{2})\sigma_2]^2}\ , \qquad m,k,\bar{n} = 0,1,2,\ldots\ . \tag{77}$$

which is similar to semi–empirical formulae like Eq. (43) described in Sec. III.E.2. The parameters entering the Rydberg–formula are now completely determined in terms of classical properties of the frozen planet orbit; $S_{\mathrm{FP}}/2$ is the (scaled) action of the orbit and σ_1, σ_2 are the winding numbers for the dynamics in the Θ – degree of freedom perpendicular to the collinear subspace and for the dynamics in the collinear plane, respectively. (We have $S_{\mathrm{FP}}/2\pi = 1.4915$, $\sigma_1 = 0.4616$ and $\sigma_2 = 0.0677$ in helium.) The classical parameters are obtained by integrating the linearized dynamics in the neighborhood of the orbit in all degrees of freedom. There are two equivalent degrees of freedom perpendicular to the collinear space, which gives rise to the additional factor

2 in Eq. (77). The quantum numbers $(m, k, \bar{n})$ can be related to excitation (of normal modes) parallel (m) and perpendicular $(\bar{n})$ to the periodic orbit and to excitation in the bending degree of freedom (k). We obtain the following identification with the Herrick/Stark quantum numbers $(N, K)_n$ in (23) and the MO-quantum numbers $(\bar{n}_\mu, \bar{n}_\lambda)_{\bar{n}}$ for planetary atom states introduced in III.B.4

FP	$r_>$ adiabatic	Herrick/Stark	
m	$= \bar{n}_\mu =$	$\frac{1}{2}(N - K - 1))$	(78a)
k	$= \bar{n}_\lambda =$	$\frac{1}{2}(N + K - 1)$	(78b)
$\bar{n}$	$= \bar{n} =$	$n - N$	(78c)

A semiclassical description of the Zee – configuration is thus equivalent to the molecular adiabatic approximation of planetary atom states (with $r_1 = r_>$ being the adiabatic invariant).

The results from Eq. (77) are in good agreement with full quantum calculations for moderate excitation in k and $\bar{n}$ as can be seen from Tab. II. The FP–approximation becomes increasingly better in the semiclassical limit $N \to \infty$ and exceeds even results obtained from the adiabatic MO – approximation in Sec. III.B.4 (Richter et al. (1992)).

The localization of Zee quantum states on the frozen planet orbit can be observed in the probability densities of numerically obtained quantum wavefunctions in the $\Theta = 0$ plane, see Fig. 24. The excitations along (m) and perpendicular $(\bar{n})$ to the periodic orbit are clearly visible as a regular node-pattern in the wave functions.

The collinear alignment is weakened with increasing excitation in k and the approximations leading to Eq. (77) break down in this limit. Similarly, the limit $\bar{n} \to \infty$ violates the assumption of being close to the center of the island. The formula (77) does indeed not converge to the correct single ionisation thresholds for $\bar{n} \to \infty$ as has been pointed out by Ostrovsky and Prudov (1993) and non–harmonic corrections have to be included into a full EBK–calculation (Wintgen and Richter (1994)), see also Section IV.D.1.

The frozen planet configuration does not exist for H^-, i.e. $Z = 1$, where the Zee – subspace is purely repulsive (Gaspard and Rice (1994), Richter et al. (1992)). The dynamical stabilization and the existence of frozen planet configurations found for two-electron atoms has also been observed for other mass ratios between the three particles and led to the prediction of a new form of a quasi-stable binding–mechanism for anti–protons in atoms (Richter et al. (1991)).

Asymmetric Stretch Orbit			Frozen Planet Orbit		
$(N, K)_n$	PO	QM	$(N, K)_n$	PO	QM
$(1, 0)_1$	3.097	2.904	——	——	——
$(2, 1)_2$	0.804	0.778	$(2, -1)_2$	——	——
$(3, 2)_3$	0.362	0.354	$(3, -2)_3$	0.248	0.257
$(4, 3)_4$	0.205	0.201	$(4, -3)_4$	0.1394	0.1411
$(5, 4)_5$	0.1317	0.1294	$(5, -4)_5$	0.0892	0.0896
$(6, 5)_6$	0.0917	0.0903	$(6, -5)_6$	0.06189	0.06205
$(7, 6)_7$	0.0675	0.0665	$(7, -6)_7$	0.04546	0.04554
$(8, 7)_8$	0.0517	0.0510	$(8, -7)_8$	0.03480	0.03484
$(9, 8)_9$	0.0409	0.0403	$(9, -8)_9$	0.02749	0.02752
$(10, 9)_10$	0.0332	0.0327	$(10, -9)_10$	0.02227	0.02228

TABLE II. Total binding energies $-E$ for $^1S^e$ states obtained by single orbit quantization of the asymmetric stretch orbit (AS) Eq. (79) and the frozen planet orbit (FP) Eq. (77) compared with full quantum calculations based on complex rotation (Bürgers et al. (1995)).

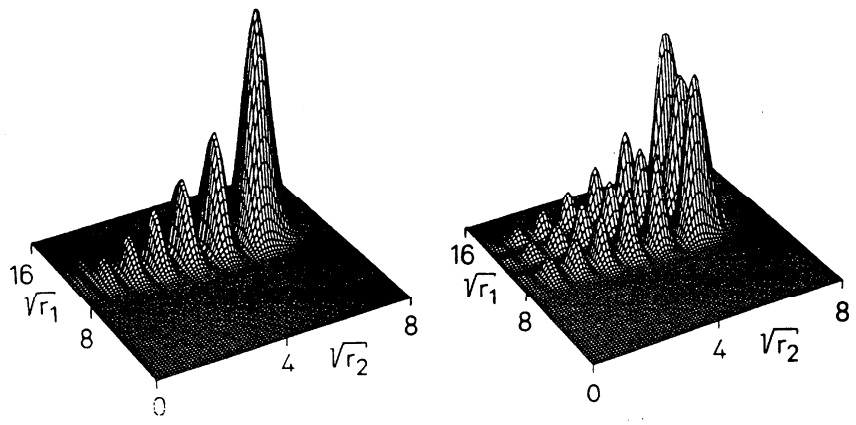

FIG. 24. Frozen planet states, localized along the classical frozen planet orbit (Fig. 20(a)), corresponding to the quantum numbers $(m, k, \bar{n}) = (6,0,0)$ (a) and (6,0,2) (b) in $^1S^e$ helium; the corresponding $(N, K)_n$ notation is: $(7,-6)_7$ (a), and $(7,-6)_9$ (b). The completely symmetrised version of the wavefunctions is obtained by reflection on the axis $r_1 = r_2$. (From Richter et al. (1992).)

b. The Langmuir orbit

A semiclassical quantization of the Langmuir orbit (see Fig. 2(b)) has been proposed by several authors to approximate the helium ground state (Langmuir (1921), Dimitrijević and Grujić (1984), Wesenberg et al. (1985)). However, the quantization failed due to the use of incorrect quantization conditions, i.e. an incorrect consideration of the motion perpendicular to the periodic orbit. Richter and Wintgen (1990) predicted long living resonant states for helium with energies given by a double Rydberg formula like Eq. (77) after discovering that the Langmuir orbit is stable in all degrees of freedom, see also Sec IV.B.2.b. The number of quantum states associated with a torus structure of a stability island is approximately given by the phase space volume of the island (Berry (1983)). The stable island around the Langmuir orbit is extremely small and even so the phase space volume increases with the energy like $|E|^{-3/2}$ for three body Coulomb problems, long–lived resonant states localized on the Langmuir orbit are expected only in the limit of extremely high double–excitation (Richter and Wintgen (1990); Müller and Burgdörfer (1993) give as an estimate $N \geq 500$). Müller et al. (1992) extended the double Rydberg formula to low energies and thus obtained approximations for low-lying resonance energies with $N \leq 15$ and moderately doubly–excited states. They proposed that these 'Langmuir - states' correspond to symmetrically excited resonances with maximal bending excitation belonging to the energetically uppermost Rydberg - series with minimal $K = 1 - N$ quantum number (Müller and Burgdörfer (1993)). Contrary, the semiclassical results of the last section and quantum calculations for doubly–excited states in helium with principal quantum numbers $N \leq 10$ suggest that resonances belonging to minimal K are of frozen planet type and are related to the collinear Zee – configuration (Richter and Wintgen (1993)). The Langmuir orbit is expected to play an important role for intermediate K values $K \approx 0$ and this point of view is supported by results from spectral Fourier transformation (Qiu et al. (1996)), see also Section IV.C.3.

c. The asymmetric stretch orbit

The most interesting invariant subspace from a quantum mechanical point of view is certainly the eZe - collinear configuration; it is energetically most favored with both electrons being far apart on opposite sites of the nucleus; the configuration is thus a candidate for a semiclassical quantization of the ground state and symmetrically excited intra-shell states (corresponding to maximal $K = N-1$ and $N = n$). The fundamental mode in the eZe - dynamics close to the nucleus is characterized by the shortest periodic orbit, the asymmetric stretch orbit (AS) in Fig. 20(b). Even so the

dynamics in the eZe - configuration is chaotic and all periodic orbits including the AS-orbit are unstable, we can perform a single periodic orbit quantization in a similar way as outlined in the last paragraphs. This step will be justified in more detail in Sec. IV.D when applying the cumulant technique for semiclassical zeta functions to collinear helium. A naive AS-quantization provides indeed a surprisingly accurate double Rydberg formula for intra-shell resonances in two electron atoms being of the form (Ezra et al. (1991), Wintgen et al. (1992))

$$E_{m,k} = -\frac{(S_{\rm AS}/2\pi)^2}{[m+\frac{1}{2}+2(k+\frac{1}{2})\sigma_{AS}]^2}, \qquad m,k = 0,1,2,\ldots . \tag{79}$$

We obtain $S_{\rm AS}/2\pi = 1.8290$ for the action in helium and $\sigma_{AS} = 0.5393$ is the winding number for the dynamics in bending degree of freedom. The quantum numbers m and k describe excitation along and perpendicular to the orbit which in turn corresponds to intra-shell excitation and vibrational excitation in the bending degree of freedom, respectively. We obtain the following identification with the Herrick and MO - quantum numbers in Eq. (23)

AS		r_{12} adiabatic	Herrick/Stark	
	m	$= [n_\mu/2] =$	$\frac{1}{2}(N+K-1)$	(80a)
	k	$= n_\lambda =$	$\frac{1}{2}(N-K-1)$.	(80b)

Note that the third quantum number $\bar{n}$ representing asymmetric excitation perpendicular to the orbit within the collinear plane in Eq. (78) is absent here due to the instability of the orbit. The collinear eZe - quantum numbers are now equivalent to the one obtained from the MA - approximation (cf. Eq. (23)) corresponding to an MO-picture with fixed inter-electronic axis as described in Section III.B.1.

A comparison of Eq. (79) with quantum results is shown in Tab. II for symmetrically excited states $N = n$, i.e. the lowest states in each Rydberg series $K = N - 1$. Especially the good approximation of the helium ground state emphasizes the importance of the asymmetric stretch orbit as a fundamental mode for bound and resonance spectrum in two electron atoms, see also Tab. I. The agreement of the Heisenberg-Sommerfeld model, Fig. 3, is not purely accidental; it captures the main ingredients of the dynamics by introducing asymmetric near collinear motion. Eq. (79) also reveals the origin of formulae for double Rydberg series found semi–empirically by Rau (1983) and Molina (1989) for symmetrically excited (intra–shell) resonances, see Eq. (43) and the discussion in Sec. III.E.2. Müller and coworkers could give a semi–empirical triple Rydberg formula which contains the semiclassical expressions Eq. (79) in the limit $K = N - 1$ but covers a wide range of K and N – values reproducing true quantum results within an astonishing accuracy (Müller 1993, Qiu et al. (1996)).

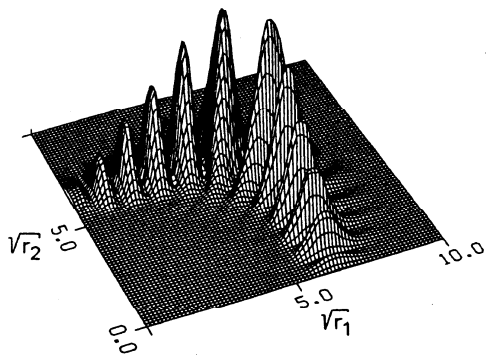

FIG. 25. The $(m,l,k) = (5,0,0)$ wavefunction (projected onto $\Theta = \pi$) in ${}^3S^e$ helium; $((N,K)_n = (6,5)_6)$; the localization along the asymmetric stretch orbit (see e.g. Fig. 20(b)) is clearly visible. (From Wintgen et al. (1992).)

The localization of intra–shell wavefunctions on the asymmetric stretch orbit is shown in Fig. 25. The nodal pattern corresponds to excitation along the orbit described by the m - quantum number. The tendency of wavefunctions being repelled from the (very unstable) triple collision and from the Wannier orbit $r_1 = r_2$ can be observed here. Similar localization phenomena are found in collinear ABA - molecules, where the corresponding wavefunctions are known as hyperspherical modes (Bisseling et al. (1987) and references therein).

To resolve asymmetric states with $n > N$ more detailed information about the chaotic electron dynamics is needed. This information is provided by other unstable periodic orbits which can be incorporated into a quantization schema when making use of the cycle – expansion technique discussed in Sec. IV.A.3.b. We will present details in Sec. IV.D.2.

3. Spectral Fourier analysis

The connection between classical periodic orbits and quantum traces as outlined in Sec. IV.A.2 allows one to analyze experimental or numerical quantum spectra by Fourier transformation. The method is based on Gutzwiller's formula (51) which for scaling systems has the form

$$d(z) = \sum_n \delta(z - z_n) \approx \bar{d}(z) + \sum_{\rm po} A_{\rm po} e^{iz S_{\rm po}}. \tag{81}$$

Here, z is the scaling parameter, i.e. we have the scaling behavior $S(E)/\hbar = z(E;\hbar) S_{\rm po}$ for the actions, and z_n are the scaled quantum eigenvalues. According to Eq. (81) a Fourier transformation of the quantum density of states with respect to z (after subtracting the smooth background $\bar{d}$ on both sides) reveals peaks at the actions of classical periodic orbits. The technique is especially useful to analyze 'chaotic' spectra, i.e. spectra which show no obvious structure in terms of good or approximate quantum numbers. The Fourier transformation uncovers long range correlation between quantum eigenvalues which may pass unobserved when studying the raw spectrum showing strong level–interference on short energy scales (Eichmann et al. (1988)).

The related scaled energy spectroscopy has first been applied to hydrogen in a constant magnetic field (Wintgen (1987), Holle et al. (1988), Friedrich and Wintgen (1989)) and has now become a standard tool in atomic and molecular spectroscopy. The method allows one to identify the classical dynamics underlying the quantum spectrum (or parts of it) and has been useful to uncover basic periodic classical motion being responsible for long range modulations in atomic or molecular spectra.

The scaled energy spectroscopy has been applied to helium by Kim and Ezra (1991) and Richter (1991), who noticed that the Wannier orbit is indeed absent in the Fourier–spectrum. This result could be traced back to the fact that the Wannier orbit is infinitely unstable, see also Section IV.B.2.b, leading to a vanishing amplitude $A_{\rm po}$ in Eq. (81). Similar results were reported by Blümel and Reinhard (1992) on the pure collinear model and by Dräger et al. (1994) on the s – wave model.

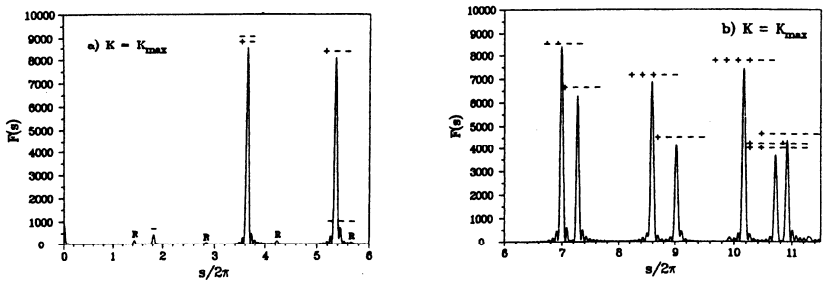

FIG. 26. Fourier transformation of the ${}^1S^e$ $(N, N-1)_n$ – spectrum corresponding to the chaotic eZe - configuration. Dominant peaks are visible at the actions s of various periodic orbits, cf. Fig. 22. (Note that the symbol code is (+,–) here corresponding to (0,1) in the notation of Section IV.B.2.a). (From Qiu et al. (1996)).

The most thorough study of the Fourier transformed helium $^1S^e$ – spectrum so far has be undertaken by Qiu et al. (1996) (see also Burgdörfer et al. (1997)) based on ab initio quantum calculations by Bürgers et al. (1995). Their results confirm the picture drawn in the previous paragraphs; the asymmetric stretch orbit and the frozen planet orbit dominate the Fourier spectrum for quantum states with maximal and minimal K, respectively. The resolution of the Fourier analysis could be considerably enhanced by extrapolating an empirical formula for the $^1S^e$ – spectrum (Burgdörfer et al. (1995)) to energies above the $N = 15$ threshold. Up to 100 orbits of the collinear subspaces could be identified in the Fourier spectrum of the empirical double Rydberg formula, see Fig. 26. Interestingly, the contribution of the Langmuir – orbit was found to dominate the spectrum for intermediate K values, i.e. $K \approx 0$, and $N > 15$.

Recently, Gremaud and Gaspard (1998) studied the Fourier transformation of the total $^1S^e$ and $^1P^o$ helium spectrum up to $N = 7$. As expected from the classical angular momentum scaling Eq. (72), the Fourier spectrum in both cases is dominated by the collinear AS and FP orbits in the $L = 0$ classical dynamics. Even P – wavefunctions localized on the asymmetric stretch orbits were found. This again emphasizes the importance of the asymmetric stretch and the frozen planet orbit as the fundamentals modes in two-electron atoms. The connection between quantum states with $L \neq 0$ and the classical $L = 0$ – dynamics can be understood in terms of the scaling relation (72).

D. Quantitative determination of resonances from semiclassical summation techniques

The semiclassical approximations for bound and resonance states in two–electron atoms in Sections IV.C.2.a and IV.C.2.c were based on a quantization of the shortest periodic orbits in the collinear subspaces. The double Rydberg – formulae (77) and (79) provide good approximations for low lying states in the corresponding $(N, K)_n$ series, i.e. for $N \approx n$. They fail, however, to reproduce asymmetrically excited states and especially the existence of Rydberg series converging to the various single ionisation thresholds $I_N = Z^2/2N^2$. Resonances close to the thresholds belong to extremely asymmetric states $\langle r_1 \rangle \gg \langle r_2 \rangle$ and can only be resolved semiclassically, if the classical dynamics in the limit $r_1 \to \infty$ is taken appropriately into account. We first consider the almost integrable Zee – configuration, which can be treated within the more conventional framework of EBK-quantization . We will then use the cycle expansion technique and obtain asymmetric excited resonances $n \geq N$ for chaotic collinear eZe – states by including long unstable periodic orbits. A special periodic orbit summation technique is introduced in Sec. IV.D.3, which contains the dynamics in the limit $r_1 \to \infty$. The corresponding zeta functions resolve the correct Rydberg structure and a semiclassical quantum defect theory can be derived.

1. EBK–quantization of asymmetric electronic excitations

The double Rydberg formula (77) is based on a harmonic approximation of the torus structure Fig. 21 (a) in the vicinity of the center fixed point. In order to describe the full dynamics of the stable island in the whole collinear subspace, we may take advantage of the near–integrable nature of the Zee – configuration. Local canonical transformations to action/angle variables can be found in principle, in which the two-electron atom – Hamiltonian takes on the form

$$H(p_1, r_1, p_2, r_2, \Theta, p_\Theta) = H(J_1, J_2, J_3, \phi_1, \phi_2, \phi_3) \approx H(J_1, J_2, J_3)\,, \tag{82}$$

and usual EBK–quantization may be performed as outlined in Section IV.A.3.a. Unfortunately, there is in general no procedure to derive the local action (and conjugated angle) variables analytically. Methods to determine such transformations numerically have been developed by Bohigas et al. (1993), (see also Percival (1974) and Martens and Ezra (1987)), and applied to the collinear Zee – problem by Wintgen and Richter (1994).

Following Wintgen and Richter (1994), we may characterize the torus structure in Fig. 21(a) not by actions J_1, J_2 but in terms of a winding number $\alpha = \omega_2/\omega_1$ with $\omega_i = \partial H/\partial J_i$, $i = 1, 2$

being the frequencies. The winding number of an (approximately) closed curve in Fig. 21(a) can be determined numerically by integrating a trajectory on that curve. The action $S = \int p\mathrm{d}q$ of a trajectory after the first return to the Poincaré section can again be obtained numerically but may be written alternatively for fixed energy as

$$S(\alpha) = 2\pi \left[J_1(\alpha) + \alpha J_2(\alpha) \right]. \tag{83}$$

In the notation above, J_1 represents approximately the radial motion of the inner, J_2 the radial motion of the outer electron. The third degree of freedom, J_3, is identified with the bending degree of freedom and we have $J_3 = 0$ in the collinear plane. A second important relation between actions and winding numbers holds on the energy manifold. Using $dE = \omega_1 dJ_1 + \omega_2 dJ_2 = 0$, we obtain

$$\frac{\partial S}{\partial \alpha} = 2\pi J_2(\alpha). \tag{84}$$

The frozen planet orbit corresponds to $S(\alpha_{\mathrm{FP}}) = S_{\mathrm{FP}}$ with α_{FP} (= 0.067650 for helium) being the stability index of the periodic orbit in the collinear plane, see Section IV.C.2.a. The periodic orbit condition implies $\mathrm{d}S/\mathrm{d}\alpha|_{\alpha_{\mathrm{FP}}} = 2\pi J_2 = 0$.

For vanishing electron – electron interaction in the limit $r_1 \to \infty$ we obtain $J_1 \to \infty$ and $\alpha \to 0$. The collinear Hamiltonian (74) then approaches the independent electron limit Eq. (75) and the action $S(\alpha)$ can be given analytically, i.e.

$$\lim_{\alpha \to 0} S(\alpha) = \frac{2\pi Z}{\sqrt{-2E}} \left[1 + \left(\frac{Z-1}{Z} \alpha \right)^{2/3} \right]^{3/2}. \tag{85}$$

The third degree of freedom J_3 perpendicular to the collinear configuration gives rise to an additional term in Eq. (83) which for small $J_3 \neq 0$ can again be written as function of α only, i.e.

$$S(\alpha) = 2\pi \left(J_1(\alpha) + \alpha J_2(\alpha) + 2\alpha_3(\alpha) J_3(\alpha) \right).$$

The winding number α_3 as function of α is obtained from the linearized dynamics perpendicular to the collinear plane, see Wintgen and Richter (1994) for details.

Inserting the EBK – quantization condition $J_1 = m + \frac{1}{2}$, $J_2 = \bar{n} + \frac{1}{2}$, $J_3 = k + \frac{1}{2}$ in Eqs. (83), (84) together with the (numerically obtained) $S(\alpha)$ curve and exploiting the scaling relation for the actions (72) leads to quantized energy levels $E_{m,k,\bar{n}}$.

The quantum numbers $(m, k, \bar{n})$ are identical to those in Eq. (78). However, the Rydberg – structure of the two – electron spectrum together with the correct single ionisation thresholds is now fully reproduced, which is already guaranteed by incorporating the asymptotic $S(\alpha)$ behavior (85). Moreover, the quantitative agreement is remarkably good even down to the lowest states in each series where strong electron–electron interaction near the frozen planet orbit contributes dominantly (Wintgen and Richter (1994)).

Ostrovsky (1992) and Ostrovsky and Prudov (1993) proposed an alternative approach by expanding the electron–electron interaction in a multipol series leading to an independent–electron type approximation. The model reproduces the structure of Rydberg series, but cannot account for the correlated electron dynamics, which is reflected in the formation of the frozen planet configuration.

2. Semiclassical zeta function and symmetrically excited states

A semiclassical treatment of the classically chaotic collinear dynamics ($\Theta = \pi$) cannot rely on a torus quantization as indicated in the previous paragraphs and must fall back upon the periodic orbit theory developed in Section IV.A. Ezra et al. (1991) (see also Wintgen et al. (1992)) were the first to study the semiclassical eZe – spectrum including all relevant degrees of freedom. Similar collinear models (neglecting, however, the stable degree of freedom perpendicular to the collinear

subspace) were studied by Blümel and Reinhard (1991), the related s-wave model by Dräger et al. (1994).

The two–electron atom bound states or resonances associated with the eZe – collinear space can be expressed as the zeros of the semiclassical zeta function (54) written as product over all periodic orbits. For the collinear subspace (including all degrees of freedom in the Monodromy matrix $\mathbf{M}$), it has the form

$$\zeta_{sc}^{-1}(z) = \prod_{k=0}^{\infty} \zeta_k^{-1}(z) = \prod_{k=0}^{\infty} \prod_{l=0}^{\infty} \prod_{\rm po} (1 - t_{\rm po}^{(k,l)}) \,. \tag{86}$$

The products over k and l originate from an expansion of $|\det(\mathbf{M} - \mathbf{1})|^{-1/2}$ in Eq. (53) in terms of the stable (k) and unstable (l) eigenvalues of $\mathbf{M}$. The higher terms in l corresponding to the unstable degree of freedom can in general be neglected and we will set $l = 0$ henceforth. The index k accounts for the stable bending dynamics in the angle Θ and corresponds already to an approximate quantum number, the vibrational quantum number introduced in Eq. (80) in Sec. IV.C.2.c. The spectrum associated with a given k-quantum number corresponds to the zeros of the individual zeta functions ζ_k^{-1}.

The periodic orbit weights $t_{\rm po}^{(k)}$ in Eq. (86) are of the form

$$t_{\rm po}^{(k)}(z) = \frac{1}{\sqrt{\Lambda_{\rm po}}} \exp[izS_{\rm po} - in_{\rm po}\pi - 4\pi i(k + \tfrac{1}{2})\sigma_{\rm po}]. \tag{87}$$

Here, $\Lambda_{\rm po}$ is the eigenvalue of $\mathbf{M}$ along the unstable direction; the winding number in the unstable degree of freedom is linked to the code length $n_{\rm po}$ of the periodic orbit in the binary symbolic dynamics introduced in Sec. IV.B.2.a. The winding number associated with the stable degree of freedom is σ_{po}. The energy dependence is contained in the scaling variable $z = \frac{1}{\hbar}\sqrt{-1/E}$,

The zeta functions ζ_k^{-1} above can be rewritten in terms of a cumulant expansion, see Section IV.A.3.b, which has the form of a perturbative series. Including only the first term in a binary cycle – expansion Eq. (68) leads to a quantization condition

$$\zeta_k^{-1} \approx 1 - t_1^{(k)} \stackrel{!}{=} 0. \tag{88}$$

The term $t_1^{(k)}$ is the contribution from the asymmetric stretch orbit (AS), the fundamental periodic mode of the collinear configuration, (see Fig. 20 (b)). Note that the orbit '0' is absent in collinear two–electron atoms. The quantization condition given by Eq. (88) is the leading term in a zeta function expansion and justifies the single periodic orbit quantization (79) introduced in Sec. IV.C.2.c.

N	n	$j=1$	$j=4$	$j=8$	$j=12$	$j=16$	$E_{\rm qm}$
1	1	3.0970	2.9692	2.9001	2.9390	2.9248	2.9037
2	2	0.8044	0.7714	0.7744	0.7730	0.7727	0.7779
2	3	—	0.5698	0.5906	0.5916	0.5902	0.5899
2	4	—	—	—	0.5383	0.5429	0.5449
3	3	0.3622	0.3472	0.3543	0.3535	0.3503	0.3535
3	4	—	—	0.2812	0.2808	0.2808	0.2811
3	5	—	—	0.2550	0.2561	0.2559	0.2560
3	6	—	—	—	0.2416	0.2433	0.2438
4	4	0.2050	0.1962	0.1980	0.2004	0.2012	0.2010
4	5	—	0.1655	0.1650	0.1654	0.1657	0.1657
4	6	—	—	0.1508	0.1505	0.1507	0.1508
4	7	—	—	0.1413	0.1426	0.1426	0.1426

TABLE III. Real part of the zeros of ζ_0^{-1} obtained by cycle expansion of length j. The exact quantum energies are in the last column. The states are labeled by their principal quantum numbers. A line as entry indicates a missing zero at that level of approximation.

The unstable AS – orbit can only account for the phase space region $r_1 \approx r_2$ and thus for intra-shell states; the dynamics for asymmetric electron motion is represented by longer periodic orbits, as e.g. shown in Fig. 22. The contributions of these orbits are included by taking into account higher terms in a cycle expansion as introduced in Sec. IV.A.3.b for each of the semiclassical zeta functions ζ_k^{-1} separately. By making use of the symbolic dynamics, we obtain an expanded zeta function of the form (68), i.e.

$$\zeta_k^{-1}(z) = \sum_{j=0}^{\infty} c_j = 1 - [t_0^{(k)} - t_1^{(k)}] - [t_{01}^{(k)} - t_0^{(k)} t_1^{(k)}] - [t_{001}^{(k)} - t_0^{(k)} t_{01}^{(k)} + t_{011}^{(k)} - t_{01}^{(k)} t_1^{(k)}] - \dots . \quad (89)$$

The weights $t_{\rm po}^{(k)}$ are given by Eq. (87) and the cumulant terms c_j defined in Eq. (65) contain all contributions of orbits and composite orbits having the same total symbol length j. The semiclassical approximations for the bound and resonance states are given by the zeros of the zeta–functions. The expanded zeta functions depend only on the classical action, stability indices and winding numbers, which have to be determined numerically by integrating the equations of motion along the periodic orbits, see Richter et al. (1993) for details. We set $t_0 = 0$ in Eq. (89) due to the absence of the orbit '0'. This fact has deep consequences which are related to the existence of Rydberg series and will be discussed in Section IV.D.3.

By including successively higher cumulants in the expansion (89) and thus longer and longer orbits, the phase space dynamics is resolved in ever finer detail. As displayed in Tab. III, the cycle-expanded zeta functions Eq. (89) yield rather precise energies for intra-shell resonant states $n = N$. Moreover, they gradually reveal subsequent states with $n > N$ in each Rydberg series with increasing j.

Even interference effects between states in overlapping Rydberg series for $N \geq 4$ can be resolved semiclassically (Wintgen et al. (1994)). Results of equal quality have been obtained for H^- (including weak magnetic field effects) by Gaspard and Rice (1994). Moderate excitation in Θ can be accounted for by choosing $k > 0$ in Eq. (89) (Wintgen et al. (1992)). Classical and semiclassical studies beyond the linear approximation in the Θ –dynamics have been reported by Grujić and Simonović (1995).

3. Rydberg series and semiclassical quantum defect theory for collinear eZe – states

The cycle expansion technique presented above provides results of considerable accuracy for intra-shell resonant states and states with moderate asymmetric excitation. However, it can not resolve the Rydberg–structure at the single ionisation thresholds, which must include the classical dynamics in the limit $r_1 \to \infty$ corresponding to very long periodic orbits and thus long symbolic codes. A connection of the phase space regions for small and large r_1 is less obvious than in the Zee – configuration, where invariant tori provide the transition. The classical dynamics in the collinear eZe – subspace shows a gradual change from chaos to regular dynamics with increasing r_1 as can be seen in Fig. 21(b); a straightforward torus–quantization of the regular region is not possible. A smooth link between the classical chaotic and regular dynamics can, however, be provided by periodic orbit theory.

Tanner and Wintgen (1995) proposed to rewrite the expansion (89) in a way that includes regular orbits stretching out along the r_1 axis up to infinity, (examples of such orbits are the 000001, and 000011 – orbit in Fig. 22) before dealing with the complicate chaotic dynamics near the nucleus (represented e.g. by the orbits 001011, 011111 in Fig. 22). This idea can be implemented systematically by making again use of the symbolic dynamics introduced in Section IV.B.2.a. The regular behavior for $r_1 \to \infty$ is reflected by the symbol '0'. The symbol '1' is always related to motion in the near core region. A single '0' can occur for arbitrary r_1 and the number of '0's following successively a '1' in the symbol code determines how far a trajectory stretches into the regular region.

The new expansion schema for the zeta function (86) corresponds to switch from the binary alphabet (0,1) to an infinite letter alphabet according to the rule (Tanner et al. (1996))

$$10^{n-1} \to n; \quad 10^{n-1}10^{m-1} \to nm \quad \ldots,$$

and '0^n' stands for n '0's occurring successively in a row. The expansion is now written in terms of infinite sums over the regular '0' tails explicitly, i.e.

$$\zeta_k^{-1}(z) = 1 - \sum_{n=1}^{\infty} t_n^{(k)} - \sum_{m=1}^{\infty}\sum_{n=1}^{\infty} \frac{1}{2}(t_{mn}^{(k)} - t_m^{(k)} t_n^{(k)}) \qquad (90)$$
$$- \sum_{l=1}^{\infty}\sum_{m=1}^{\infty}\sum_{n=1}^{\infty} \ldots,$$

and the periodic orbit weights are again given by Eq. (87). The fundamental term $1 - \sum_{n=1}^{\infty} t_n^{(k)}$ is build up by periodic orbits with code '10^{n-1}'. It can be seen as the building block for the zeta function and its zeros reproduce already the gross structure of the Rydberg spectrum. The subsequent terms give corrections which account for interactions between overlapping Rydberg series corresponding to different N quantum numbers. The various quantities entering the periodic orbit weights (87) can be written as smooth functions of n, i.e.

$$S(n) = 2\pi n \frac{Z}{\sqrt{2}} \left[1 + (\frac{Z}{Z-1} n)^{-\frac{2}{3}}\right]^{\frac{3}{2}} + s_0 + s_{2/3} n^{-2/3} + \ldots \qquad (91)$$
$$\sigma(n) = \frac{n}{2} + \sigma_0 + \sigma_{2/3} n^{-2/3} + \ldots$$

The leading terms are universal for all infinite sums and can be obtained from the asymptotic behavior $n \to \infty$, i.e. $r_1 \to \infty$ as indicated in Section Eq. IV.D.1 (see also Wintgen and Richter (1994), Tanner and Wintgen (1995)). The subsequent coefficients contain information about the chaotic near–core dynamics. They are obtained by fitting Eq. (91) to the periodic orbit data.

A quasi–EBK (QEBK) formula can be derived revealing the basic quantitative structure of the spectrum by approximating the zeta function by its fundamental term only (Tanner and Wintgen (1995)), i.e.

$$\zeta_k^{-1}(z) \approx 1 - \sum_{n=1}^{\infty} t_n^{(k)}(z) \approx 1 - \sum_{m=-\infty}^{\infty} \int_1^{\infty} \mathrm{d}n\, e^{2\pi i m n}\, t_n^{(k)}(z). \qquad (92)$$

Poisson summation has been used in the last step and n is now a continuous variable.

$\bar{n}$	N=1		N=4	
	QM	QEBK	QM	QEBK
0	2.90372	2.78475	0.20099	0.19888
1	2.14597	2.14907	0.16573	0.16669
2	2.06127	2.06162	0.15082	0.15110
3	2.03359	2.03363	0.14260	0.14266
4	2.02118	2.02117	0.13769	0.13766
5	2.01456	2.01455	0.13455	0.13449
6	2.01063	2.01062	0.13245	0.13236
7	2.00809	2.00809	0.13100	0.13087
8	2.00637	2.00636	0.12999	0.12979
(N=5,$\bar{n}$=0)	$\longrightarrow$		0.12932	
9	2.00514	2.00514	0.12878	0.12898
10	2.00424	2.00424	0.12826	0.12835
11	2.00356	2.00355	0.12782	0.12787
12	2.00302	2.00302	0.12745	0.12758
∞	2.0	2.0	0.125	0.125

TABLE IV. Quantum energies of the bound Rydberg states $N = 1$ and the resonance series $N = 4$ are compared with semiclassical quasi EBK results in ${}^1S^e_{m=0}$ – helium

Approximating the integrals in Eq. (92) by stationary phase yields the condition

$$\frac{\partial}{\partial n}\left(z\frac{S(n)}{2\pi} - (m+\frac{1}{2})n - 2(k+\frac{1}{2})\sigma(n)\right) = 0. \tag{93}$$

The solutions $n_0(z)$ of Eq. (93) tend to infinity for $\hbar z \equiv (-E)^{-1/2} = \sqrt{2}N/Z$, i.e. at the single ionisation thresholds $I_N = -Z^2/(2N^2)$, $N = m + k + 1$. The quantization condition $\zeta_k^{-1}(E) \approx 1 - \sum_{n=1}^{\infty} t_n^{(k)} \stackrel{!}{=} 0$ implies now (in stationary phase approximation) the phase quantization

$$z\frac{S(n_0)}{2\pi} - (m+\frac{1}{2})\,n_0 - 2(k+\frac{1}{2})\,\sigma(n_0) = \bar{n} + \frac{1}{8} \tag{94}$$

with $\bar{n} \geq 0$ integer. Eqs. (93), (94) correspond exactly to the EBK quantization in Eqs. (83), (84). The regular – chaos transition producing non-closed tori in phase space leads to the unusual action quantization condition $\bar{n} + 1/8$ for the motion of the outer electron.

The QEBK - quantization using Eqs. (93) and (94) in the same way as in Sec. IV.D.1 reproduces the (real parts) of full three-dimensional quantum calculations already surprisingly well, especially in the large $\bar{n}$ limit, see Tab. IV. The QEBK – approach does not capture the interaction between overlapping Rydberg series manifesting itself in perturber states, see e.g. the spectral region around the first perturber (N, l) =(5,0) in helium in Tab. IV. These states can be resolved by including higher terms in the expansion (90) (Tanner and Wintgen (1995)).

The QEBK – formalism allows to derive a simple estimate for the quantum defects at the threshold energies. The quantum defect $\nu_{N,K}(E)$ is defined as the smooth function through the points (Friedrich (1990))

$$E_{(N,K)_n} = I_N - \frac{1}{2[n - \nu(E_{(N,K)_n})]^2}, \tag{95}$$

where $n \geq N$ counts the states successively up to the threshold energy I_N. The QEBK approximation for the threshold values $\nu_{N,K}$ are given by the simple formula,

$$\nu_{N,K}(I_N) = (1+s_0)\,N - 2(k+\frac{1}{2})\,\sigma_0 - \frac{1}{8} + n_{\rm per}, \tag{96}$$

where $n_{\rm per}$ counts the number of perturber states in the N series. Information about electron-electron interaction in the near core region enters the quantum defect through the leading coefficients s_0, σ_0, in Eq. (91), ($s_0 = -0.43709$, $\sigma_0 = 0.30491$ for helium). Eq. (96) is in good agreement with quantum results, see Tab. V. Especially the unusual phase 1/8, arising from the non–closure of the tori in phase space, is crucial at the thresholds.

Hence, the following overall picture emerges; the infinite periodic orbit sums account for the quasi–regular dynamics in the separable limit of non–interacting electrons. The Rydberg series as a highly ordered structure in the spectrum are correctly described, and the spectrum follows a simple QEBK–quantization scheme near the thresholds. The chaoticity of the central phase space region plays, however, a crucial role to reproduce the mixing and interference between overlapping series.

N	1	2	3	4	5	6	7
MQDT	0.140	0.685	1.272	2.785	3.410	4.953	6.391
QEBK	0.133	0.696	1.259	2.822	3.385	4.948	6.510

TABLE V. Quantum defects at the various threshold energies $I_N = -2/N^2$ (from Rost and Tanner (1997)).

V. CONCLUSION AND OUTLOOK

A. Summary

We can distinguish roughly three periods in which characteristic problems in two-electron atoms, most clearly exemplified in helium, have been addressed and which arose with increasing excitation energy:

1. Helium after 1920: The quest for quantum mechanics

The failure of the old quantum theory to describe a stable two-electron atom, as described in Chapter II, triggered the invention and development of quantum mechanics. Once the basic formalism had been established by Heisenberg and Schrödinger early variational calculations produced remarkably good results for the ground state. The quick success was possible because the variational technique was already known (the Rayleigh-Ritz variational principle). The central field approximation together with the Hartree-Fock self consistent field method finally made it possible to understand and compute large parts of the periodic table including excited bound states in particular of helium. The pictures and ideas developed in a semi-classical context for two electron atoms within the old quantum mechanics were obsolete and quickly forgotten over the success of the new quantum wave mechanics.

2. Helium after 1960: The need to go beyond the Hartree-Fock approximation

With the seminal synchrotron absorption experiments leading to doubly-excited states in the early 60ies it became clear that the effective single particle picture, familiar from the successful Hartree-Fock approximation, was inadequate to understand two-electron resonances. As a consequence, sophisticated alternative quantum approximations were developed over the next 30 years. The most important concepts were a group theoretical approach and two adiabatic approximations as described in Chapter III. These concepts successfully explained the high degree of nontrivial regularity in the spectra of two-electron resonances, i.e. features which could and can not be accounted for by an effective single particle picture. Rather, they are intrinsically related to the *correlated* dynamics of two electrons.

3. Helium after 1990: The quest for new concepts to understand the extreme excitation regime

Over the last decade the regime of extremely high excitation of both electrons, i.e. $N \approx n \geq 10$, has become feasible, both, experimentally and computationally. For these high excitations the approximate quantum numbers begin to loose their meaning and the regularities in the two-electron resonance spectrum start to dissolve. Moreover, even if applicable, the spectroscopic concept of isolated resonances identified by a set of quantum numbers becomes very questionable if the density of resonances per unit energy tends to infinity which is the case towards the three body break up limit $E = 0$ with $N \approx n \to \infty$. Hence, one needs an alternative concept to understand two-electron dynamics in this regime of extreme double-excitation. The concept is provided by a modern semiclassical approach. Its development over the last few years, reviewed in chapter IV, reveals an impressive progress in the quantitative description of the resonances by the cycle expansion and the QEBK approach. The backbone of these semiclassical descriptions are the periodic orbits of the full classical two-electron system without approximations.

It is very gratifying to see that from the shortest and simplest periodic orbits and from their stability properties one can draw a picture of two-electron excitation dynamics which agrees perfectly well with the results of the quantum approximations explaining the regular spectrum of intermediate double excitation. The asymmetric stretch and the frozen planet orbit can carry quantized

two-electron resonances. The third fundamental collinear orbit, the Wannier orbit, is too unstable for resonance formation. Instead, it represents the main decay path for the resonances.

However, the periodic orbits have one advantage that goes beyond the simple structural picture discussed above: A representation of the spectra in terms of periodic orbits, in particular through periodic orbit spectroscopy, does not rely on an explicit quantization scheme based on some the quasi-spearability of the problem in (collective) coordinates or the existence of approximate quantum numbers. This advantage might lead the way into the extreme excitation regime where the increase of resonances renders a description in terms of the assignment of quantum numbers meaningless. Moreover, the limit of high excitations naturally calls for semiclassical methods. One tool, which has already been proven to be very useful to characterize dynamical features in the extreme excitation limit for hydrogen in the magnetic field, is scaled periodic orbit spectroscopy. As described in section IV.C.3 the incredibly complex energy spectrum with many (overlapping) resonances can look quite ordered, if properly Fourier transformed into the time domain where peaks at certain times indicate the periods of relevant periodic orbits.

B. Outlook

One of the important and interesting issues for the future concerning two-electron dynamics is the behavior in the extreme excitation limit towards the three-body break up threshold.

- Which kind of resonances will survive as isolated identifiable structures?
- Will collective effects arise and which observable signature do they produce?
- Is chaotic behavior directly observable?

We expect that most of these questions can be discussed theoretically in the context of classical nonlinear dynamics. Some of them have already been addressed. In particular, it has been argued that Ericson fluctuations (Ericson (1960)) may occur in two-electron spectra (Blümel and Reinhardt 1997, Rost and Wintgen (1996), Burgdörfer et al. (1997), Gremaud and Delande (1997)). This shows that in the extreme excitation regime features could be possible which are common to many few-body systems.

Working towards a solution of these questions can make the helium atom once again to the point of condensation at which novel concepts and perspectives for few-body physics are developed.

C. Acknowledgements

We acknowledge fruitful collaboration with J.S. Briggs, A. Bürgers, J.T. Broad, G. Ezra, J. Feagin, D. Herschbach, M. Domke, G. Kaindl, E.A. Solovev, R. Thürwächter, A. Vollweiter, and D. Wintgen. For frequent discussions on two electron dynamics we thank R. Blümel, E. Bogomolny, J. Burgdörfer, P. Cvitanović, D. Delande, U. Eichmann, C.H. Greene, H. Friedrich, R. Gersbacher, H. Klar, W. Sandner, and V. Schmidt. Finally, we are grateful for the financial support of this work by the DFG, in particular within the Sonderforschungsbereich 276 at Freiburg University. Partial support from the DFG under contract Wi877/2 (KR), Wi877/5 (GT), TA181/1 (GT) and under the Gerhard Hess-Programm (JMR), as well as from the A. von Humboldt Foundation (KR, JMR) and the DAAD (JMR) is also acknowledged. We also thank the Isaac Newton Institute for Mathemtical Sciences, Cambridge, where part of this review was prepared.

REFERENCES

Aarseth, S. J., and K. Zare, 1974, Celest. Mech. **10**, 185.

Abramov, D. I., Gusev. V. V., and Ponomarev. L. I, 1997, Physics of Atomic Nuclei, **60**, 1133.

Abrashkevich A. G., D. G. Abrashkevich, and M. Shapiro, 1995, Comp. Phys. Commun. **90**, 311.

Arnold, V. I., 1979, *Mathematical Methods in Classical Mechanics* (Springer, New York).

Arnold, V. I., 1991, *Dynamical Systems III; Mathematical Aspects of Classical and Celestical Mechanics*, ed. V. I. Arnold (Springer, Berlin).

Artuso, R., E. Aurell and P. Cvitanović, 1990, Nonlinearity **3**, 325 and 361.

Atsumi T., T. Isihara, M. Koyama, and M. Matsuzawa, 1990, Phys. Rev. A **42**, 6391.

Aurich, R., M. Sieber, and F. Steiner, 1988, Phys. Rev. Lett. **61**, 483.

Aymar, M., C. H. Greene, and E. Luc-Koenig, 1996, Rev. Mod. Phys. **68**, 1015.

Bachau, H., 1984, J. Phys. B **17**, 1771.

Bachau, H., 1988, J. Phys. B **21**, 3547.

Bachelard, G., 1941, *Le Nouvel Esprit Scientifique* (Presses Universitaires de France, Paris), p. 152.

Balazs, N. L., and A. Voros, 1986, Phys. Rep. **143**, 109 .

Balslev, E., and J. M. Combes, 1971, Comm. Math. Phys. **22**, 280.

Bathia, A. K., and A. Temkin, 1975, Phys. Rev. A **11**, 2018.

Bathia, A. K., and A. Temkin, 1984, Phys. Rev. A **29**, 1895.

Belov, A. A., and D. V. Khveshchenko, 1985, Sov. Phys. JETP **62**, 1138.

Bergeson, S. D. et. al., 1998, Phys. Rev. Lett. **80**, 3475.

Berry, M. V., and M. Tabor, 1976, Proc. Roy. Soc. London A **349**, 101.

Berry, M. V., 1977, Phil. Trans. R. Soc. Lond. A **287**, 237.

Berry, M. V., and M. Tabor, 1977, J. Phys. A **10**, 371.

Berry, M. V., 1983, *Chaotic behaviour of Deterministic Systems*, eds. G. Iooss et al. (Amsterdam: North Holland), p. 172.

Berry, M. V., and J. P. Keating, 1990, J. Phys. A, **23** 4839.

Berry, M. V., and C. J. Howls, 1994, Proc. Roy. Soc. Lond. A. **447**, 527.

Bethe, H. A., and E. E. Salpeter, 1977, *Quantum mechanics of one- and two-electron atoms* (Plenum, New York).

Bisseling, R. H., R. Kossloff, J. Manz, F. Mrugala, J. Römelt, G. Weichselbaum, 1987, j. Chem. Phys. **86**, 2626.

Bloomfield, L. A., R. R. Freeman, W. E. Cooke, and J. Bokor, 1984, Phys. Rev. Lett. **53**, 2234.

Blümel, R., and W. P. Reinhardt, 1991, *Directions in Chaos Vol 4*, eds. B. L. Hao et al. (World Scientific, Hongkong).

Blümel, R., and W. P. Reinhardt, 1992, *Quantum Non-Integrability*, eds. D. H. Feng and J.-M. Yuan (World Scientific, Singapore).

Blümel, R., and W. P. Reinhardt, 1997, *Chaos in Atomic Physics* (Cambridge University Press, Cambridge).

Bogomolny, E., 1992, Nonlinearity **5**, 805.

Bohigas, O., 1991, *Chaos and Quantum Physics*, Les Houches, Session LII 1989, eds. M. J. Giannoni, A. Voros and J. Zinn–Justin (Elsevier, Amsterdam).

Bohigas, O., S. Tomsovic, and D. Ullmo, 1993, Phys. Rep. **223**, 44.

Bohr, N., 1913, Phil. Mag. **26**, 476.

Born, M., and W. Heisenberg, 1923, Z. Phys. **16**, 229.

Born, M., 1925, *Vorlesungen über Atommechanik* (Springer, Berlin); english translation: *The Mechanics of the Atom* (Ungar, New York, 1927).

van den Brink, J. P., G. Nienhuis, J. van Eck, and H. G. M. Heideman, 1989, J. Phys. B **22**, 3501.

Brotton, S. J., S. Cvejanovic, F. J. Currell, N. J. Bowring, and F. H. Read, 1997, Phys. Rev. A **55**, 318.

Buckmann, S. J., P. Hammond, F. H. Read, and G. C. King, 1983, J. Phys. B **16**, 4039.

Buckmann, S. J., and D. S. Newman, 1987, J. Phys. B **20**, L711.

Buckman, S. J., and C. W. Clark, 1994, Rev. Mod. Phys. **66**, 539.

Buchleitner, A., B. Grémaud, and D. Delande, 1994, J. Phys. B **27**, 2663.

Burgdörfer, J., X. Yang, and J. Müller, 1995, Chaos, Solitons and Fractals **5**, 1235.

Burgdörfer, J., Y. Qiu and J. Müller, 1997, *Classical, Semiclassical and Quantum Dynamics in Atoms*, eds. H. Friedrich and B. Eckhardt (Springer-Verlag, Berlin, Heidelberg, New York), p. 304.

Bürgers, A., D. Wintgen, and J.-M. Rost, 1995, J. Phys. B **28**, 3163.

Byron, F. W., and C. J. Joachim, 1989, Phys. Rep. **179**, 212.

Camus, P., T. F. Gallagher, J. M. Lecomte, P. Pillet, L. Pruvost, and J. Boulmer, 1989, Phys. Rev. Lett. **62**, 2365.
Chen, Z., C. G. Bao, and C. D. Lin, 1992, J. Phys. B **25**, 61.
Cheng-Pan, A. F. Starace, and C. H. Greene, 1994, J. Phys. B **27**, L137.
Chrysos, M., Y. Komninos, Th. Mercouris, and C. A. Nicolaides, 1990, Phys. Rev. A **42**, 2634.
Chrysos, M., G. Aspromallis, Y. Komninos, and C. A. Nicolaides, 1992, Phys. Rev. A **46**, 5789.
Cooper, J. W., U. Fano, and F. Prats, 1963, Phys. Rev. Lett. **10**, 518.
Cortés, M., and F. Martin, 1993, Phys. Rev. A **48**, 1227.
Creagh, S. C., J. M. Robbins, and R. G. Littlejohn, 1990, Phys. Rev. A **42**, 1907.
Cvitanović, P., 1988, Phys. Rev. Lett. **61**, 2729.
Cvitanović, P., and B. Eckhardt, 1989, Phys. Rev. Lett. **63**, 823.
Cvitanović, P., 1998, *Classical and Quantum Chaos: A Cyclist Treatise (Das Buch)*, http://www.nbi.dk/ChaosBook/.
Dietz, B., and U. Smilansky, 1993, Chaos **3**, 581.
Dimitrijević, M. S., and P. V. Grujić, 1984, Z. Naturforschung **39a**, 930.
Dmitrieva, I. K., and G. I. Plindov, 1988, J. Phys. B **21**, 3055.
Dmitrieva, I. K., and G. I. Plindov, 1988a, Opt. Spectrosc. **64**, 162.
Dmitrieva, I. K., and G. I. Plindov, 1989, J. Phys. B **22**, 1297.
Dmitrieva, I. K., and G. I. Plindov, 1990, J. Phys. B **23**, 693.
Dmitrieva, I. K., and G. I. Plindov, 1991, J. Phys. B **24**, 3149.
Domke, M., C. Xue, A. Puschmann, T. Mandel, E. Hudson, D. A. Shirley, G. Kaindl, C. H. Greene, H. R. Sadeghpour, and H. Petersen, 1991, Phys. Rev. Lett. **66**, 1306.
Domke, M., G. Remmers, and G. Kaindl, 1992, Phys. Rev. Lett. **69**, 1171.
Domke, M., K. Schulz, G. Remmers, A. Gutiérrez, G. Kaindl, and D. Wintgen, 1995, Phys. Rev. A **51**, R4309.
Domke, M., K. Schulz, G. Remmers, G. Kaindl, and D. Wintgen, 1996, Phys. Rev. A **53**, 1424.
Doolen, G. D., J. Nuttall, and R. W. Stagat, 1974, Phys. Rev. A **10**, 1612.
Doron, E., and U. Smilansky, 1992, Nonlinearity **5**, 1055.
Drake, G. W. F., 1988, Nucl. Instrum. Methods, B **31**, 7.
Drake, G. W. F., 1993, in *Long-Range Casimir Forces: Theory and Recent Experiments on Atomic Systems*, Eds. F. S. Levin and D. A. Micha (Plenum, New York).
Dräger, M., G. Handke, W. Ihra, and H. Friedrich, 1994, Phys. Rev. A, **50**, 3793.
Duan, Y., C. Browne, and J.-M. Yuan, 1998, submitted to Phys. Rev. A.
Eckhardt, B., and E. Aurell, 1989, Europhys. Lett. **9**, 509.
Eckhardt, B., 1991, Habilitationsschrift, Universität Marburg.
Eichmann, U., K. Richter, D. Wintgen, and W. Sandner, 1988, Phys. Rev. Lett. **61**, 2438.
Eichmann, U., P. Brockmann, V. Lange, and W. Sandner, 1989, J. Phys. B **22**, L361.
Eichmann, U., V. Lange, and W. Sandner, 1990, Phys. Rev. Lett. **64**, 274.
— 1992, Phys. Rev. Lett. **68**, 21.
Eikema, K. S. E., W. Ubachs, W. Vassen, and W. Hogervorst, 1996, Phys. Rev. Lett. **76**, 1216.
Einstein, A., 1917, Verhandl. der Deutschen Physik. Gesellschaft **19** No. 9/10, 82.
Ericson, T., 1960, Phys. Rev. Lett. **5**, 430.
Ezra, G. S., K. Richter, G. Tanner, and D. Wintgen, 1991, J. Phys. B **24**, L413.
Fano, U., 1961, Phys. Rev. **124**, 1866.
Fano U., and J. W. Cooper, 1965, Phys. Rev. **137**, 1364.
Fano, U., 1983, Rep. Prog. Phys. **46**, 97.
Fano, U., and A. R. P. Rau, 1986, *Atomic Collisions and Spectra* (Academic Press, New York).
Feagin, J. M., and J. S. Briggs, 1986, Phys. Rev. Lett. **57**, 984.
Feagin, J. M., and J. S. Briggs, 1988, Phys. Rev. A **37**, 4599.
Feynman, R. P., and A. R. Hibbs, 1965, *Quantum Mechanics and Path Integrals* (McGraw–Hill, New York).
Friedrich, H., and D. Wintgen, 1989, Phys. Rep. **183**, 37.
Friedrich, H., 1990 *Atomphysik* (Springer, Berlin).
Froese–Fischer, C., and M. Indrees, 1990, J. Phys. B **23**, 679.
Fukuda, H., N. Koyama, and M. Matsuzawa, 1987, J. Phys. B **20**, 2959.
Gallagher, T., 1994, *Rydberg atoms* (Cambridge University Press, Cambridge).
Gaspard, P., and S. A. Rice, 1994, Phys. Rev. A **48**, 838.
Gerasimovich, E. A., I. K. Dmitrieva, and G. I. Plindov, 1996, J. Phys. B **29**, 5227.
Goldstein, H., 1980, *Classical Mechanics* (Addison–Wesley, Reading MA).

Gou, B. C., Z. Chen, and C. D. Lin, 1991, Phys. Rev. A **43**, 3260.
Grémaud, B., and D. Delande, 1997, Europhys. Lett. **40**, 363.
Grémaud, B., and P. Gaspard, 1998, J. Phys. B. **31**, 1671.
Gu, Y., and J.-M. Yuan, 1993, Phys. Rev. A **47** , R2442.
Guhr, T., A. M. Müller–Groeling and H. A. Weidenmüller, 1998, Phys. Rep., to be published.
Grujić, P. V., and N. S. Simonović, 1995, J. Phys. B. **28**, 1159.
Gutzwiller, M. C., 1967, J. Math. Phys. **8**, 1979.
— 1971, J. Math. Phys. **12**, 343.
— 1990, *Chaos in Classical and Quantum Mechanics* (Springer, New York).
— 1994, AIP conference procceedings **334**, ed. Gross, F., 275.
— 1998, Rev. Mod. Phys. **70**, 589.
Halzen F., and A. D. Martin, 1984, *Quarks and Leptons: An Introductory Course in Modern Particle Physics* (Wiley, New York).
Hamacher, P., and J. Hinze, 1989, J. Phys. B **22**, 3397.
Handke, G., M. Dräger, and H. Friedrich, 1993, Physica A **197**, 113.
Harris, P. G., H. C. Bryant, A. H. Mohaghegli, R. A.Reeder, H. Sharifian, H. Tootoonchi, C. Y. Tang, J. B. Donahue, C. R. Quick, D. C. Rislove, and W. W. Smith, 1990, Phys. Rev. Lett. **65**, 309; P. G. Harris, H. C. Bryant, A. H. Mohaghegli, R. Reeder, C. Y. Tang, J. B. Donahue, and C. R. Quick, 1990, Phys. Rev. A **42**, 6443.
Hayes, M. A., and M. P. Scott, 1988, J. Phys. B **21**, 1499.
Heitmann, D., and J. P. Kotthaus, 1993, Phys. Today **46**, 56.
Heller, E. J., and S. Tomsovic, 1993, Physics Today **46**, 38.
Heim, T. A., G. B. Armen, and A. R. P. Rau, 1997, Phys. Rev. A **55**, 2674.
Heisenberg, W., 1922, letter of Heisenberg to Sommerfeld, 28 October 1922; archive of the *Deutsches Museum*, Munich. The role of W. Heisenberg at this stage of the "old quantum theory" is also described in: D. C. Cassidy, 1995, *Werner Heisenberg* (Spektrum Akademischer Verlag Heidelberg), Sec. II.8: "Der blonde Bauernjunge".
Heisenberg, W., 1925, Z. Phys. **33**, 879.
Heisenberg, W., 1926, Z. Phys. **39**, 499.
Hernandez, M. I., and D. C. Clary, 1996, J. Chem. Phys. **104**, 8413
Herrick, D. R., and F. H. Stillinger, 1975, Phys. Rev. A **11**, 42.
Herrick, D. R., and A. O. Sinanoglu, 1975, Phys. Rev. A **11**, 97.
Herrick, D. R., 1975, Phys. Rev. A **12**, 413.
Herrick, D. R., 1975a, J. Math. Phys. A **16**, 281.
Herrick, D. R., and M. E. Kellman, 1980, Phys. Rev. A **21**, 418.
Herrick, D. R., M. E. Kellman, and R. D. Poliak, 1980, Phys. Rev. A **22**, 1517.
Herrick, D. R., 1983, Adv. Chem. Phys. **52**, 1.
Herschbach, D. R., 1986, J. Chem. Phys. **84**, 838.
Herschbach, D. R., 1993, Dudley Herschbach Festschrift, J. Chem. Phys. **97**.
Herschbach, D. R., O. Goscinsci, and J. S. Avery (eds.), 1993, *Dimensional scaling in Chemical Physics* (Kluwer, Dordrecht).
Hicks, P. J., and J. Comer, 1975, J. Phys. **8**, 1866.
Ho Y. K., 1983, Phys. Rep. **99** 1.
— 1986, Phys. Rev. A **34** 4402.
— 1989, Z. Phys. D **11**, 277.
— 1990, J. Phys. B **23**, L71.
— 1992, Phys. Rev. A **45** 148.
Ho, Y. K., and J. Callaway, 1985, J. Phys. **18**, 3481.
Ho, Y. K., and A. K. Bhatia, 1992, Phys. Rev. A **45** 6268.
Hogervorst, W., 1993, Comments At. Mol. Phys. **29**, 245.
Holle, A., J. Main, G. Wiebusch, H. Rottke, and K. H. Welge, 1988, Phys. Rev. Lett. **61**, 161.
Hunter, III, J. E., and R. S. Berry, 1987, Phys. Rev. A **36**, 3042 .
Hunter, G., and H. O. Pritchard, 1967, J. Chem. Phys. **46**, 2146.
Hunter, G., and H. O. Pritchard, 1967a, J. Chem. Phys. **46**, 2153.
Hunter, G., B. F. Gray, and H. O. Pritchard, 1968, J. Chem. Phys. **45**, 3806.
Hylleraas, E. A., 1928, Z. Phys. **48**, 469.
Hylleraas, E. A., 1929, Z. Phys. **54**, 347.
James, H. M, and A. S. Coolidge, 1937, Phys. Rev. **51**, 857.

Jones, R. R., and T. F. Gallagher, 1990, Phys. Rev. A **42**, 2655.
Junker, B. R., 1982, Adv. At. Mol. Phys. **18** 207.
Keating, J. P., and M. Sieber, 1994, Proc. Roy. Soc. Lond. A. **447**, 413.
Keller, J. B., 1958, Ann. Phys. NY **4**, 180.
Kellman, M. E., and D. R. Herrick, 1980, Phys. Rev. A **22**, 1536.
Kellner, G. W., 1927, Z. Phys **44**, 91.
Kemble, E. C., 1921, Phil. Mag. **42**, 123.
Kilgus, G. et. al., 1990, Phys. Rev. Lett. **64**, 737.
Kim, J. H., and G. S. Ezra, 1991, *Proc. Adriatico Conf. on Quantum Chaos*, eds. H. Cerdeira et al. (World Scientific, Singapore).
Klar, H., and M. Klar, 1980, J. Phys. B **13**, 1057.
Klar, H., 1986, Phys. Rev. Lett. **57**, 66.
Kinoshita, T., 1959, Phys. Rev. **115**, 366.
Kossmann, H., B. Krässig, and V. Schmidt, 1988, J. Phys. B **21**, 1489.
Koyama, N., H. Fukuda, T. Motoyama, and M. Matsuzawa, 1986, J. Phys. B **19**, L331.
Koyama, N., A. Takafuji, and M. Matsuzawa, 1989, J. Phys. B **22**, 553.
Kramers, H. A., 1923, Z. Phys. **13**, 312.
Krein, M., 1953, Mat. Sborn. **33**, 597; for a more recent discussion see also J. S. Faulkner, 1977, J. Phys. C **10**, 4661.
Kustaanheimo, P., and E. Stiefel, 1965, Comt. Rend. **260**, 805.
Langmuir, I., 1921, Phys. Rev. **17**, 339.
Landé, A., 1919, Phys. Zeitschr. **20**, 228.
Leopold, J. G., I. C. Percival, and A. S. Tworkowski, 1980, J. Phys. B **13**, 1025.
Leopold, J. G., and I. C. Percival, 1980, J. Phys. B **13**, 1037.
Lin, C. D., 1982, Phys. Rev. A **25**, 76.
— 1982a, Phys. Rev. A **26**, 2305.
— 1983, Phys. Rev. Lett. **51**, 1348.
— 1983a, Phys. Rev. A **27**, 22.
— 1984, Phys. Rev. A **29**, 1019.
Lin, C. D., and J. Macek, 1984, Phys. Rev. A **29**, 2317.
Lin, C. D., 1986, Adv. At. Mol. Phys. **22**, 77.
Lin, C. D., and S. Watanabe, 1987, Phys. Rev. A **35**, 4499.
Lin, C. D., 1989, Phys. Rev. A **39**, 4355
Lin, C. D., 1995, Phys. Rep. **257**, 1.
Liu, C. H., N. Y. Du, and A. F. Starace, 1991, Phys. Rev. A **43**, 5891.
Lyman, T., 1924, Astroph. Journ. **60**, 1.
Macek, J., 1968, J. Phys. B **1**, 831.
Macias, A., and A. Riera, 1986, Europhys. Lett. **2**, 351.
Macias, A., and A. Riera, 1986a, Phys. Lett. A **119**, 28.
Mack, M., J. H. Nijland, P. van der Straten, A. Niehaus, and R. Morgenstern, 1989, Phys. Rev. A **39**, 3846.
MacKay, R. S., J. D. Meiss, and I. C. Percival, 1984, Phys. Rev. Lett. **52**, 697.
Madden, R. P., and K. Codling, 1963, Phys. Rev. Lett. **10**, 516.
Main J., and G. Wunner, 1992, Phys. Rev. Lett. **69**, 586.
Mandelshtam, V. A., T. R. Ravuri, and H. S. Taylor, 1993, Phys. Rev. Lett. **70**, 1932.
Martens, C. C., and S. E. Ezra, 1987, J. Chem. Phys. **86**, 279.
Martin, F., A. Riera, M. Yanez, and H. Bachau, 1988, J. Phys. B **21**, 2261.
Mehra, J., and H. Rechenberg, 1982, *The Historical Development of Quantum Theory* (Springer-Verlag, Heidelberg); see in particular Vol. I, Part 2 and Vol. II, Chap. 3.
Menzel, A., S. P. Frigo, S. B. Whitfield, C. D. Caldwell, M. O. Krause, J-Z. Tang, and I. Shimamura, 1995, Phys. Rev. Lett. **75**, 1479.
Menzel, A., S. P. Frigo, S. B. Whitfield, C. D. Caldwell, and M. O. Krause, 1996, Phys. Rev. A **54**, 2080.
Miller, W. H., 1972, J. Chem. Phys. **56**, 38.
Miller, W. H., 1974, Adv. Chem. Phys. **25**, 69.
Miller, W. H., 1975, J. Chem. Phys. **63**, 996.
Molina, Q., 1989, Phys. Rev. A **39**, 3298.
Moretto-Capelle, P., D. Bordenave-Montesquieu, A. Bordenave-Montesquieu, A. L. Godunov, and V. A. Schipakov, 1997, Phys. Rev. Lett. **79**, 5230.

Morgan, H. D., and D. L. Ederer, 1984, Phys. Rev. A **29**, 1901.
Morita, N., and T. Suzuki, 1988, J. Phys. B **21**, L439.
Müller, J., 1993, PhD thesis, University of Frankfurt, Reihe Physik (Verlag Deutsch, Frankfurt), **19**, 1.
Müller, J., J. Burgdörfer, and D. W. Noid, 1992, Phys. Rev. A **45**, 1471.
Müller, J., and J. Burgdörfer, 1993, Phys. Rev. Lett. **70**, 2375.
Müller, J., X. Yang, and J. Burgdörfer, 1994, Phys. Rev. A **49**, 2470.
Nikitin, S. I., and V. N. Ostrovsky, 1982, J. Phys. B **15**, 1609, and references therein.
Ostrovsky, V. N., 1992, Phys. Rev. A **46**, R5309.
Ostrovsky, V. N., and N. V. Prudov, 1993, J. Phys. B **26**, L263.
Oza, D. H., 1986, Phys. Rev. A **33**, 824.
Ozorio de Almeida, A. M., and J. H. Hannay, 1983, Ann. Phys. **145**, 100.
Ozorio de Almeida, A. M., and J. H. Hannay, 1987, J. Phys. A **20**, 5873.
Park, C. H., A. F. Starace, J. Tan, and C. D. Lin, 1991, Phys. Rev. A **33**, 1000.
Pars L. A., 1965, *A Treatise on Analytical Dynamics* (Heinemann, London).
Pauli, W., 1922, PhD thesis, unpublished.
Pekeris, C. L., 1958, Phys. Rev. **112**, 1649.
Pekeris, C. L., 1959, Phys. Rev. **115**, 1216.
Pelikan, E., and H. Klar, 1983, Zeits. Phys. A **310**, 153.
Percival I. C., 1974, J. Phys. A **7**, 794.
Percival, I. C., 1977, Proc. Roy. Soc. Lond. A **353**, 289.
Prosen, T., 1994, J. Phys. A **27**, L709.
— 1995, J. Phys. A **28**, 4133.
— 1996, Physica D **91**, 244.
Qiu, Y., J. Müller, and J. Burgdörfer, 1996, Phys. Rev. A **54**, 1922.
Rau, A. R. P., 1983, J. Phys. B **16**, L699.
Rau, A. R. P., 1984, Phys. Rep. **110**, 369.
Read, F. H., 1977, J. Phys. B **12**, 449.
Read, F. H., 1982, Aust. J. Phys. **35**, 475.
Read, F. H., 1990, J. Phys. B **23**, 951.
Reed, M., and B. Simon, 1972, *Methods of Modern Mathematical Physics* (Academic Press, New York), see Vol. **I** Chap. VI and Vol. **IV** Chap. XIII.
Reinhardt W. P., 1982, Ann. Rev. Phys. Chem. **33**, 223.
Richter, K., and D. Wintgen, 1990, J. Phys. B **23**, L197.
Richter, K., and D. Wintgen, 1990a, Phys. Rev. Lett. **65**, 1965.
Richter, K., 1991, *Semiklassik von Zwei-Elektronen-Atomen*, PhD thesis, Universität Freiburg (unpublished).
Richter, K., and D. Wintgen, 1991, J. Phys. B **24**, L565.
Richter, K., J. M. Rost, R. Thürwächter, J. S. Briggs, D. Wintgen, and E. A. Solov'ev, 1991, Phys. Rev. Lett. **66**, 149.
Richter, K., and D. Wintgen, 1992, in *Atomic Physics 13*, eds. H. Walther, T. W. Hänsch, and B. Neizert (American Institute of Physics, New York), p. 388.
Richter, K., J. S. Briggs, D. Wintgen, and E. A. Solov'ev, 1992, J. Phys. B **25**, 3929.
Richter, K., G. Tanner, and D. Wintgen, 1993, Phys. Rev. A **48**, 4182.
Richter, K., and D. Wintgen, 1993, J. Phys. B **26**, 3719.
Robbins, J. M., 1991, Nonlinearity **4**, 343.
Rost, J. M., and J. S. Briggs, 1988, J. Phys. B **21**, L233.
Rost, J. M., and J. S. Briggs, 1989 J. Phys. B **22**, 3587.
Rost, J. M., and J. S. Briggs, 1990, J. Phys. B **23**, L339.
Rost, J. M., J. S. Briggs, and J. M. Feagin, 1991, Phys. Rev. Lett. **66**, 1642.
Rost, J. M., and J. S. Briggs, 1991, J. Phys. B **24**, 4293.
Rost, J. M., R. Gersbacher, K. Richter, J. S. Briggs, and D. Wintgen, 1991a, J. Phys. B **24**, 2455 .
Rost, J. M., S. M. Sung, D. R. Herschbach, and J. S. Briggs, 1992, Phys. Rev. A **46**, 2410.
Rost, J. M., 1994, Phys. Rev. Lett. **72**, 1998.
Rost, J. M., 1995, J. Phys. B **28**, 3003.
Rost, J. M., and Wintgen D., 1996, Europhys. Lett. **35**, 19.
Rost, J. M., and G. Tanner, 1997, *Classical, Semiclassical and Quantum Dynamics in Atoms*, eds. H. Friedrich and B. Eckhardt (Lecture Notes in Physis 485, Springer, Berlin), p. 274.
Rost, J. M., K. Schulz, M. Domke, and G. Kaindl, 1997, J. Phys. B **30**, 4663.

Rost, J. M., 1998, Phys. Rep., to be published.
Roussel, F., M. Cheret, L. Chen, T. Bolzinger, G. Spiess, J. Hare, and M. Gross, 1990, Phys. Rev. Lett. **65**, 3112.
Rouvinez, C., and U. Smilansky, 1995, J. Phys. A **28**, 77.
Sadeghpour, H. R., and C. H. Greene, 1990, Phys. Rev. Lett. **65**, 313.
Sadeghpour, H. R., 1991, Phys. Rev. A **43**, 5821.
Sadeghpour, H. R., C. H. Greene, and M. Cavagnero, 1992, Phys. Rev. A **45**, 1587.
Sadeghpour, H. R., 1991, Phys. Rev. A **43**, 5821.
Sakaue, H. A., Y. Kanai, K. Ohta, M. Kushima, T. Inaba, S. Ohtani, K. Wakiya, H. Suzuki, T. Takayanagi, T. Kambara, A. Danjo, M. Yoshino, and Y. Awaya, 1990, J. Phys. B **23**, L401.
Sánchez, I., and F. Martin, 1993, Phys. Rev. A **48**, 1243.
Schiff, L. I., 1968, *Quantum mechanics* (McGraw Hill, Singapore).
Schrödinger, E., 1926, Ann. Physik **79**, 361.
Schulz, K., G. Kaindl, M. Domke, J. D. Bozek, P. A. Heimann, A. S. Schlachter, and J. M. Rost, 1996, Phys. Rev. Lett. **77**, 3086.
Schuster, H. G., 1989, *Deterministic Chaos* (VCH, Weinheim).
Schutte, C. J. H., 1976, *The theory of molecular spectroscopy* (Elsevier, Amsterdam).
Seaton, M. J., 1983, Rep. Prog. Phys., **64**, 167.
Selberg, A., 1956, J. Indian Math. Soc. **20**, 47.
Seng, M., M. Halka, K.-D. Heber, and W. Sandner, 1995, Phys. Rev. Lett. **74**, 3344.
Sieber, M., and F. Steiner, 1990, Phys. Lett. A **144**, 159.
Sieber, M., and F. Steiner, 1991, Phys. Rev. Lett. **67**, 1941.
Sinanoglu, O., and D. E. Herrick, 1975, J. Chem. Phys. **62**, 886.
Slater, J. C., 1927, Proc. Nat. Acad. Amer. **13**, 423.
Slater J. C., 1977, *Quantum theory of matter* (Krieger, Huntington).
Smilansky, U., and I. Ussishkin, 1996, J. Phys. A **29**, 2587.
Sokell, E, A. A. Wills, P. Hammond, M. A. MacDonald, and M. K. Odling-Smee, 1996, J. Phys. B **29**, L863.
Solov'ev, E. A., 1985, Sov. Phys. JETP **62**, 1148; Zh. Eksp. Teor. Fiz. **89**, 1991.
Sommerfeld, A., 1923, Jour. Opt. Soc. America, **7**, 509.
Starace, A. F., 1988, *Fundamental Processes of Atomic Dynamics*, Eds. J.S. Briggs, H. Kleinpoppen, and H.O. Lutz (Plenum, New York).
Stolterfoth, N., C. C. Havener, R. A. Phaneuf, J. K. Swenson, S. M. Shafroth, F. W. Meyer, 1986, Phys. Rev. Lett. **57**, 74.
Strand, M. P., and W. P. Reinhardt, 1979, J. Chem. Phys. **70**, 3812.
Tang, J. Z., S. Watanabe, and M. Matsuzawa, 1992, Phys. Rev. A **46** 2437.
Tang, J. Z., S. Watanabe, M. Matsuzawa, and C. D. Lin, 1992a, Phys. Rev. Lett. **69**, 1633.
Tang, J. Z., and I. Shimamura, 1994, Phys. Rev. A **50**, 1321.
Tang, X., Y. Gu, and J.-M. Yuan, 1996, Phys. Rev. A **54** , 496.
Tanner, G., P. Scherer, E. B. Bogomolny, B. Eckhardt, and D. Wintgen, 1991, Phys. Rev. Lett. **67**, 2410.
Tanner, G., and D. Wintgen, 1995, Phys. Rev. Lett. **75**, 2928.
Tanner, G., K. Hansen, and J. Main, 1996, Nonlinearity **9**, 1641.
Tanner, G., 1997, J. Phys. A **30**, 2863.
Taylor, J. R., 1972, *Scattering Theory* (Wiley&Sons, New York).
Titchmarsh, E. C., 1986, *The theory of the Riemann zeta function* (Clarendon Press, Oxford).
Tolstikhin, O. I., S. Watanabe, and M. Matsuzawa, 1995, Phys. Rev. Lett. **74**, 3573.
Unsöld, A., 1927, Ann. Physik, **82**, 355.
van Vleck, J. H., 1922, Phil. Mag. **44**, 842.
van Vleck, J. H., 1928, Proc. Natl. Acad. Sci. **14**, 178.
Vollweiter, A., J. M. Rost, and J. S. Briggs, 1991, J. Phys. B **24**, L155.
Voros, A., 1987, Commun. Math. Phys. **110**, 439.
Voros, A., 1988, J. Math. Phys. **21**, 685.
Wang, H., 1986, J. Phys. B **19**, 3401.
Wannier, G., 1953, Phys. Rev. **90**, 817.
Watanabe, S., and C. D. Lin, 1986, Phys. Rev. A **34**, 823.
Wesenberg, G. E., D. W. Noid, and J. B. Delos, 1985, Chem. Phys. Lett. **118**, 72.
Wintgen, D., 1987, Phys. Rev. Lett. **58**, 1589.
Wintgen, D., K. Richter, and G. Tanner, 1992, Chaos **2**, 19.

Wintgen, D., and D. Delande, 1993, J. Phys. B **26**, L399.
Wintgen, D., and K. Richter, 1994, Comm. At. Mol. Phys. **29**, 261.
Wintgen, D., A. Bürgers, K. Richter, and G. Tanner, 1994, Proc. Theo. Phys. Supp. **116**, 121.
Wintgen, D., 1994, private communication.
Wirzba, A., 1992, Chaos **2**, 77.
Wirzba, A., 1997, Habilitationsschrift, Darmstadt.
Witten, E., 1980, Physics Today **33**, 38.
Woodruff, P. R., and J. A. R. Samson, 1982, Phys. Rev. A **25**, 848.
Wulfman, C., 1968, Phys. Lett. A **26**, 397.
Wulfman, C., 1973, Chem. Phys. Lett. **23**, 370.
Yamamoto, T., and K. Kaneko, 1993, Phys. Rev. Lett. **70**, 1928.
Yuh, H. J., G. S. Ezra, P. Rehmus, and R. S. Berry, 1981, Phys. Rev. Lett. **47**, 497.
Zubek, M., G. C. King, P. M. Rutter, and F. H. Read, 1989, J. Phys. B **22**, 3411.